The 13th School of Mesoscopic Physics:
Mesoscopic Quantum Devices
May 24, 2024
Pohang, Korea

Part I Basics of semiconductor QC
Part II Advances in semiconductor QC

**RIKEN Center for Emergent Matter Science &
Quantum Computing**

Seigo Tarucha

1. Fundamentals for quantum computer
2. Advances in spin quantum computer

Approx. 2,000 scientists
3,400 people

Tokyo

RIKEN Research Center for Quantum Computing

SC

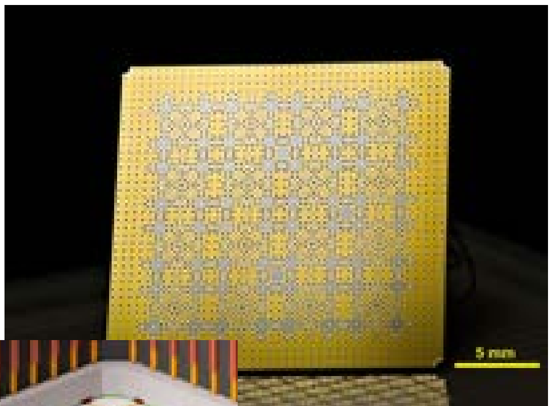

RIKEN/FUJI
・64 qubit
services

Optical

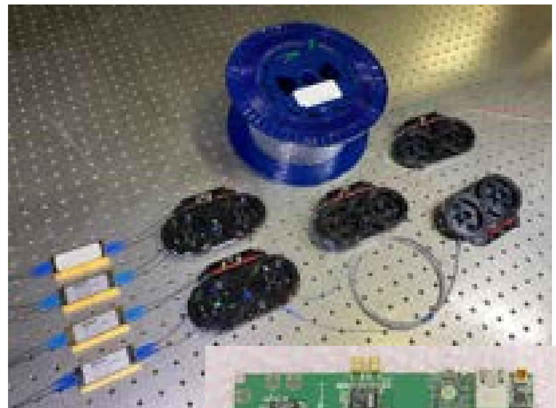

ement-
QC

New project for integrated use of QC and supercomputers

Nov. 2023

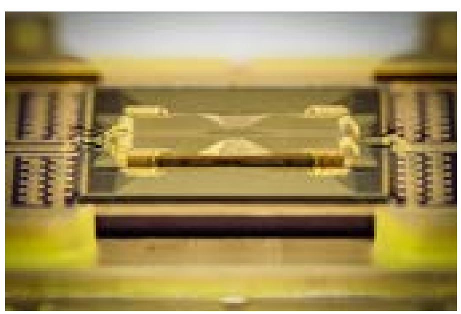

Quantinuum Model H1

Semiconductor

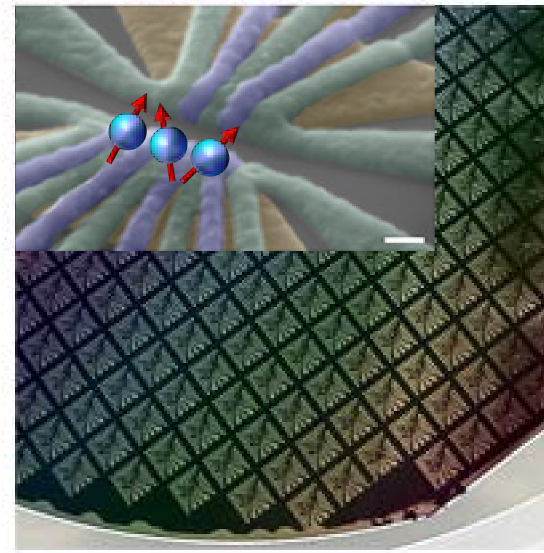

- Spin-based QC in 28Si

ST and DL

Part I Basics of semiconductor QC

- Concepts of quantum bits and computation
- Implementation of single and two qubit gates
- Readout and initialization
- Quantum coherence and phase noise

Part II Advances in semiconductor QC

- Features of quantum computing in silicon
- High-fidelity quantum gates and readout
- Quantum error correction
- Multi-qubit devices for scale-up

Spin Qubit

$|\varphi\rangle = a|0\rangle + b|1\rangle$

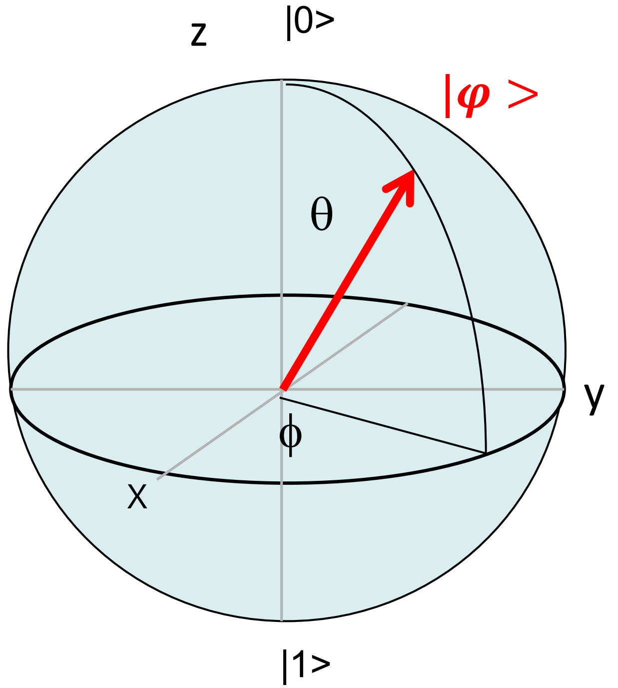

Qubit = Superposition of |0> and |1>

Only for operation time < coherence time

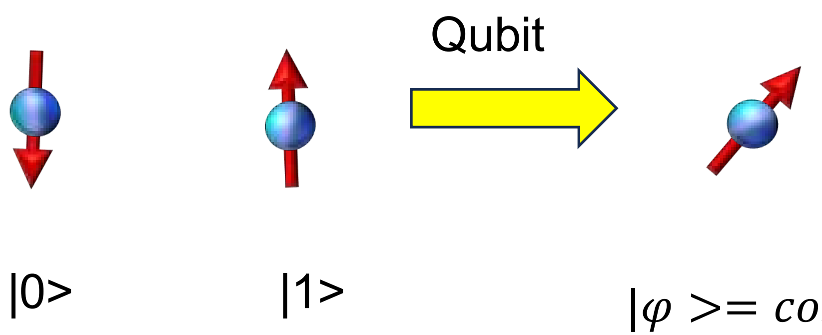

a|0> + b|1>
Basis {|0>, |1>}

$$|\varphi> = cos\frac{\theta}{2}\,|0> + e^{i\emptyset} sin\frac{\theta}{2}\,|1>$$

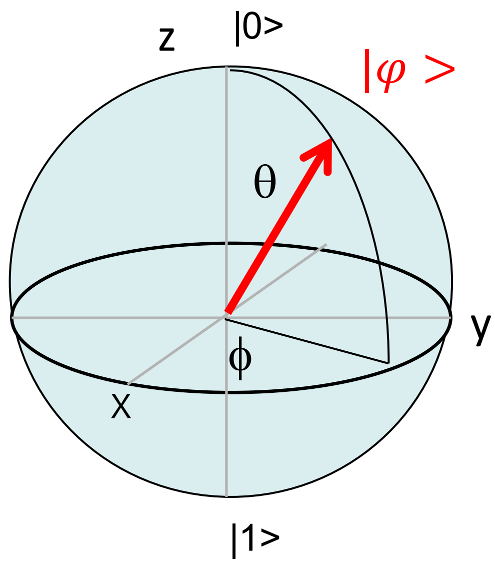

$$i\hbar \frac{d|\varphi(t)>}{dt} = \hat{H}|\varphi(t)>$$

$H = H_0 + H_1$

H_0 to define the steady states
$H_0|0> = E_0|0>$、$H_0|1> = E_1|1>$

H_1 to superpose the steady states

Spin Qubit Manipulation

Only for time < coherence time

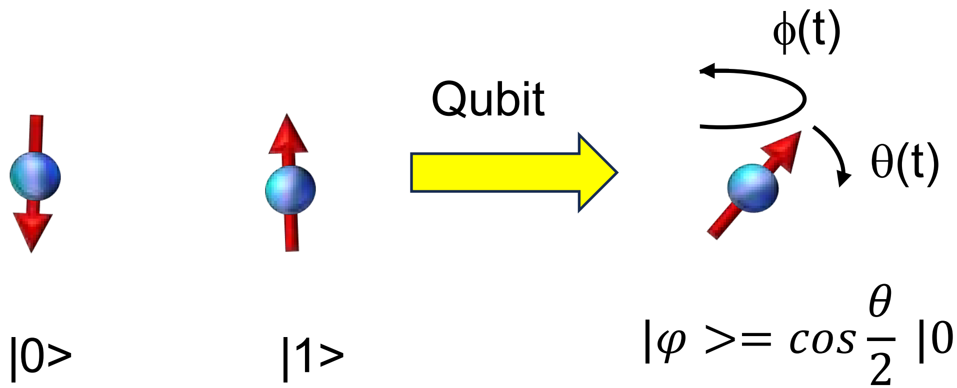

a|0> + b|1>

Basis {|0>, |1>}

$$|\varphi >= cos\frac{\theta}{2}\ |0> +e^{i\phi}sin\frac{\theta}{2}\ |1>$$

$$i\hbar\frac{d|\varphi(t)>}{dt} = \hat{H}_1|\varphi(t)>$$

$$U(t,0) = \exp[-\frac{i}{\hbar}\hat{H}_1 t]$$

$|\varphi(t)>=a(t)|0>+b(t)|1>$

$=\begin{pmatrix} a(t) \\ b(t) \end{pmatrix}=U(t,0)\begin{pmatrix} a(0) \\ b(0) \end{pmatrix}$

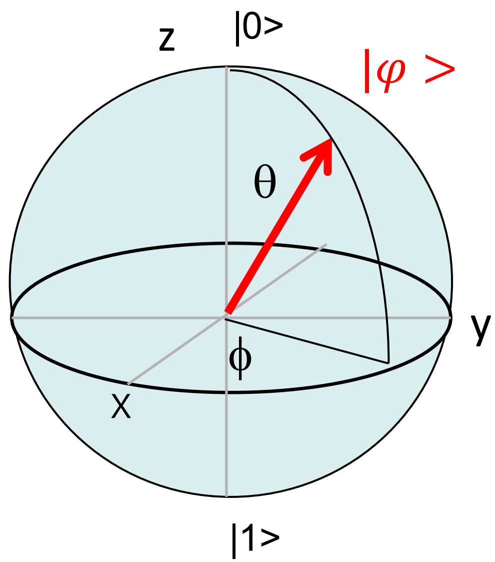

Qubit control

= Control of rotation about x-axis, θ(t), and z-axis, ϕ(t), respectively.

Spin Manipulation for Quantum Computing

Baisi $\{|0>_A|0>_B,\ |0>_A|1>_B,\ |1>_A|0>_B,\ |1>_A|1>_B\}$

$|00>$ $|01>$ $|10>$ $|11>$

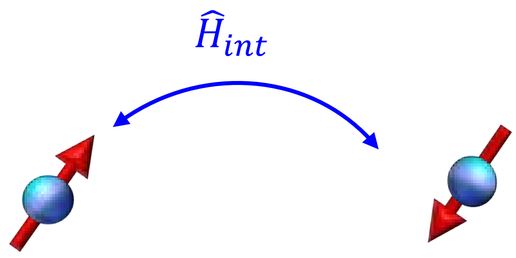

$|\varphi>=a|0>+b|1>$ $|\varphi>=c|0>+d|1>$

$$|\varphi_1,\varphi_2> = \alpha|00>+\beta|01>+\gamma|10>+\delta|11> = \begin{pmatrix}\alpha(t)\\ \beta(t)\\ \gamma(t)\\ \delta(t)\end{pmatrix} = U(t,0)\begin{pmatrix}\alpha(0)\\ \beta(0)\\ \gamma(0)\\ \delta(0)\end{pmatrix}$$

$$i\hbar\frac{d|\varphi_1,\varphi_2>}{dt} = \widehat{H}|\varphi_1,\varphi_2>$$

$$\widehat{H} = \widehat{H}_1 + \widehat{H}_{int}$$

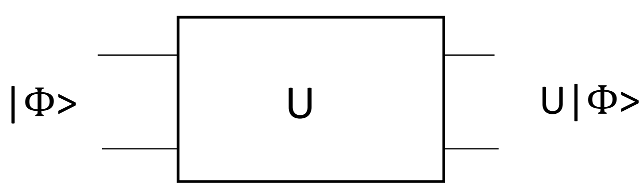

Quantum Entanglement

2qubit system

|A>=a|0> + b|1>
|B>=c|0> + d|1>

Simple product $|A\rangle \otimes |B\rangle = ac|0\rangle_A|0\rangle_B + ad|0\rangle_A|1\rangle_B + bc|1\rangle_A|0\rangle_B + bd|1\rangle_A|1\rangle_B$

Inseparable two-qubit state ＝ a|00>+b|01>+g|10>+d|11>

$$\left\{ \begin{array}{l} \dfrac{|0\rangle|0\rangle \pm |1\rangle|1\rangle}{\sqrt{2}} \\[2ex] \dfrac{|0\rangle|1\rangle \pm |1\rangle|0\rangle}{\sqrt{2}} \end{array} \right.$$

Maximally entangled states
＝Bell states

Spin singlet |S>、Spin triplet $|T_0\rangle$

$$|S\rangle = \frac{|\downarrow\rangle|\uparrow\rangle - |\uparrow\rangle|\downarrow\rangle}{\sqrt{2}}$$

$|T_+\rangle = |\uparrow\rangle|\uparrow\rangle$

$|T_0\rangle = \dfrac{|\downarrow\rangle|\uparrow\rangle + |\uparrow\rangle|\downarrow\rangle}{\sqrt{2}}$

$|T_-\rangle = |\downarrow\rangle|\downarrow\rangle$

Logical Calculation

Fidelity > 99%

Initialization

Readout Fidelity > 99%

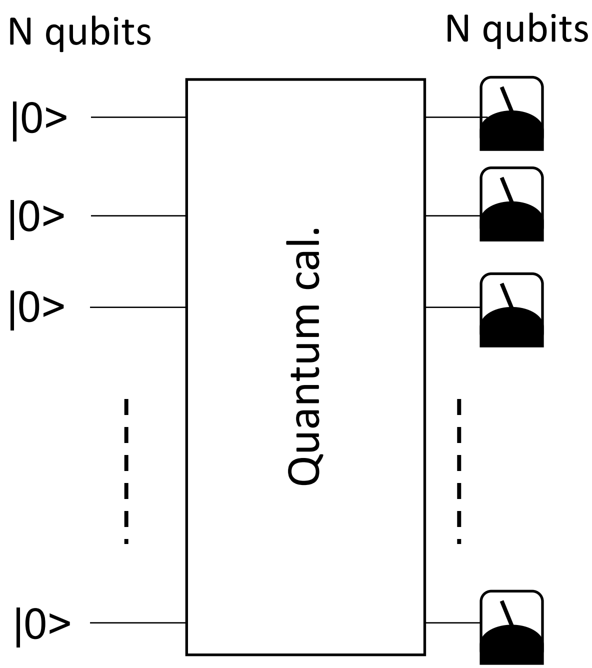

Multi-qubit gates consisting of single qubit gates and two-qubit gates

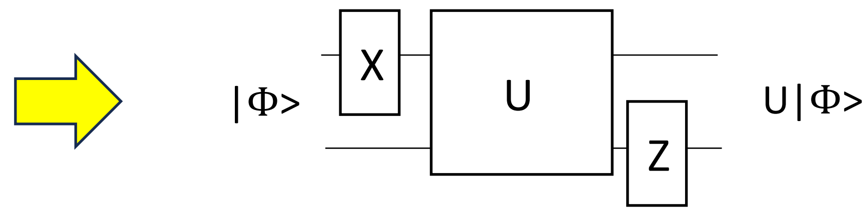

Single qubit op. Fidelity > 99.9%
Two-qubit op. Fidelity > 99%

Scale-up of qubit devices required for large scale calculation but all operations must complete within dephasing time.

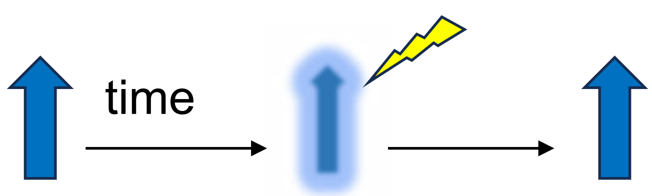

Error correction

DiVincenzo’s criteria

1. Long coherence time
2. Universal quantum gate set
   （Single and two-qubit gates）
3. Quantum bit readout
4. Quantum bit initialization
5. Qubit scalability

Summary: Why quantum computation fast?

1. Superposition of n qubits in 2^n basis states $\{|000..0>, |000..1>, ..., |111..1>\}$

$$|\varphi> = \frac{1}{2^{\frac{n}{2}}}[|000..0> + |000..1> + ... + |111..1>]$$

2. Quantum entanglement

$$\frac{|0>|0> \pm |1>|1>}{\sqrt{2}}$$ Correlation in 2 or more qubits

Used in logical calculations

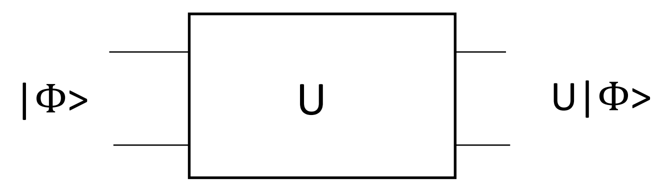

3. Quantum parallelism

Parallel calculation of superposed n qubits

$$U|\varphi> = \frac{1}{2^{\frac{n}{2}}}[U|000..0> + U|000..1> + ... + U|111..1>]$$

Part I   Basics of semiconductor QC

- Concepts of quantum bits and computation
- Implementation of single and two qubit gates
- Readout and initialization
- Quantum coherence and phase noise

Part II   Advances in semiconductor QC

- Features of quantum computing in silicon
- High-fidelity quantum gates and readout
- Quantum error correction
- Multi-qubit devices for scale-up

Spin Qubit Manipulation using Concept of Spin Resonance

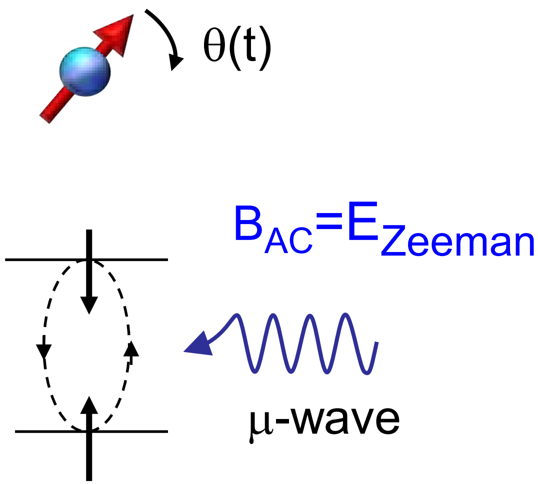

Rotation about x-axis

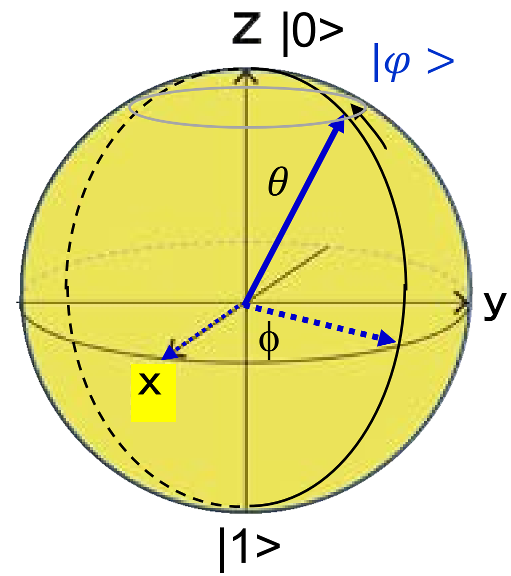

θ control by B_{AC} burst

ϕ control by B_{AC} phase

Physical Implementation of Spin Qubits
: Spin Resonance for Single Electrons in QD

ESR using Microwave
induced ac E-field

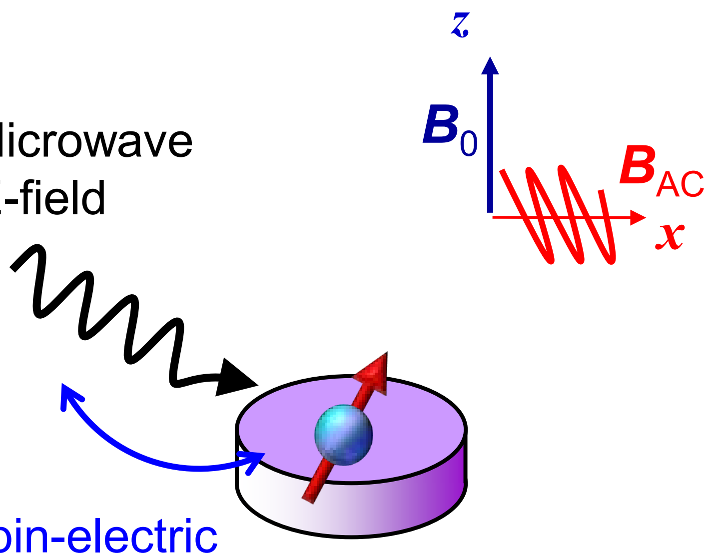

a.c. electric field of μ-wave is converted to a.c. magnetic field through spin-electric coupling mechanism of spin-orbit coupling, on-chip coil, μ-magnet,….

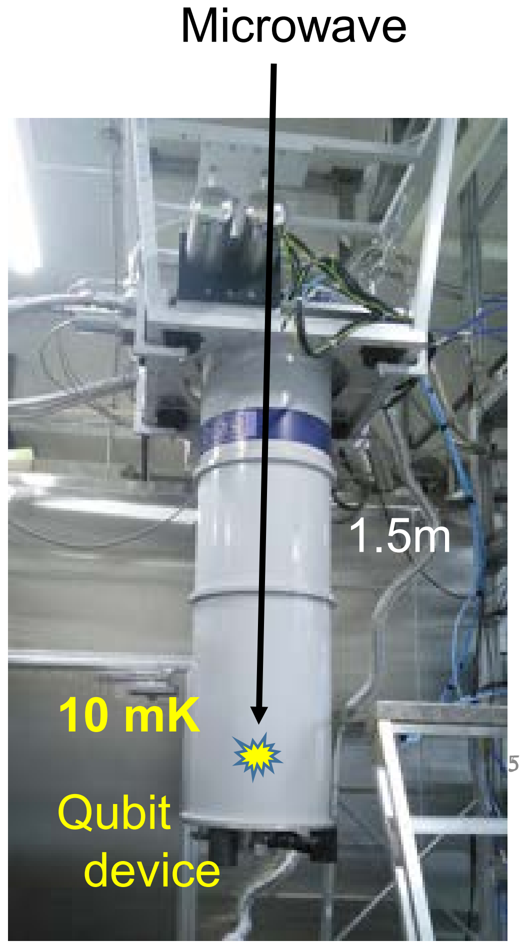

Generation of Local AC Magnetic Field

Ampère's circuital law

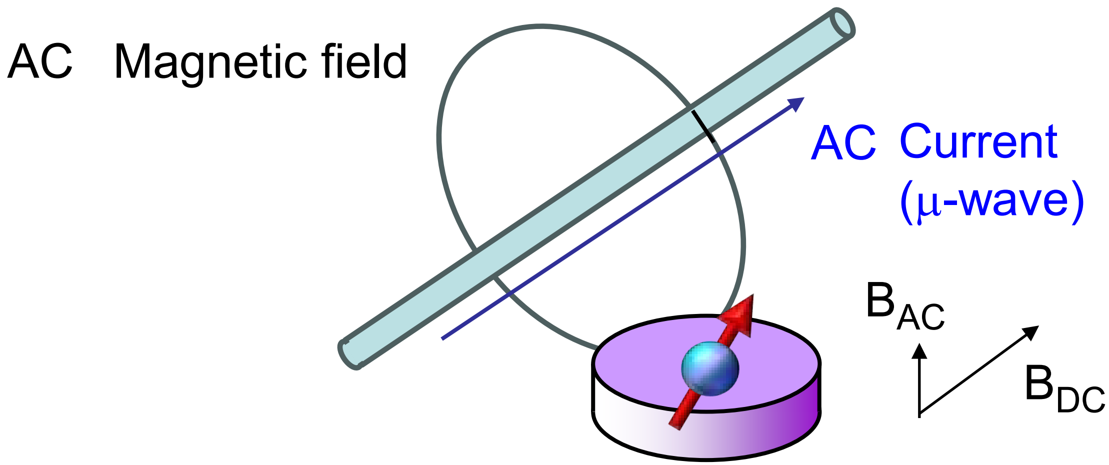

But the generated AC field is weak and the qubit rotation is slow.

Spin Resonance with Spin-electric Coupling

UNSW

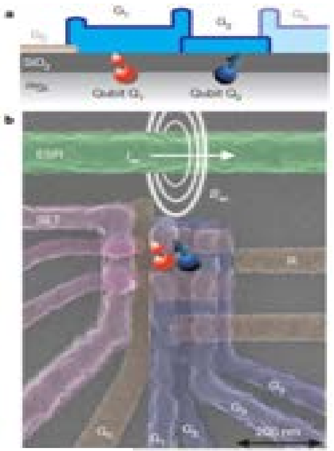

0.3 MHz

RIKEN, Wisconsin/TuDelft, Princeton, Sherbrook

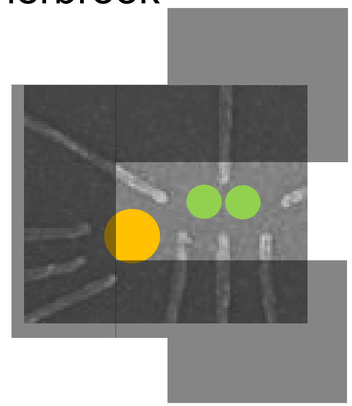

Grenoble/Leti

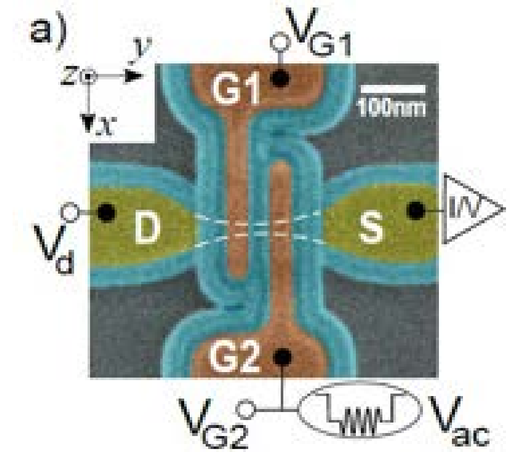

On-chip coil

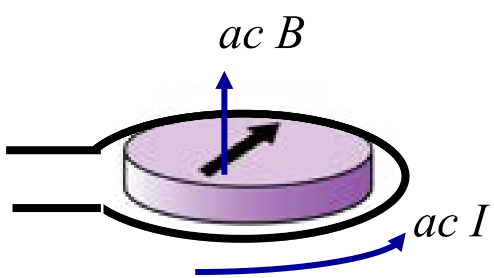

μ-magnet

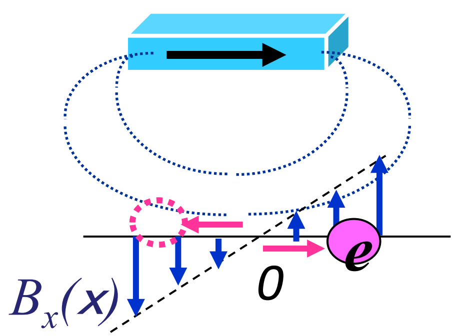

Spin-orbit int.

$B_{loc}=(Exp)\sigma$

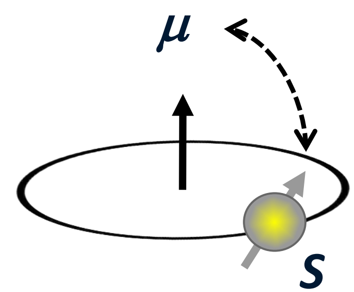

Spin Qubits in Si QD Devices

n-MOS with μ-wave antenna

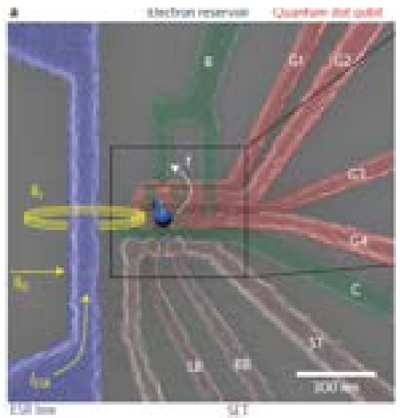

M. Veldhorst et al. Nat. Nanotechnol. 2014

Si/SiGe with μ-magnet

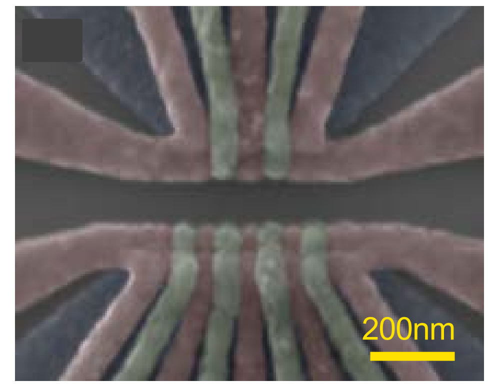

K. Takeda et al. Nat. Nanotechnol. 2021

P donors in Si with μ-wave antenna

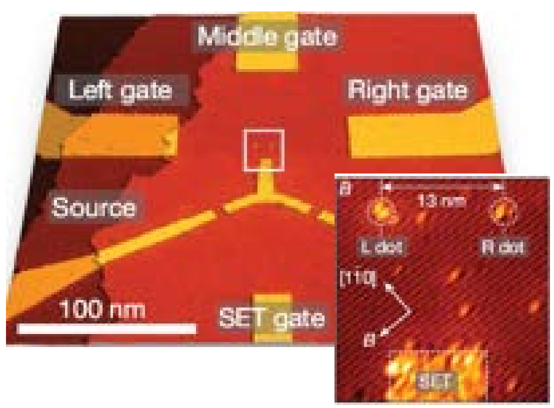

Y. He et al. Nature 2019

p-MOS with spin-orbit effect

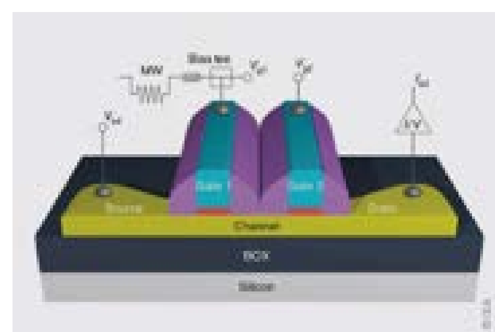

R, Maurand et a. Nat. Commun. 2016

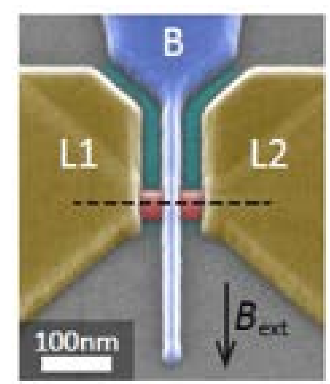

LC. Camenzind et al. Nat. Electron. 2020

Rotation about x-axis

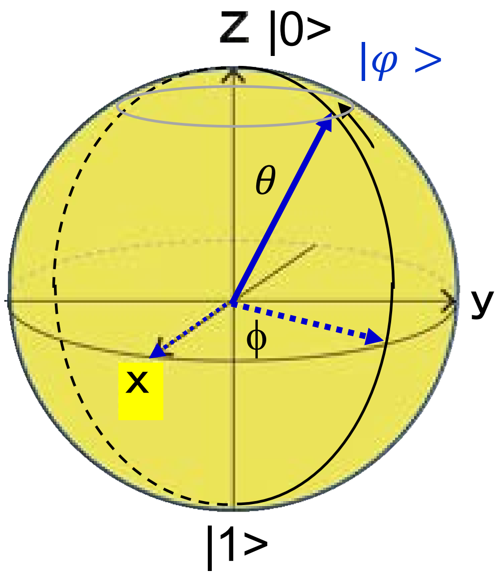

$$|\varphi>= cos\frac{\theta}{2}\ |0>+e^{i\emptyset}sin\frac{\theta}{2}\ |1>$$

$$\theta = \frac{\omega_1 t}{2}$$

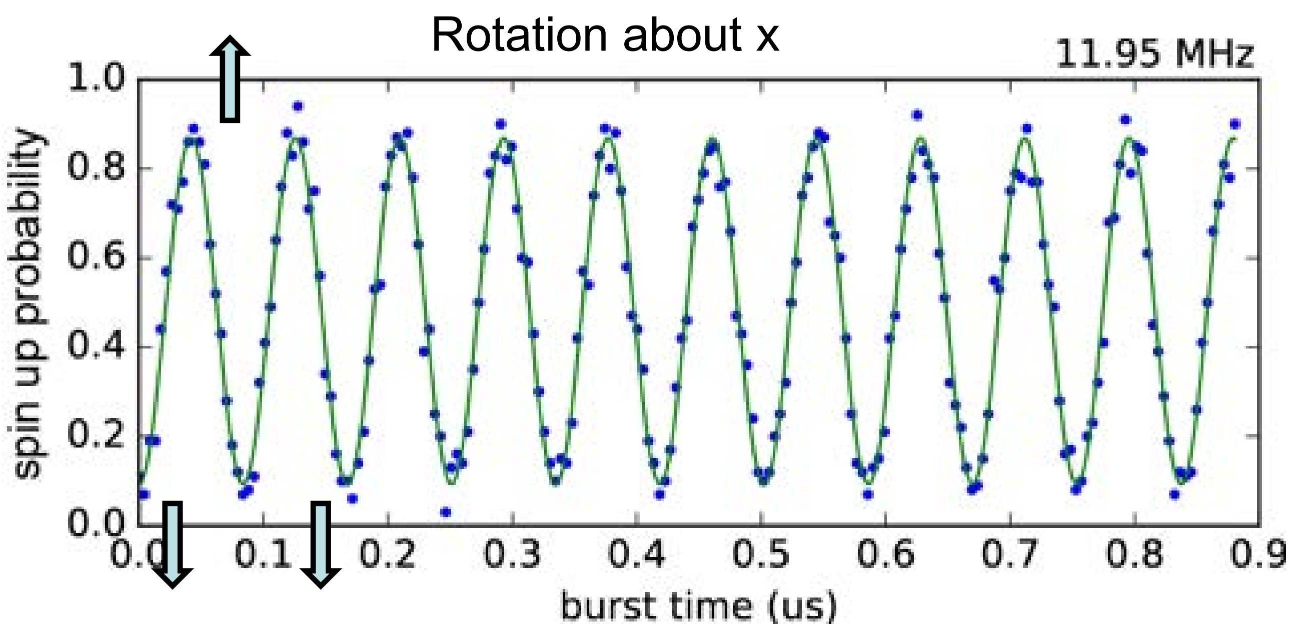

Measurement of Superposition State

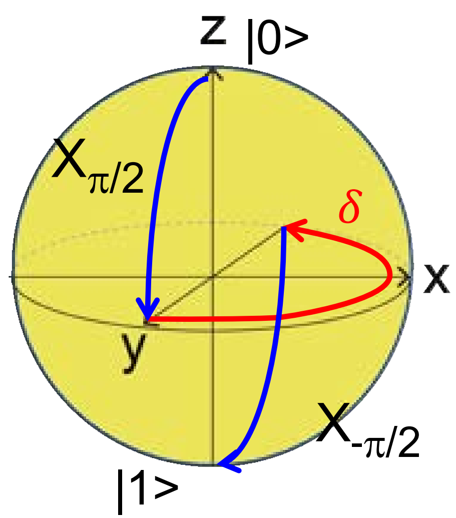

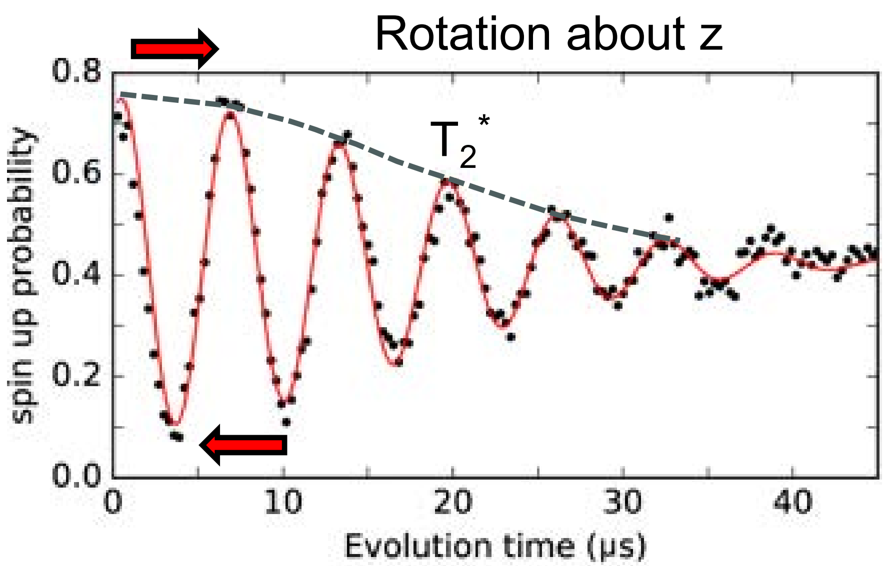

$$A cos(2\pi f t + \varphi)\exp(-(\frac{t}{T_2^*})^2) + B$$

Spin Echo Measurement

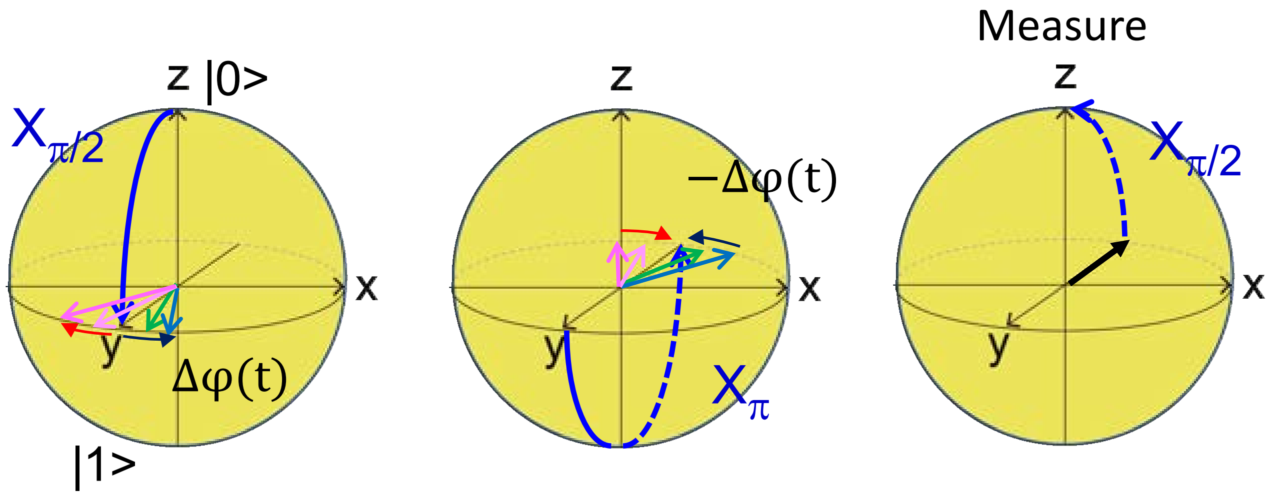

Free evolution In x-y with τ_1

Refocus in $\tau_2=\tau_1$ after π-pulse

Measure after τ_2

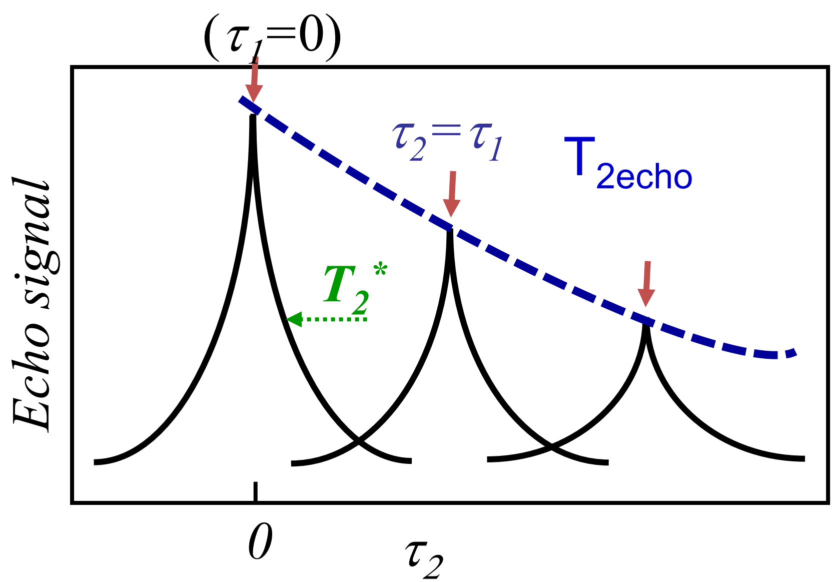

Only good for the phase fluctuation frequency lower than the focusing frequency.

Compensation of the faster phase fluctuations.

Hahn echo and CPMG

CP-Meiboom-Gill (CPMG) decoupling

$$X/2\text{-}(\tau\text{-}Y\text{-}\tau)_n\text{-}X/2$$

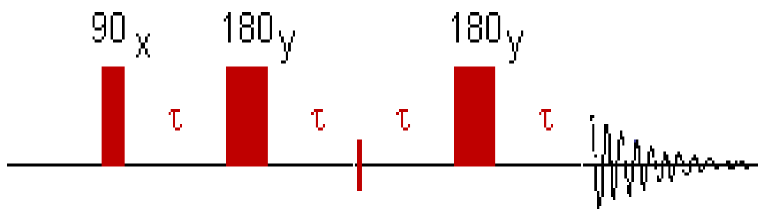

n = 512 number of π pulses

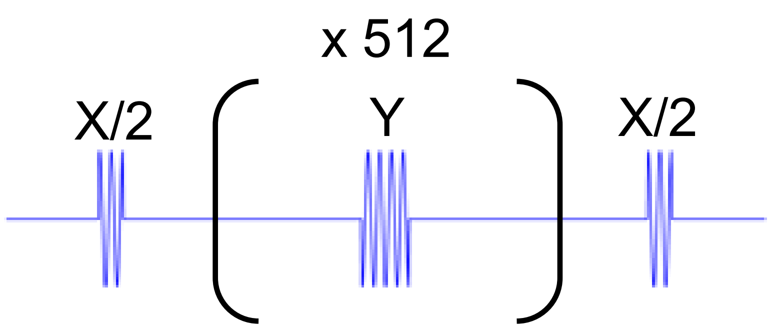

$$T_2^{CPMG} = 2.4 \text{ ms}$$

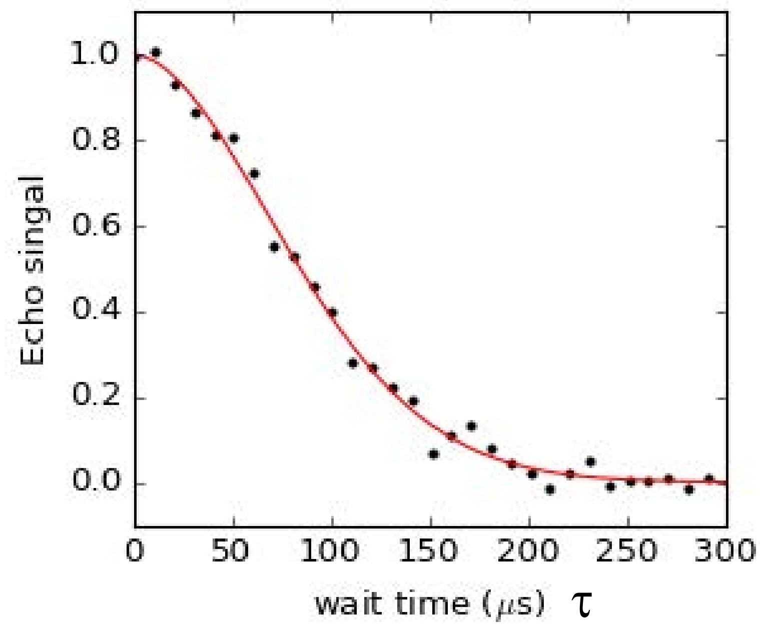

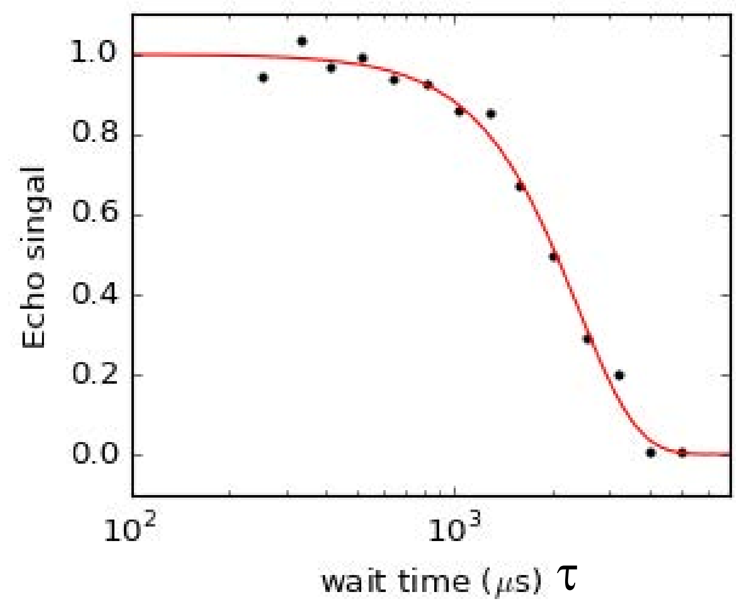

Hahn Echo and CPMG

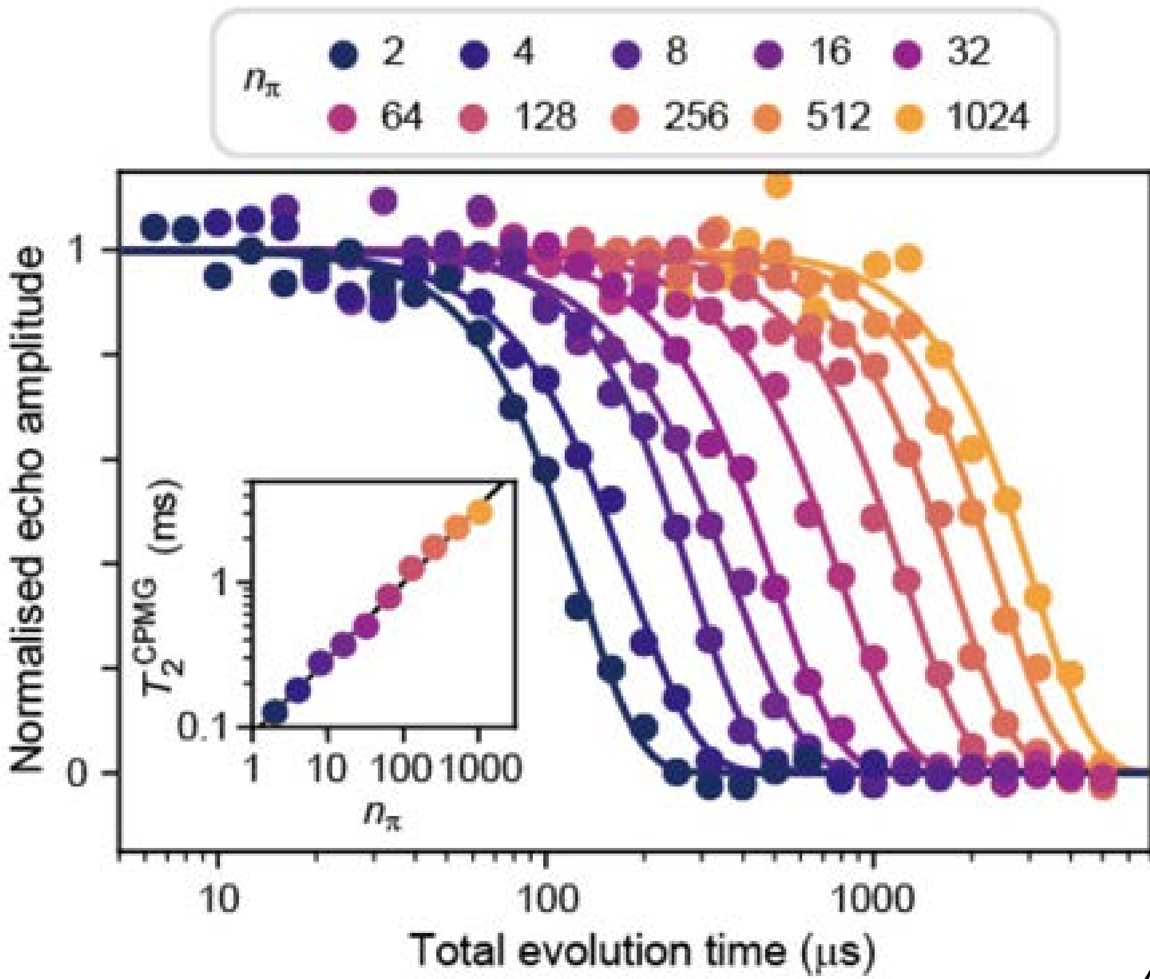

n_π=1: Hahn echo

T_2^{echo} =100 μsec

n_π>1: power-law

$T_2^{echo} \propto n_\pi^{0.526}$

\> msec

Ref.
Medford et al. PRL 2012

$$A\exp(-(\frac{t_{wait}}{T_2^{CPMG}})^2) + B$$

J. Yoneda et al., Nat. Nanotechnol. 2018

High-fidelity Two-qubit Gates

Two-qubit gate using spin-exchange interaction and Zeeman energy difference

Exchange coupling controlled by tunnel coupling (up to 10MHz)

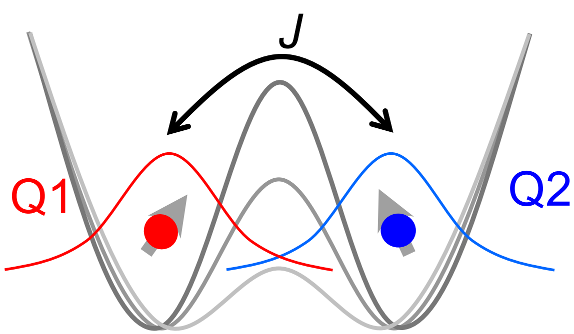

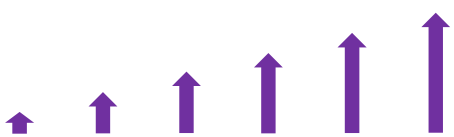

Zeeman energy gradient (ΔE_Z) induced by MM

ΔE_Z ~ a few 100 MHz

$\Delta E_Z \gg J$

"Heisenberg" *"Ising"*

$$H_{\mathrm{int}} = \frac{J}{4}\boldsymbol{\sigma}_1 \cdot \boldsymbol{\sigma}_2 \approx \frac{J_{12}}{4}\sigma_{z1}\sigma_{z2}$$

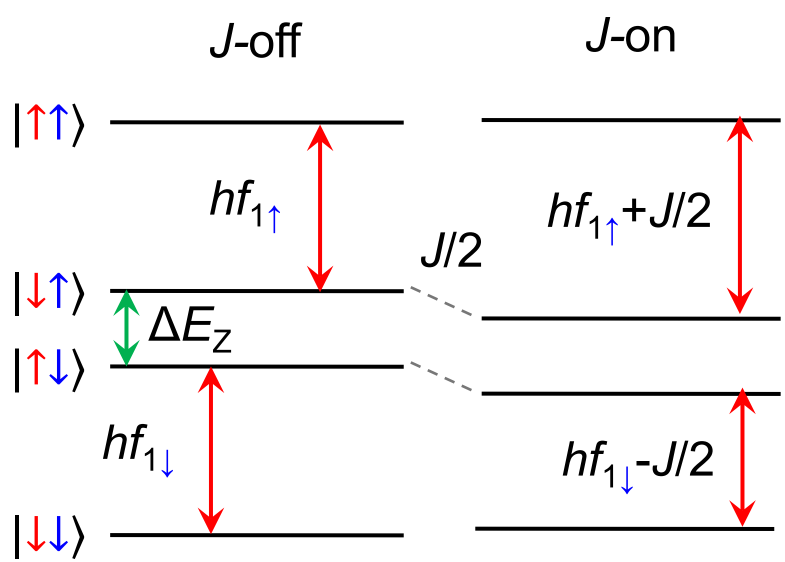

CPHSE (CZ)

Energy shift ΔE=J/2 for time t generates a phase accumulation in $|\uparrow\downarrow>$ and $|\downarrow\uparrow>$:

$$|\uparrow\downarrow> \rightarrow e^{\frac{i\Delta E t}{\hbar}}|\uparrow\downarrow>= i|\uparrow\downarrow> \text{ for } Jt= \frac{\pi}{\hbar}$$

In	Out
$\|\uparrow\uparrow\rangle$	$+\|\uparrow\uparrow\rangle$
$\|\uparrow\downarrow\rangle$	$i\|\uparrow\downarrow\rangle$
$\|\downarrow\uparrow\rangle$	$i\|\downarrow\uparrow\rangle$
$\|\downarrow\downarrow\rangle$	$+\|\downarrow\downarrow\rangle$

… represented by a unitary transformation:

$$U_{CZ}=\begin{pmatrix} 1 & 0 & 0 & 0 \\ 0 & 1 & 0 & 0 \\ 0 & 0 & 1 & 0 \\ 0 & 0 & 0 & -1 \end{pmatrix} = Z_1(-\frac{\pi}{2})Z_2(-\frac{\pi}{2})\begin{pmatrix} 1 & 0 & 0 & 0 \\ 0 & i & 0 & 0 \\ 0 & 0 & i & 0 \\ 0 & 0 & 0 & 1 \end{pmatrix}$$

Rotation about z-axis by $-\pi/2$

CPHSE (CZ)

Additional phase of
$\phi/2$ to the 1st bit

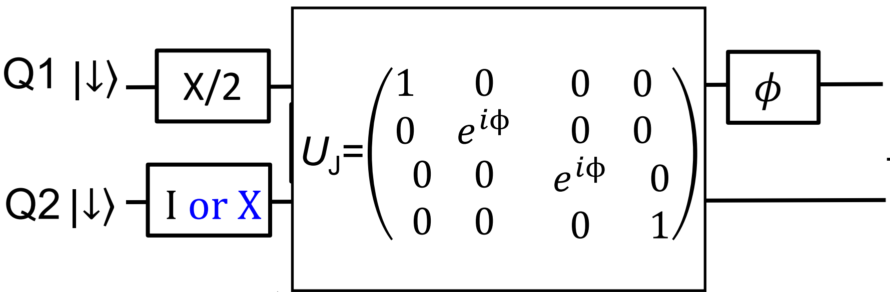

$\frac{|\downarrow> - ie^{i\phi}\,|\uparrow>}{\sqrt{2}}\,|\downarrow>$ or $\frac{e^{i\phi}\,(|\downarrow> - ie^{-i\phi}\,|\uparrow>)}{\sqrt{2}}\,|\uparrow>$

$\frac{|\downarrow> - i|\uparrow>}{\sqrt{2}}\,|\downarrow>$ or $\frac{|\downarrow> - i|\uparrow>}{\sqrt{2}}\,|\uparrow>$

Conditional phase accumulation
depending on Q2, ↑ or ↓

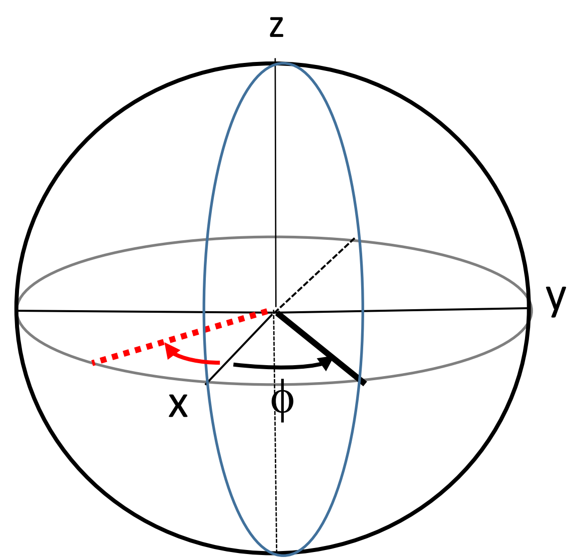

If Q2 is |↑>, clockwise rotation of Q1 about z-axis or positive phase ϕ accumulation, while
if Q2 is |↓>, counterclockwise rotation of Q1 or negative phase ϕ accumulation.

CPHASE is the case for $\phi = \pi/2$.

CPHASE

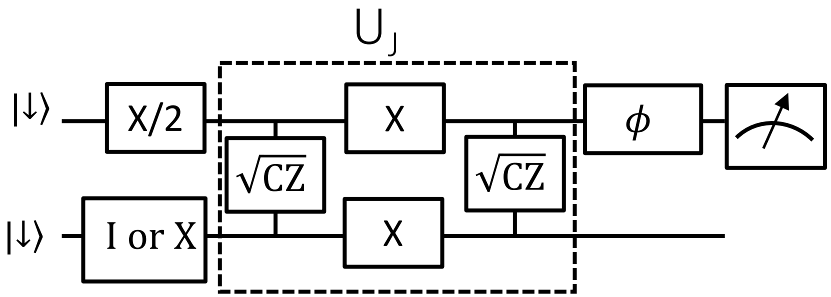

Q2 phase accumulation measurement

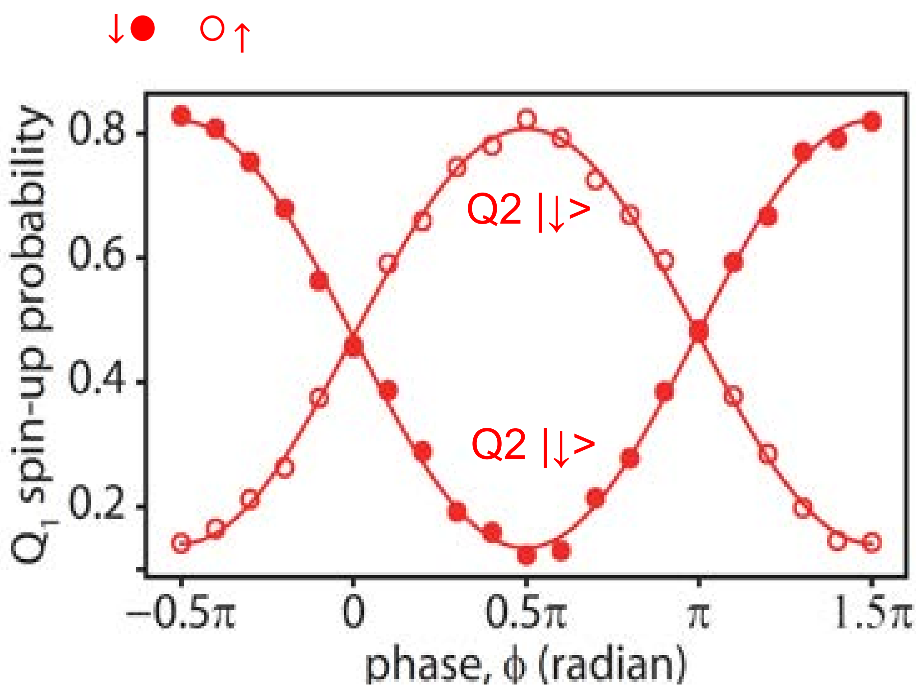

CNOT

$$U_{CNOT12} = (I_1 \otimes U_{\mathrm{Hadamard2}}) U_{CPhase} (I_1 \otimes U_{\mathrm{Hadamard2}})$$

$$U_H = \frac{1}{\sqrt{2}} \begin{pmatrix} 1 & 1 \\ 1 & -1 \end{pmatrix}$$

$$U_{CNOT12} = \begin{pmatrix} 1 & 0 & 0 & 0 \\ 0 & 1 & 0 & 0 \\ 0 & 0 & 0 & 1 \\ 0 & 0 & 1 & 0 \end{pmatrix}$$

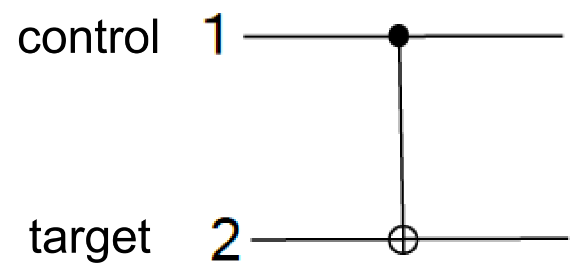

$U_{CNOT}|00> = |00>$

$|01> = |01>$

$|10> = |11>$

$|11> = |10>$

The second spin only flips when the first spin is in the up-state (|1>).

Part I Basics of semiconductor QC

- Concepts of quantum bits and computation
- Implementation of single and two qubit gates
- Readout and initialization
- Quantum coherence and phase noise

Part II Advances in semiconductor QC

- Features of quantum computing in silicon
- High-fidelity quantum gates and readout
- Quantum error correction
- Multi-qubit devices for scale-up

Spin Readout

Information conversion from spin to charge

Spin-dependent dot to lead tunneling

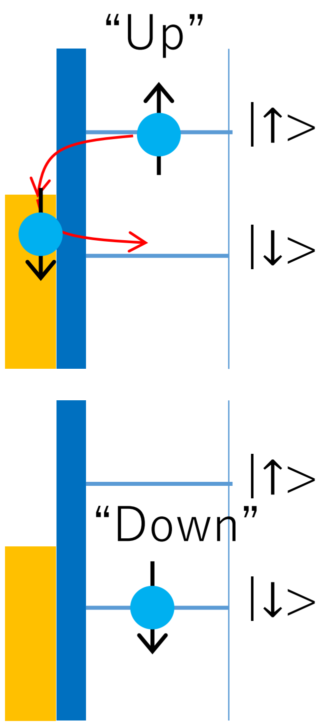

Zeeman split states

N=1 to 0 to 1

N=1

J. Elzerman et al. Nature 2004

Pauli spin blockade between dots

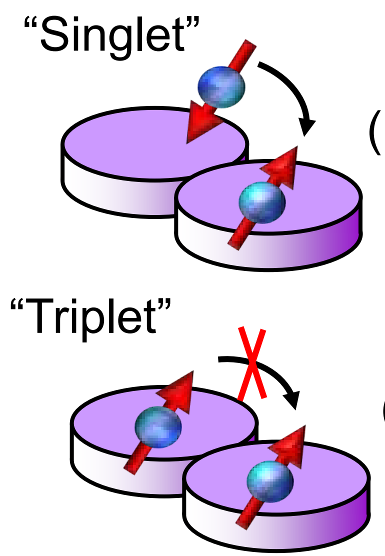

(N, M)=(1,1) to (0, 2)

(N, M)=(1,1)

K. Ono et al. Science 2002

Charge State Detection

Measurement of conductance change with N

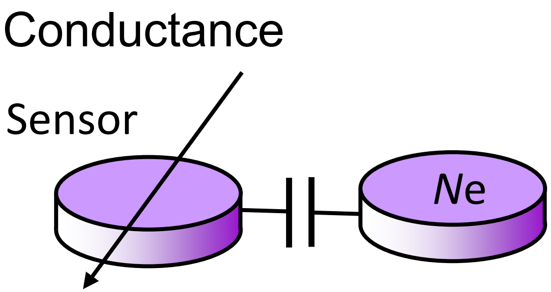

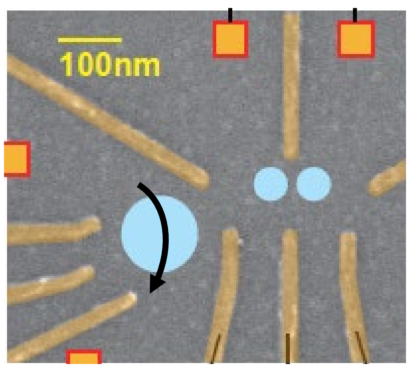

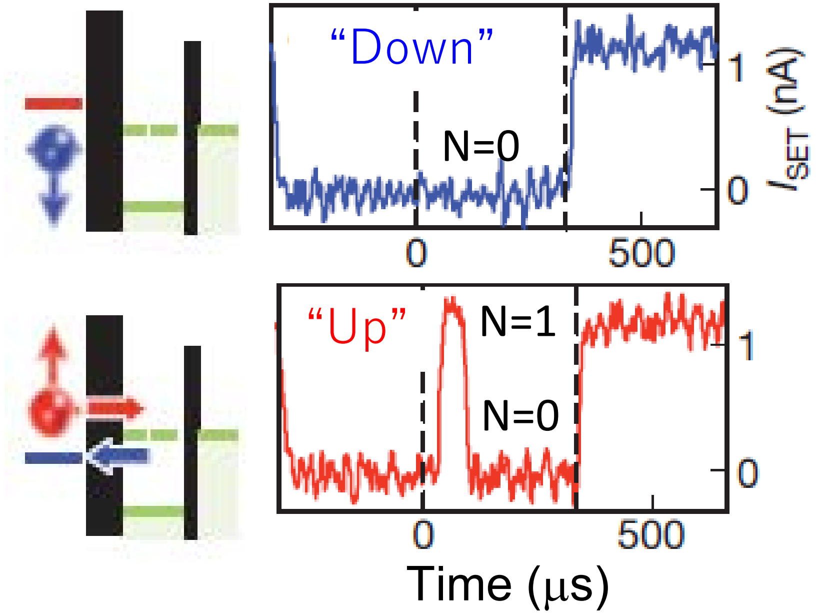

A. Morello et al., Nature 2010

Advanced Method of Charge Sensing

conductance measurement
with RF reflectometry

Resonance circuit

QD sensor

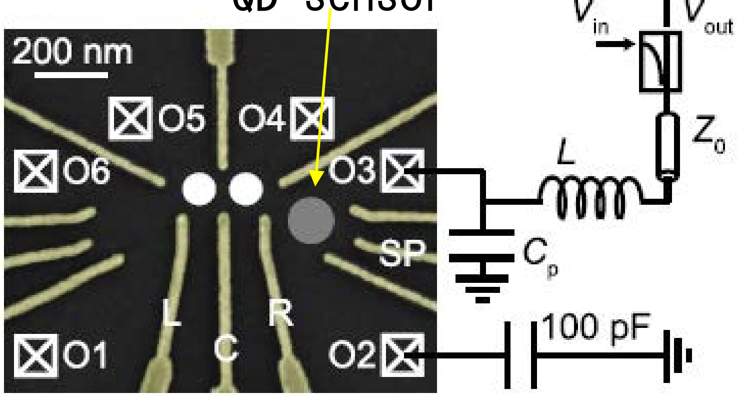

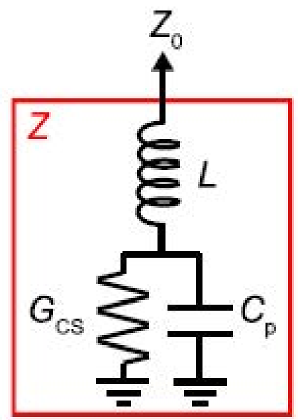

Change of charge
number in objective QD

⬇

Change of sensor QD
conductance, G_{CS}

⬇

Change of resonance
characteristic

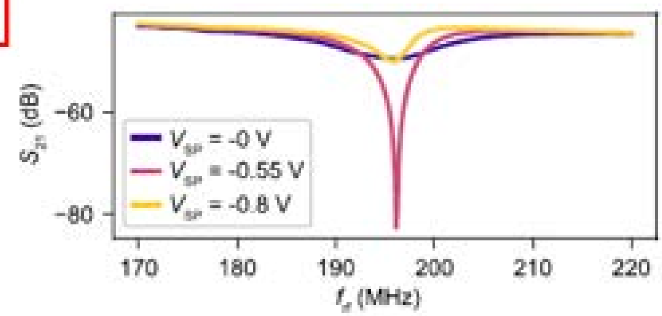

D. Reilley et al.
Appl. Phys. Lett.
(2007)

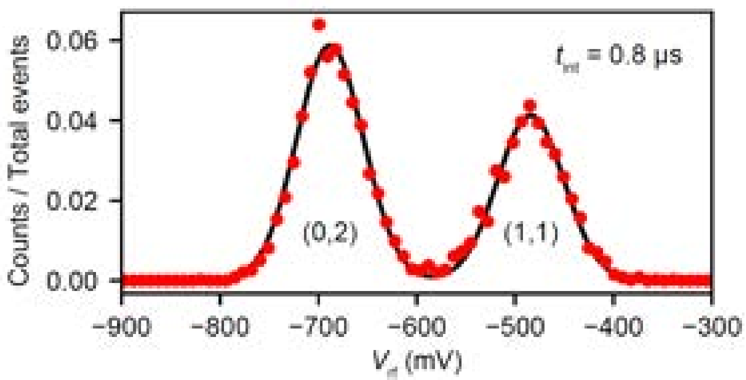

SNR = 6 (F>99%) @0.8 μs (SiGe)
<< T1 (10 to 100msec)

A. Noiri et al., Nano Lett. (2020).

Initialization

Final state after spin readout is |0> = Initialization

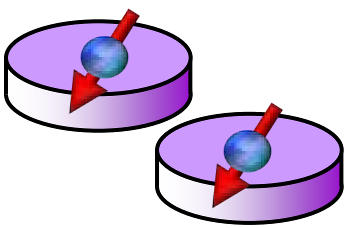

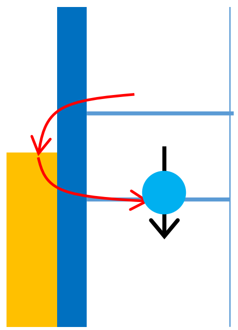

Long-time waiting (>> T1) provides |0>.

Application of Entanglement I: Quantum Non-demolition Readout using an Ancillary Qubit

… useful to improve the readout and initialization fidelity

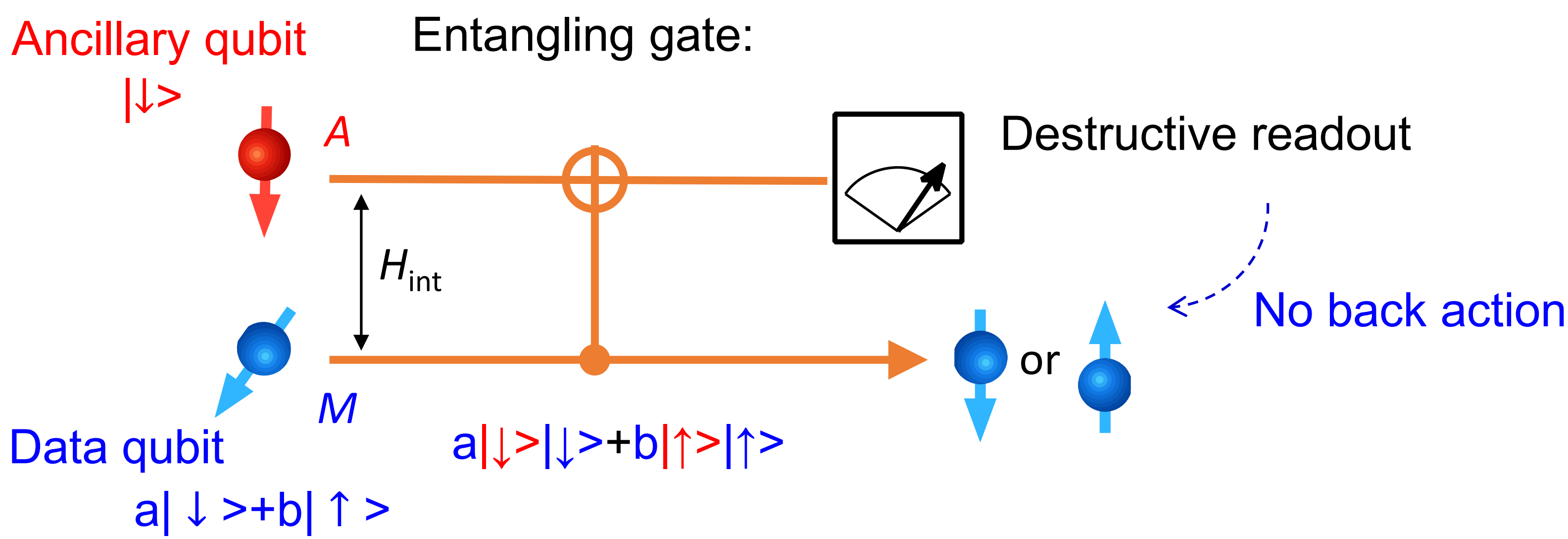

Previous work Quantum optics: Grangier et al. Nature 1998; Nougues et al. Nature 1999.
Cavity QED with Rydberg atoms: Geremia et al. Science 2004
Trapped single electrons: Peil et al. PRL 1999
Superconducting circuits: Lupascu et al. Science 2007
Nuclear spin with donor P: Pla et al. Nature 2013

QND Measurement with Si/SiGe DQD

J. Yoneda et al. Nat. Commun. 2020

Rabi measurement
after a waiting time

$H_{\text{int}} = \frac{J_{12}}{4}\sigma_{zL}\sigma_{zR}$
for $E_Z \gg J_{12}$

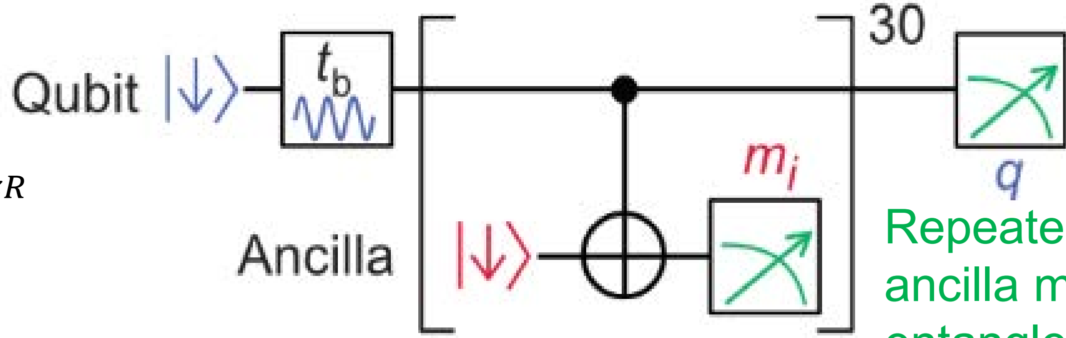

Repeated cycle (60 μs):
ancilla measured after
entangled with data

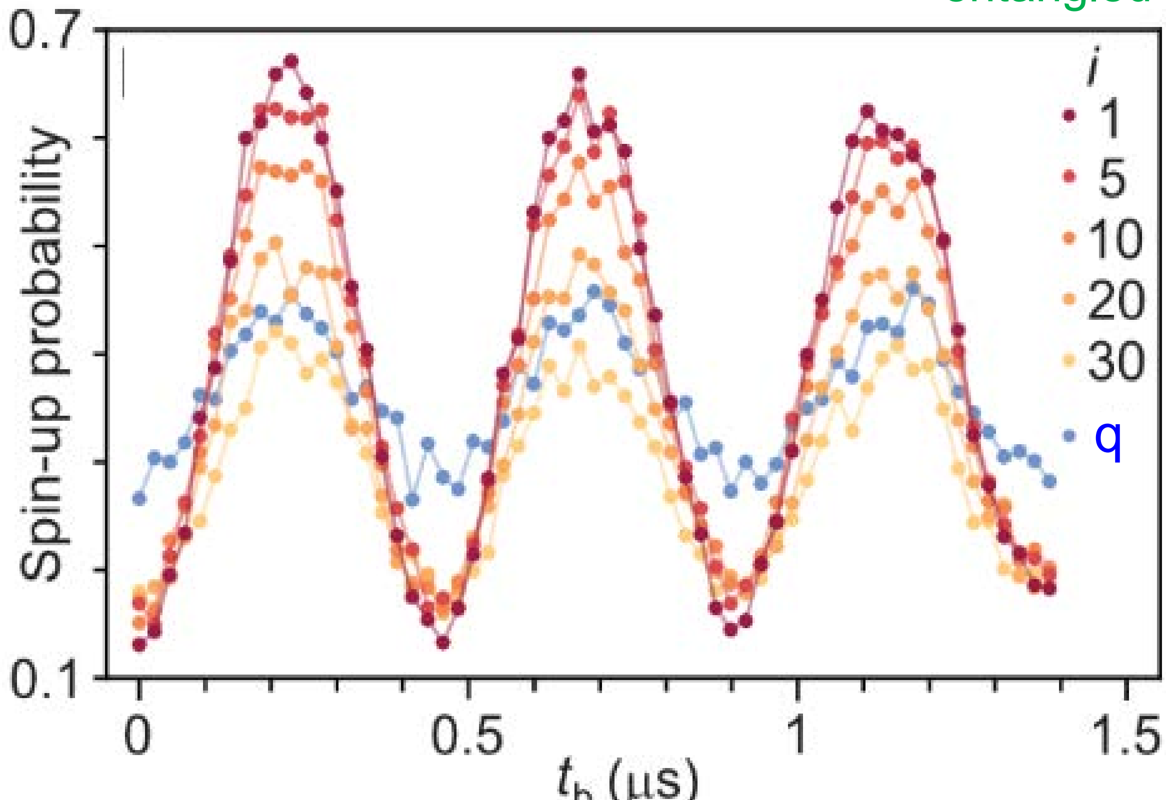

Ancilla

Data

Improved Readout and Initialization Fidelity by QND Measurement

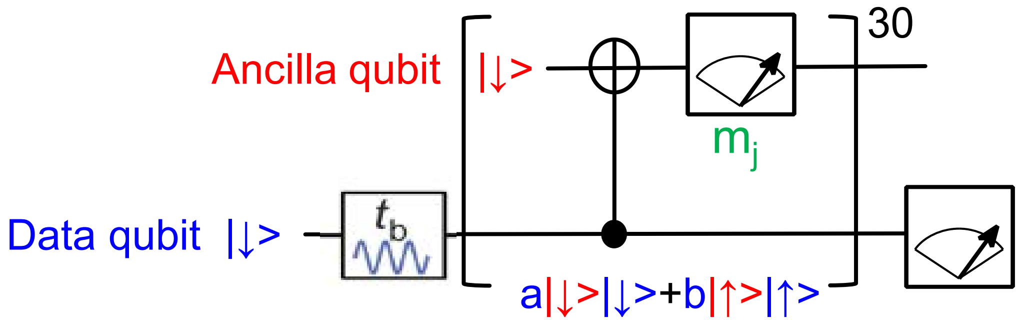

T. Nakajima et al. Nature Nanotechnol. 2019; J. Yoneda et al. Nature Commun. 2020

Accumulation of repeated QND ancilla measurements

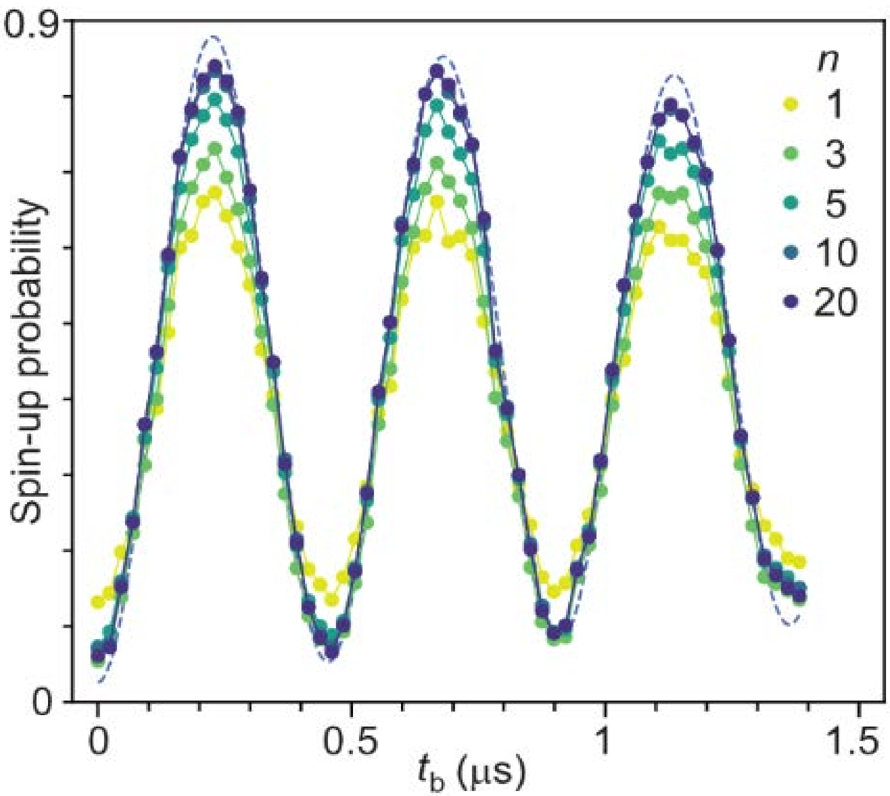

Measurement fidelity :

By repeated QND measurement

$F_M^{\downarrow(\uparrow)}$= 88 % for n=1 (60 μs << T1)

95.6% (94.6%) for *n* = 20

(1.2 msec << T1)

Measurement-based Initialization

T. Kobayashi et al. (2021)

Initialization of the data qubit to spin-down

a|↓>|↓>+b|↑>|↑>

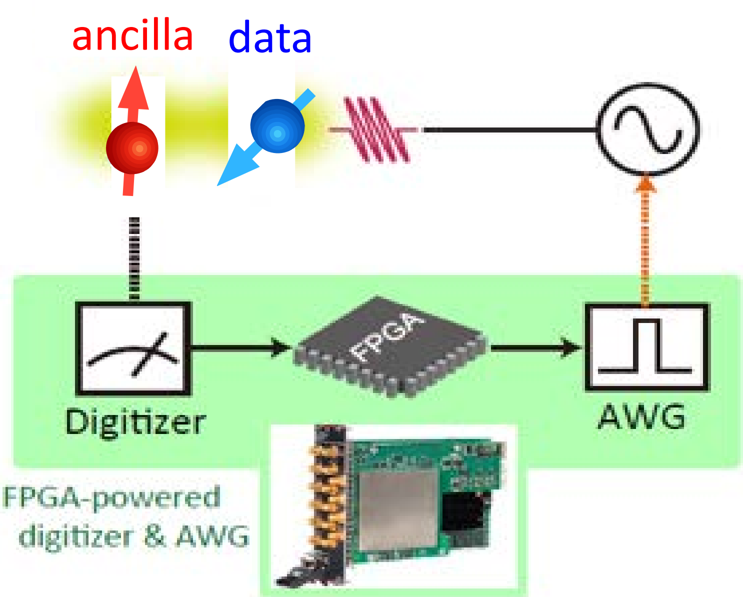

Initialization fidelity increased from 86 to 97%.

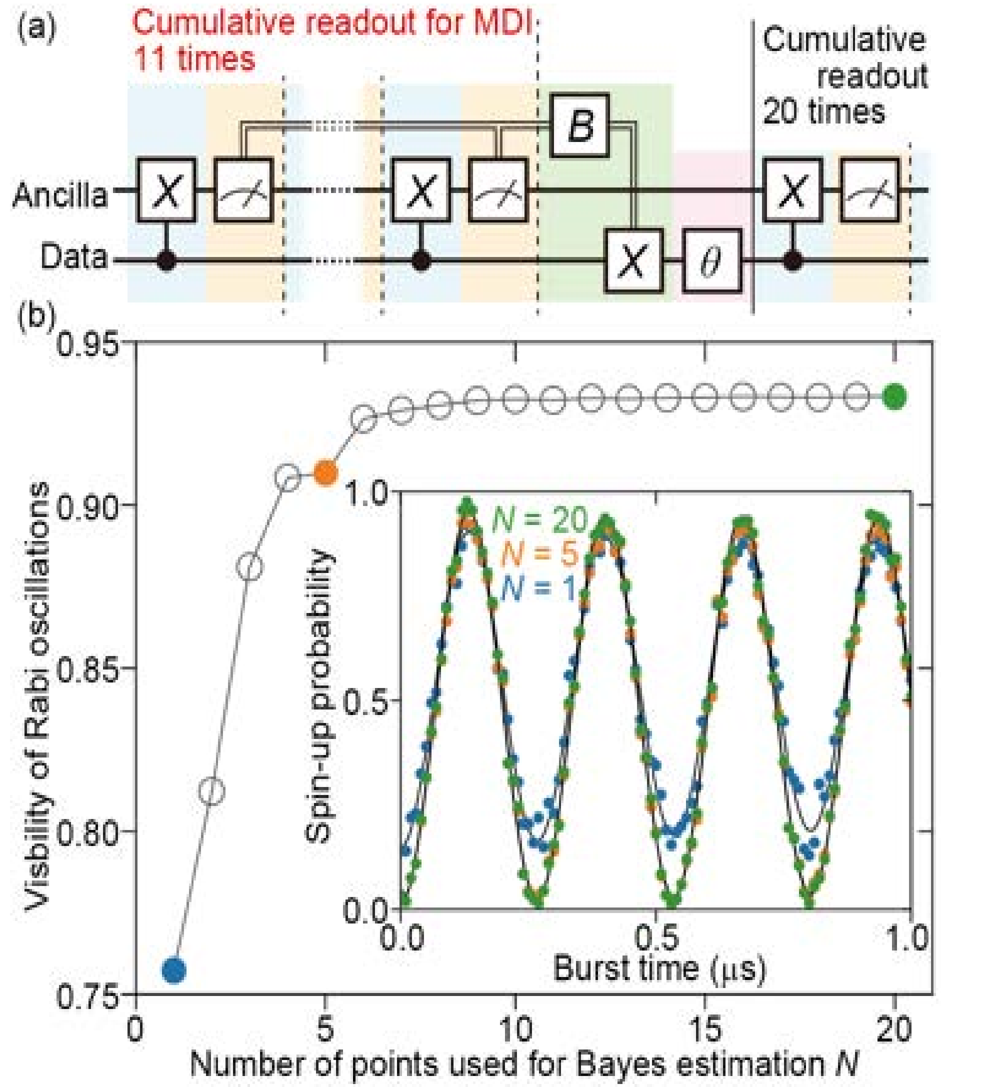

Part I Basics of semiconductor QC

- Concepts of quantum bits and computation
- Implementation of single and two qubit gates
- Readout and initialization
- Quantum coherence and phase noise

Part II Advances in semiconductor QC

- Features of quantum computing in silicon
- High-fidelity quantum gates and readout
- Quantum error correction
- Multi-qubit devices for scale-up

Dephasing time T_2^*, Hahn-echo time T_2^H, CPMG time T_2^C and Rabi decay time T_2^R

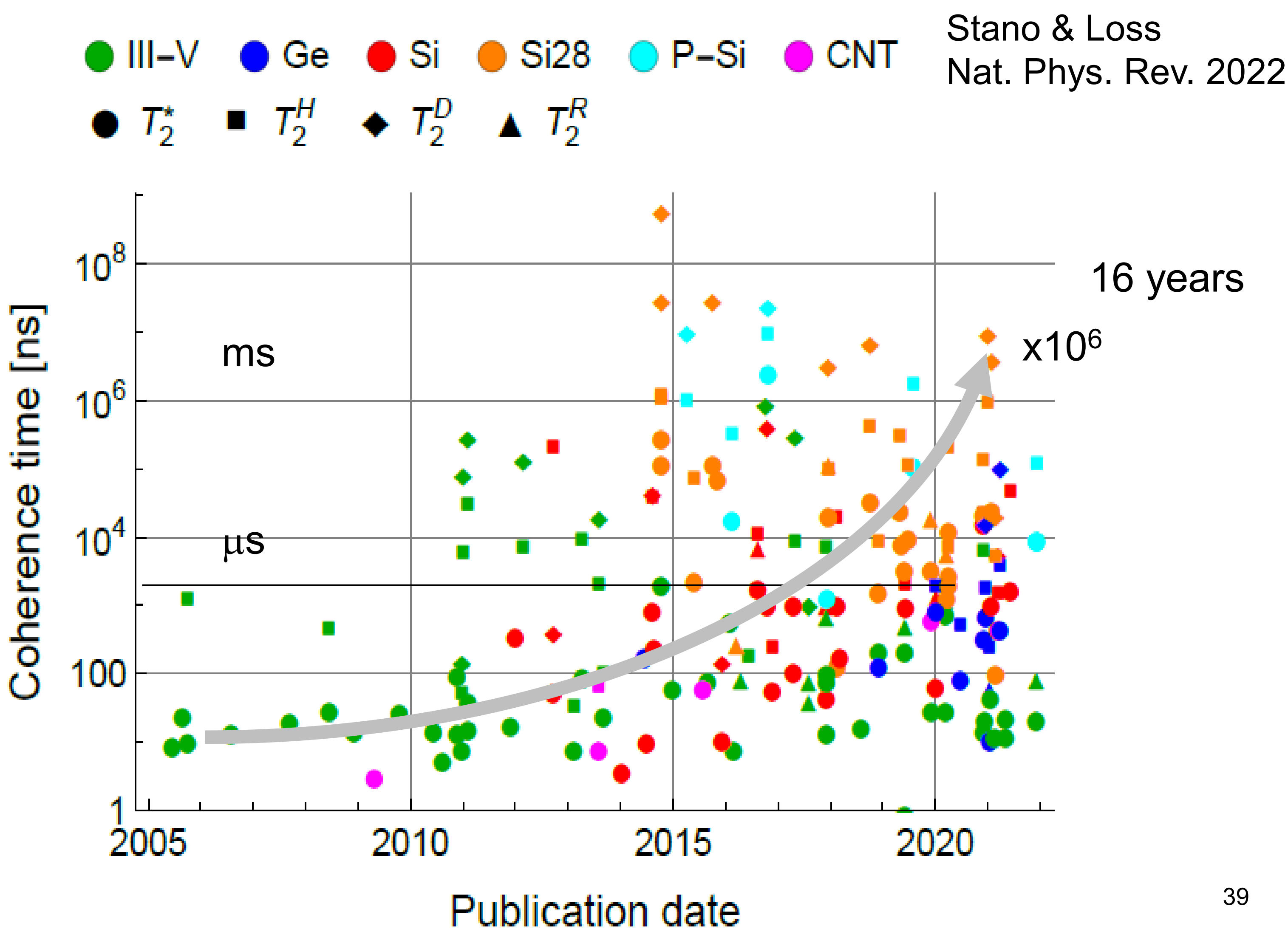

Dephasing and Depolarization of Spin

Larmor precession about $\boldsymbol{B}_{\mathrm{DC}}$
: Coherent state

$$|\varphi >= a|0 > +be^{i\omega_L t}|1 >$$

$$\omega_L = g\mu_B B_{DC}/\mathrm{h}$$

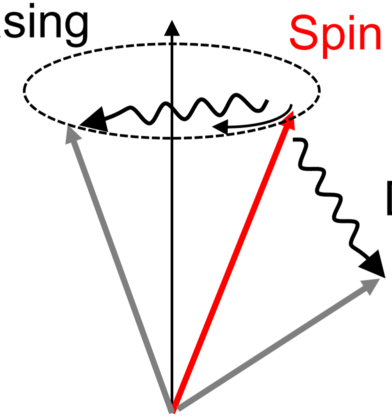

Dephasing T_2^* due to magnetic noise

$$\longrightarrow \quad |a|^2|0 >< 0| + |b|^2|1 >< 1|$$

$$T_2^* = \frac{1}{\pi\sqrt{2 < \delta\omega^2 >}}$$

Measure $\delta\omega_L = \frac{g\mu_B}{h}\delta B$

Depolarization T_1
due to phonon+spin orbit interaction

$$\longrightarrow \quad (1-p)|0 >< 0| + p|1 >< 1|$$

Measure polarization p $= e^{-\frac{t}{T1}}$

Charge Noise and Nuclear Spin Noise in GaAs and Si

1) Ensembles of nuclear spins cause statistical fluctuations of B field

2) Two-level fluctuators (impurities, defects,..) cause fluctuation of electron position. This causes fluctuation of electron Zeeman energy in the presence of magnetic field inhomogeniety or spin-orbit interaction.

Nuclear spin noise $H_{\mathrm{HF}} = A|\psi(\mathrm{x})|^2\left(\frac{I_+S_- + I_-S_+}{2} + I_Z S_Z\right)$

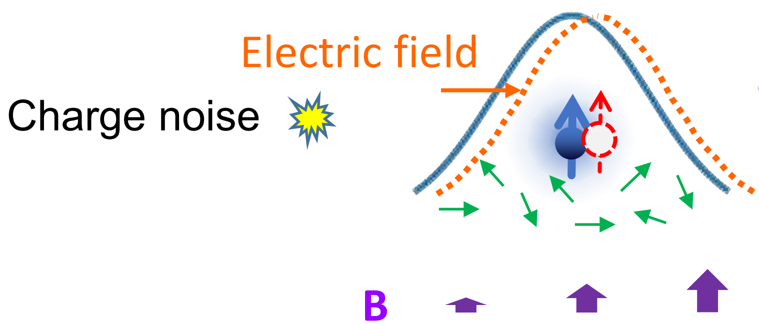

$$\delta B(t) = \delta B_{nuclear}(t) + \delta B_{charge}(t)$$

Phase Measurement of Spin

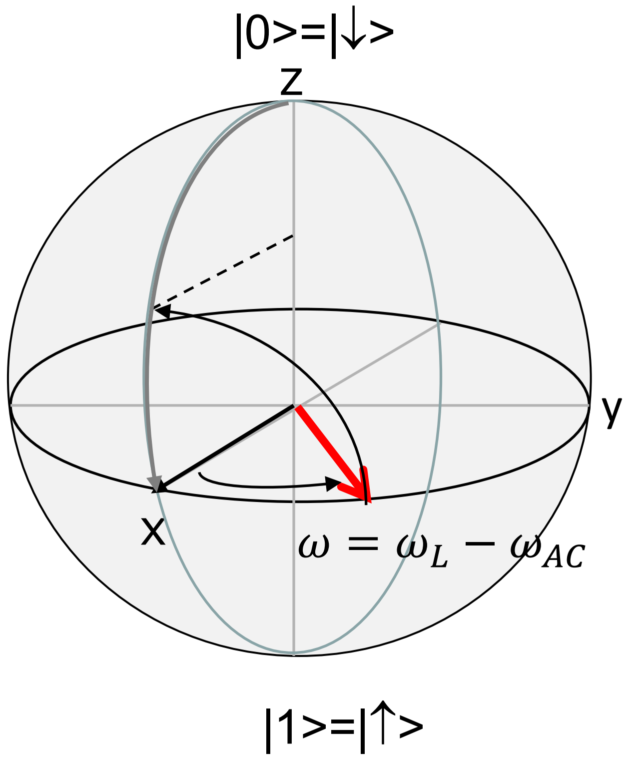

Prepare a state along x-axis : $\frac{|0>+|1>}{\sqrt{2}}$

Rotation about z-axis with detuning frequency $\omega = \omega_L - \omega_{AC}$ (<< ω_L)

$$|\varphi>= \frac{|0> + e^{i\omega t}|1>}{\sqrt{2}}$$

Rotating frame about z with ω_{AC}

After π/2 rotation about x-axis

Probability of finding the state in | ↓ >

$= \frac{1+sin\omega t}{2}$

Measure ω(t) for z-axis rotation within T2*

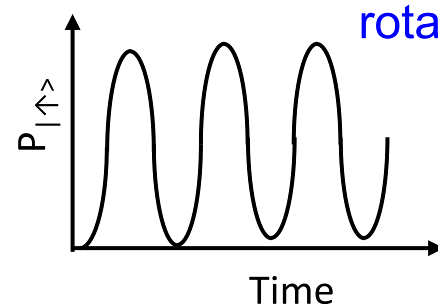

$\longrightarrow \delta\omega_L$(t)

Ramsey Measurement to Evaluate the Fluctuating B_{Zeeman}

GaAs: 10^5 to 10^6 n-spins

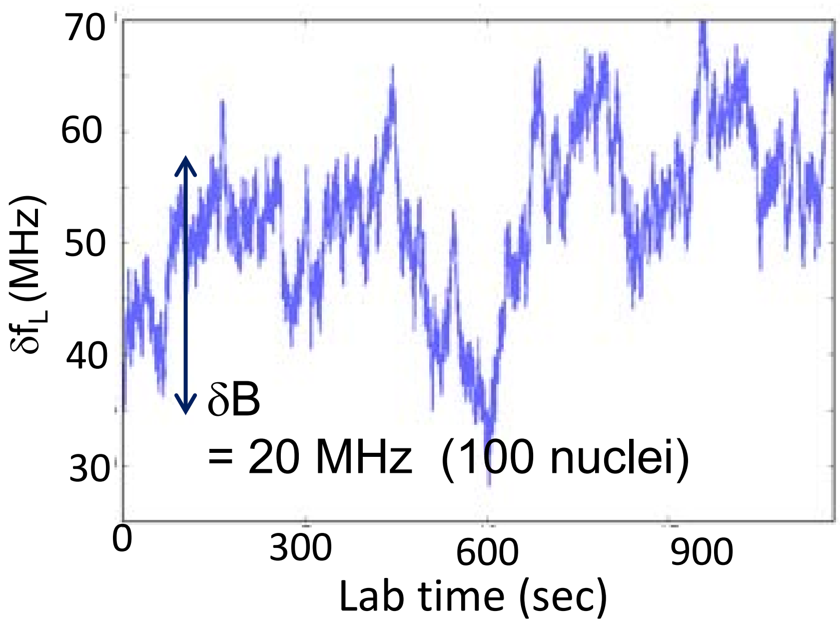

^{28}Si (0.08% ^{29}Si): 10 to 10^2 n-spins

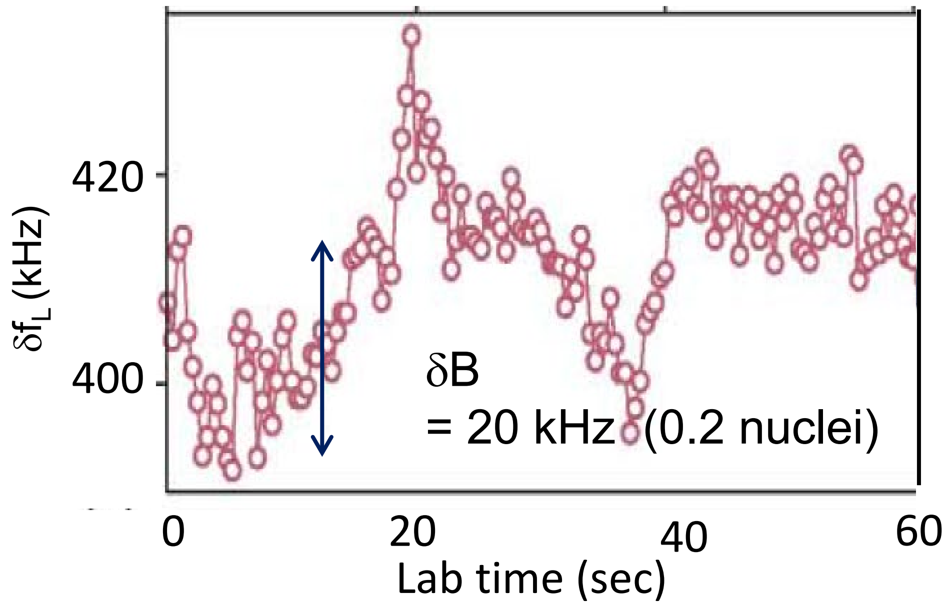

$\delta B_{1nuc} = \frac{A(GaAs)}{\sqrt{N}}$
= 20 MHz

$\delta B_{1nuc} = = \frac{A(29Si)}{\sqrt{N}}$
=0.1 MHz

Time resolution = 100 μs
(=1μsx100)

Dynamics of Nuclear Spin Fluctuation

Magnetic, Non-Markov, Non-ergodic, Diffusive,…

Variance of the correlator $C(\Delta t) = B_{\mathrm{N}}(t+\Delta t) - B_{\mathrm{N}}(t)$

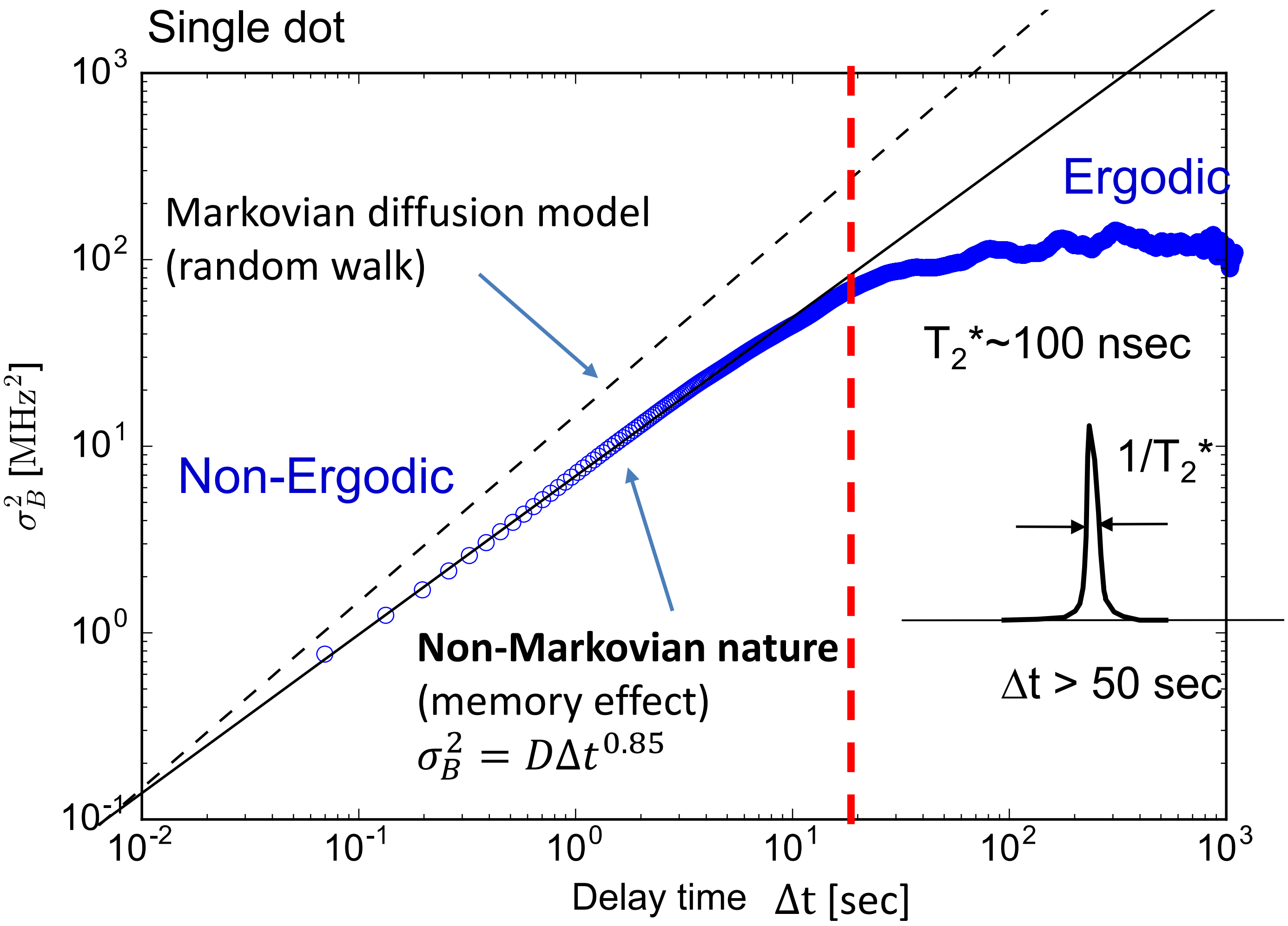

Reduced Dephasing of Single Spins by Fast Measurement

- Non-ergodic spin dynamics in the fluctuating environment is demonstrated
- Two-orders of magnitude improvement of the spin coherence with a feedback control is shown

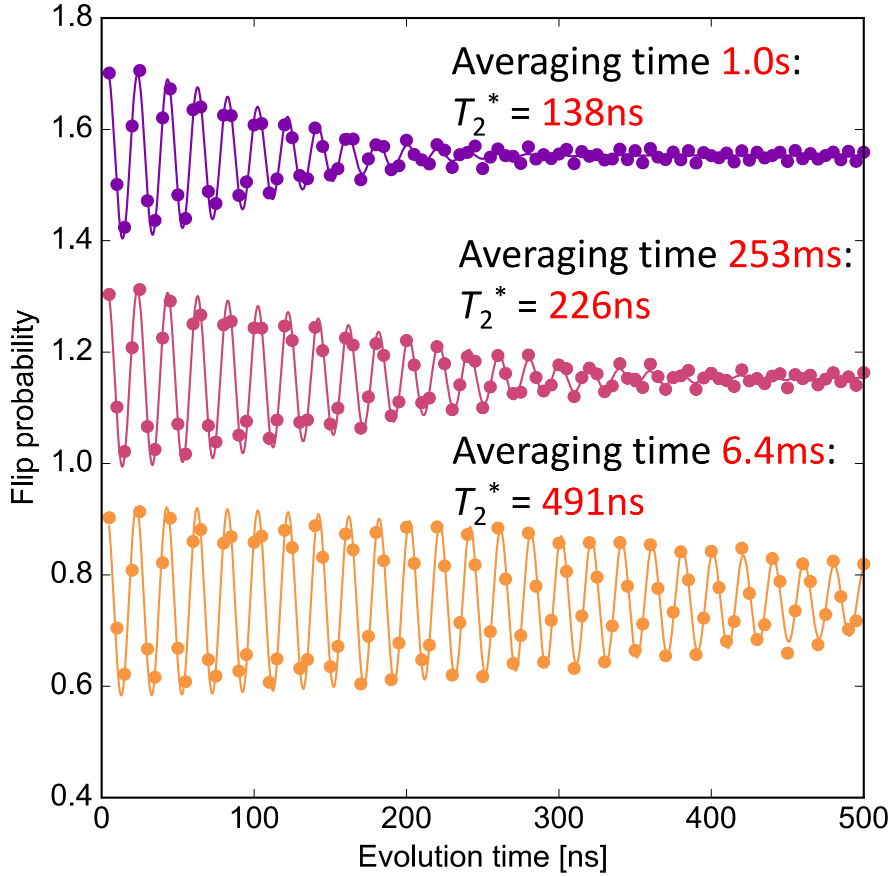

Real-time Feedback of Spin Noise Measurement to Control Spin Dynamics

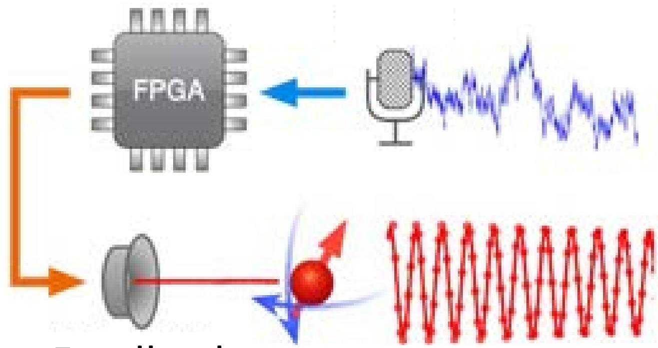

$T_M + T_{FB} < T1$ (> 10 msec), F > 99%

Tracking the magnetic field fluctuation by changing the MW frequency

M. Delbecq et al. Phys. Rev. Lett.

T. Nakajima et al. Phys. Rev. X 2019

Low-frequency fluctuation compensated

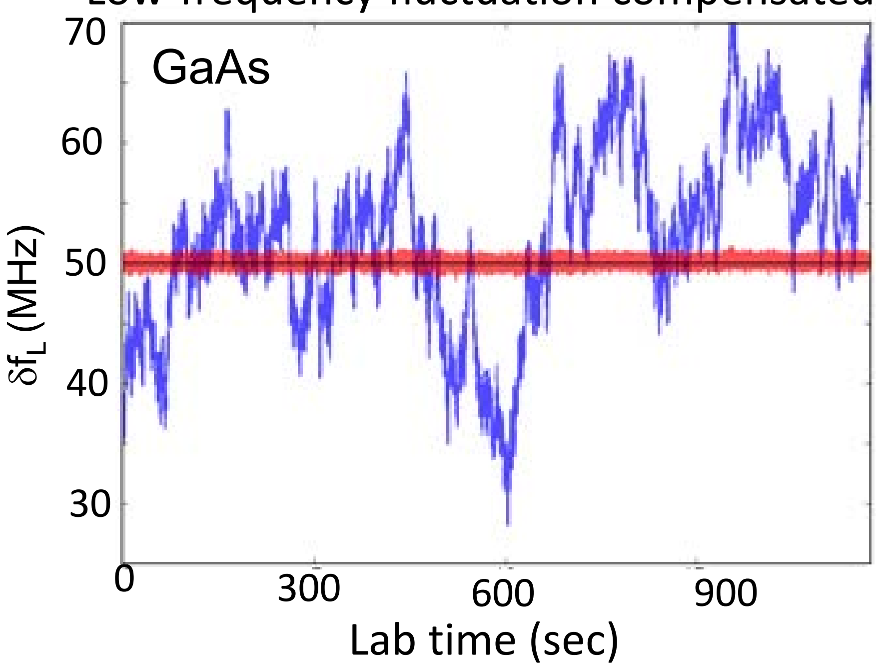

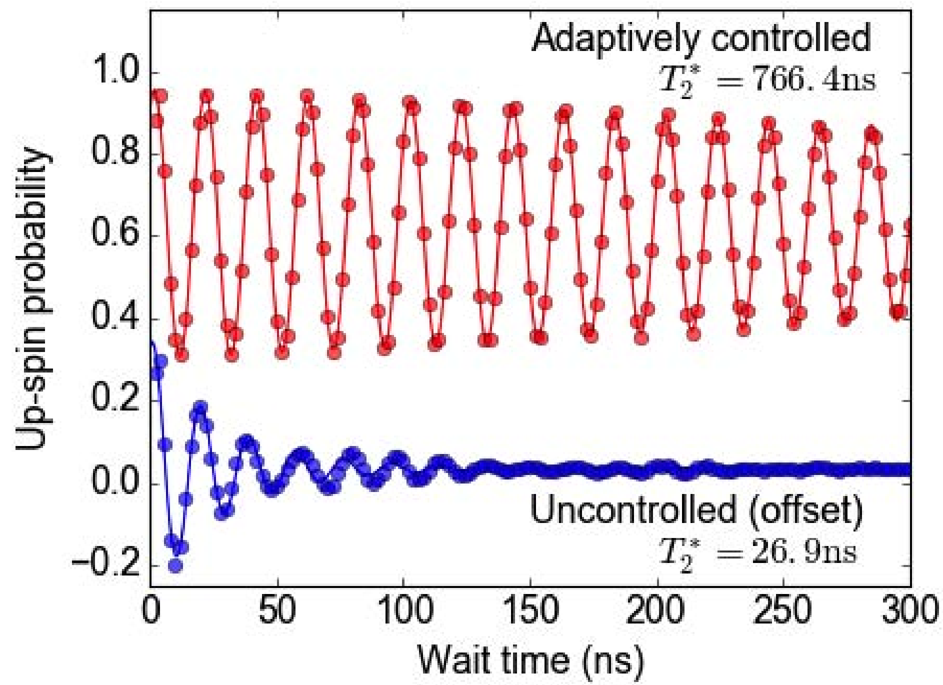

Nuclear Spins in GaAs, nat. Si and 28Si

	GaAs	Nat. Si	28Si
Nuclear spin	100%	4.7%	0.08%
T2*	10 nsec	1.5 μsec	10 μsec
Noise source	nuclear spin (>> charge noise)	nuclear spin (> charge noise)	charge noise (>> nuclear spin)

$$H_{\mathrm{HF}} = A\left|\psi(\mathrm{x})\right|^2\left(\frac{I_+S_- + I_-S_+}{2} + I_Z S_Z\right)$$

T1 > 10 to 1000 msec

Statistical fluctuation : $\delta A = A/\sqrt{N}$

Part I Basics of semiconductor QC

- Concepts of quantum bits and computation
- Implementation of single and two qubit gates
- Readout and initialization
- Quantum coherence and phase noise

Part II Advances in semiconductor QC

- Features of quantum computing in silicon
- High-fidelity quantum gates and readout
- Quantum error correction
- Multi-qubit devices for scale-up

Why Silicon?

^{28}Si

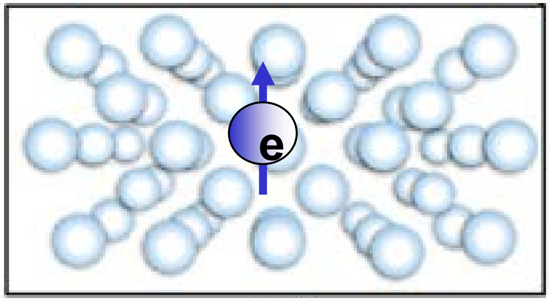

Long-intrinsic coherence time in isotopically purified ^{28}Si

Compatibility with CMOS based manufacturing techniques

Possible high-temperature operation at > 1 K
- A larger number of qubits
- On-chip integration with cryo-electronics

> 1K

< 0.1 K

Quantum processor

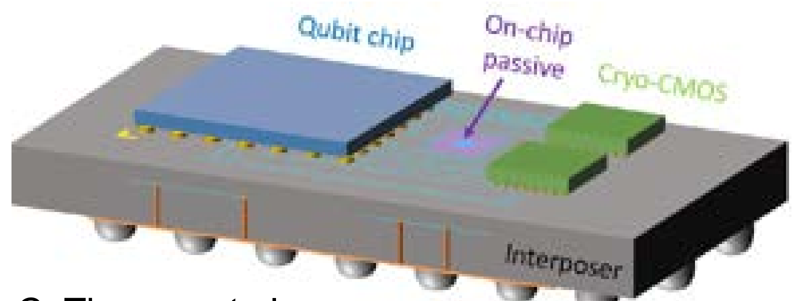

C. Thomas et al.
arXiv: 2022

49

Integration of Quantum Processors and Cryo-CMOS Controller

B. Patra et al. IEEE J. Solid-State Circuits, 33, 309 (2018)
E. Charbon et al., IEDM Tech. Dig., 5 (2016)
F. Sebastiano et al., Proc. 54th Annu. Des. Autom. Conf. (DAC) 13-1 (2017).

C. Thomas et al. arXiv: 2206.14082

Quantum processor vs classical control for control/readout

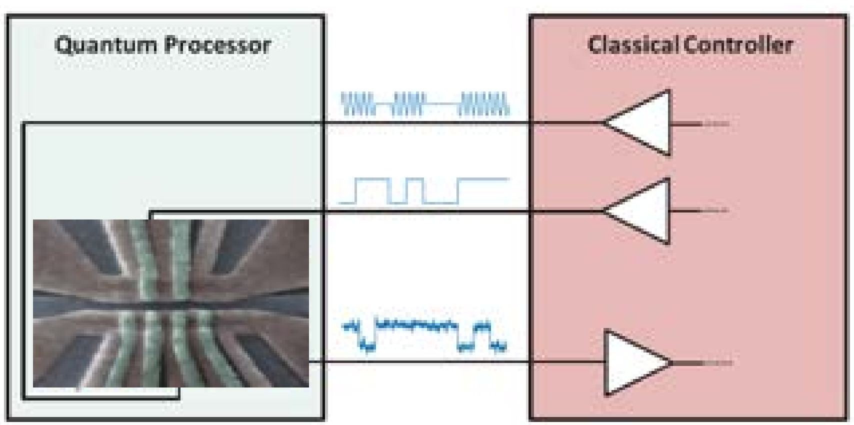

< 0.1 K

300K

X. Xue et al. Nature 2021

Block diagram of cryo-CMOS controller for the control and readout of qubits.

Integration

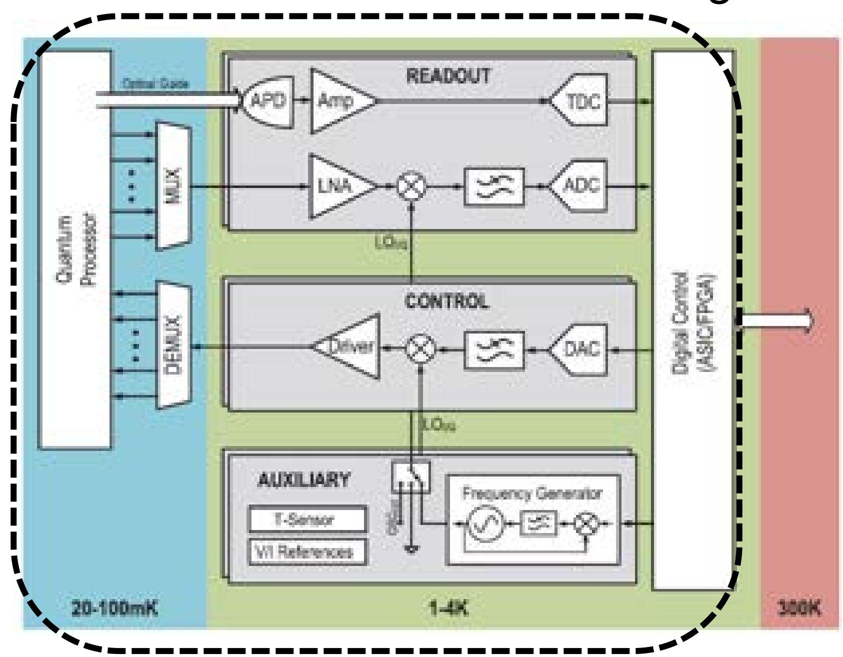

< 0.1 K | 1 to 4 K | 300K

Cooling power ~ mW | ~ W

Si Qubits at High Temperature > 1 K

High-temperature operation of a Si qubit

K. Ono et al. RIKEN
Sci. Rep. 2019

1.5 K to 10 K

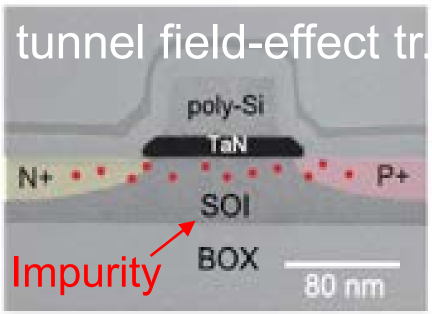

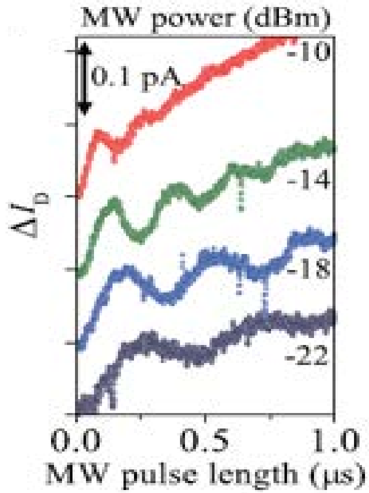

Si quantum processor unit cell operation > 1K

CH Yang et al. UNSW
Nature 2020, 2024

single qubit F=99.85%
DCZ F=98.92%

28Si n-MOS

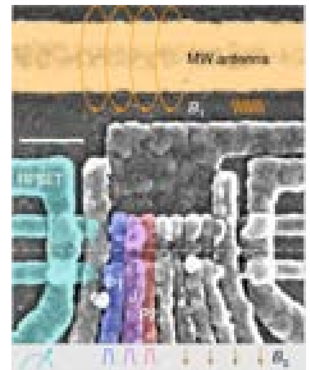

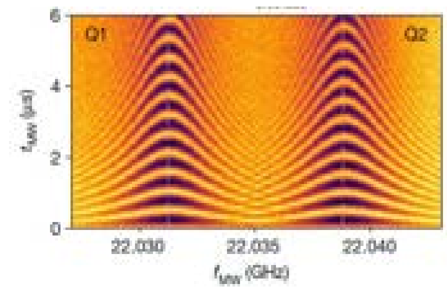

High-temperature operation of hole qubit

LC. Camenzind et al. Basel, IBM Zurich
arXiv 2103.07369v1 2021

1.5K hole qubit F=98.9%

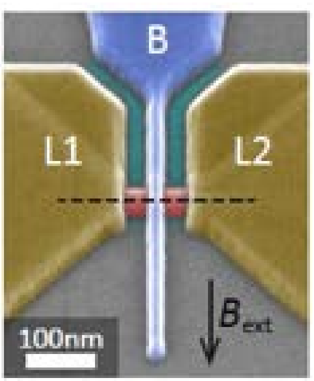

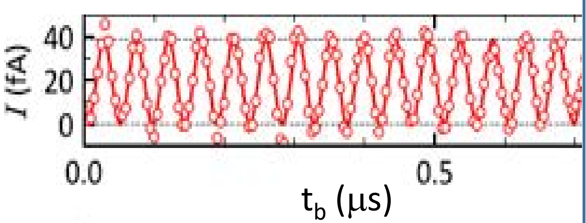

nat. Si Fin-FET

Universal logic in hot Si qubits

L. Petit et al. TuDelft
Nature 2020

1.1K single qubit F=99.3%
Two qubit CROT F=86%

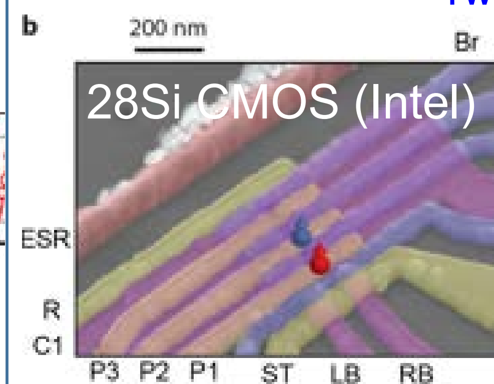

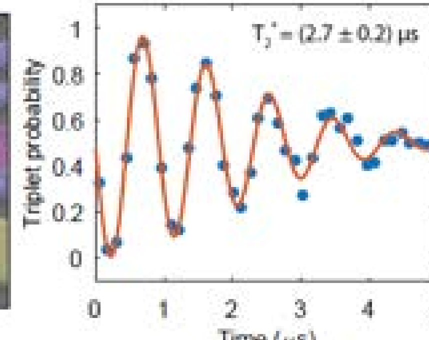

Part I Basics of semiconductor QC

- Concepts of quantum bits and computation
- Implementation of single and two qubit gates
- Readout and initialization
- Quantum coherence and phase noise

Part II Advances in semiconductor QC

- Features of quantum computing in silicon
- High-fidelity quantum gates and readout
- Quantum error correction
- Multi-qubit devices for scale-up

Challenges in Si QC

High fidelity in two-qubit gates
Error correction
Scale-up
… not yet well studied in semiconductor QC before

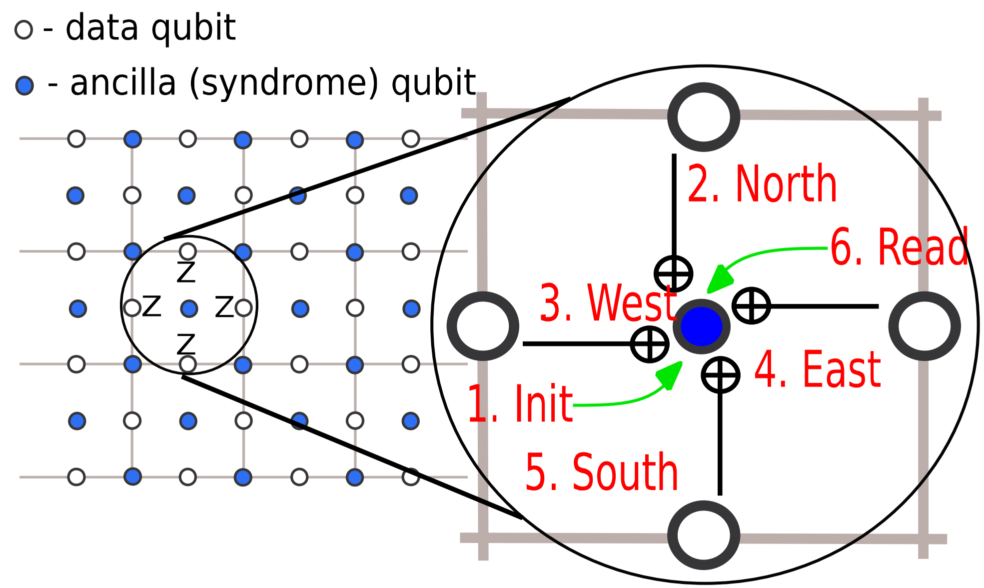

A. G. Fowler *et al.*, *Phys. Rev. A* (2009)

Introduction of semiconductor manufacturing tech. for scale-up

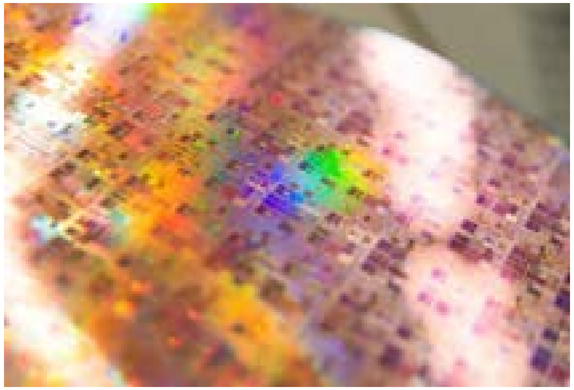

Error correction thresholds

Fidelity (1 qubit) > 99.9%
Fidelity (2 qubit) > 99%
Initialization F > 99%
Readout F > 99%

Micro-magnet Method for Implementing Spin Qubits Based on ESR

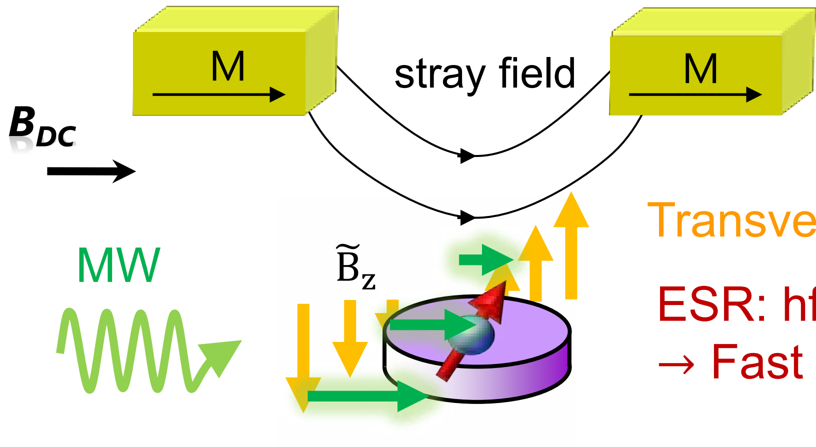

Transverse field

ESR: $hf_{MW} = g\mu_B B_{total}$
→ Fast single qubit drive

Longitudinal field

ΔE_{Zeeman} between QDs
→ Addressability to each qubit
→ Fast two-qubit gate

Y. Tokura et al. PRL 2008;
M. Pioro-Ladriere et al. Nature Phys. 2011

Three Qubit Si/SiGe Device with a Micro-magnet

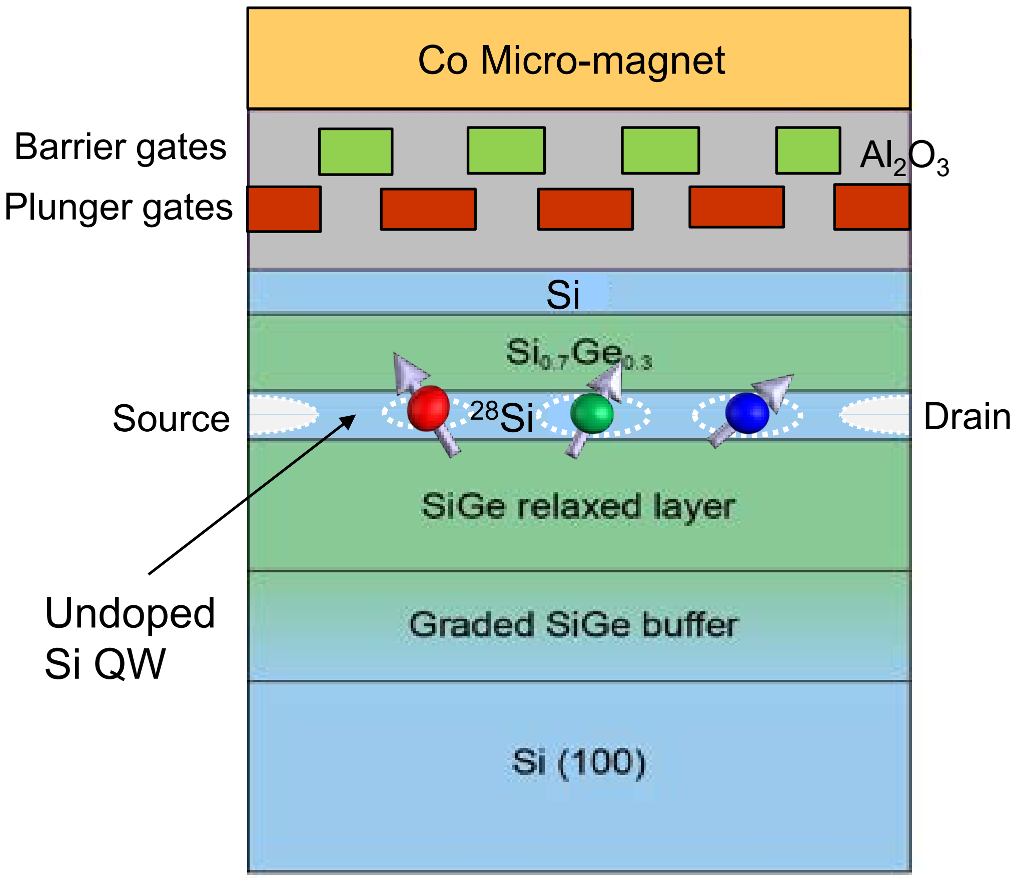

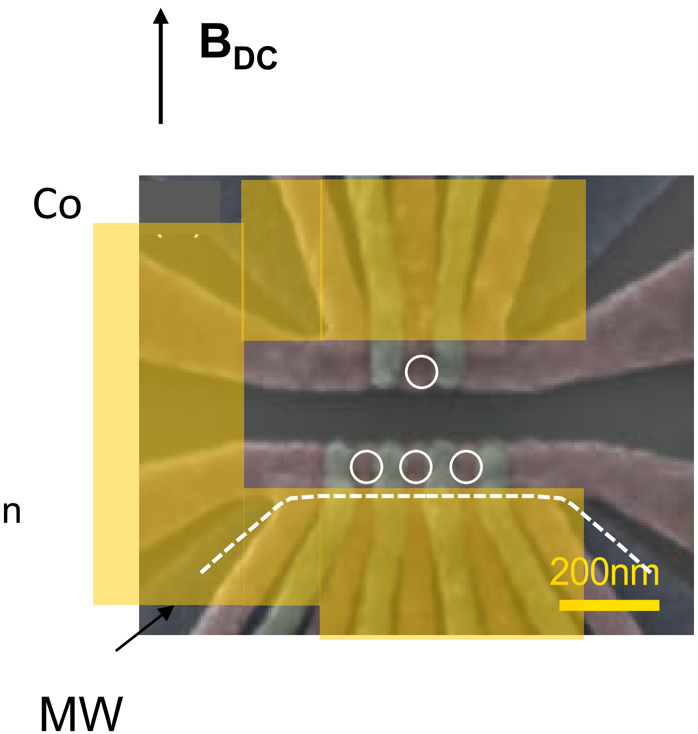

High-fidelity of three single qubits

Nat. Nanotechnol. 2021

f_{Rabi}= 5 MHz

$Ramsey\ T_2^* \cong 1.5 \mu sec$

$Hahn\ echo\ \ T_2 \cong 15\ \mu sec$

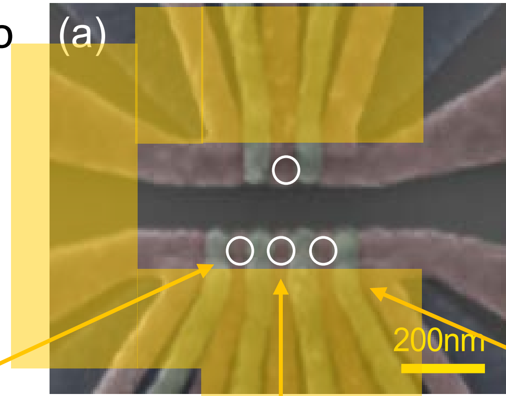

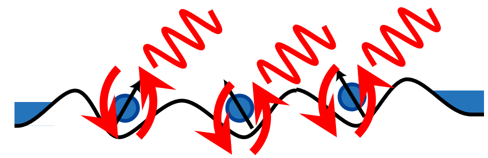

Qubit 1 Qubit 2 Qubit 3

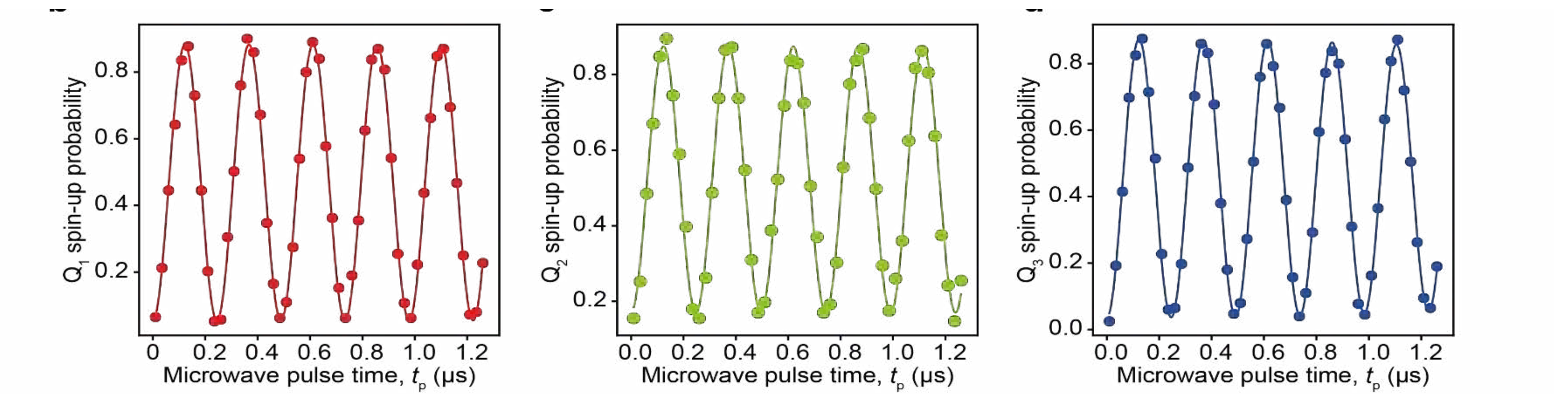

Δf_{Larmor} = 400 to 500 MHz

Fidelity = 99.6 % on average for Nat. Si/SiGe
= 99.8 % on average for 28Si/SiGe

Toward Multiple Qubits

6 qubits in 1x6 28Si/SiGe QDs

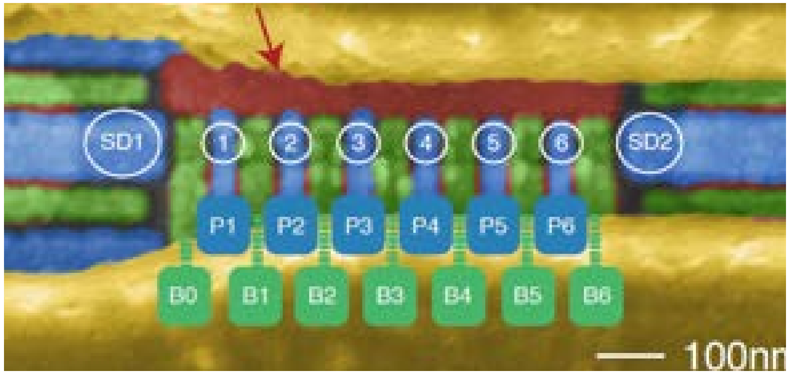

S.G.J. Philips et al.
Nature (2022)

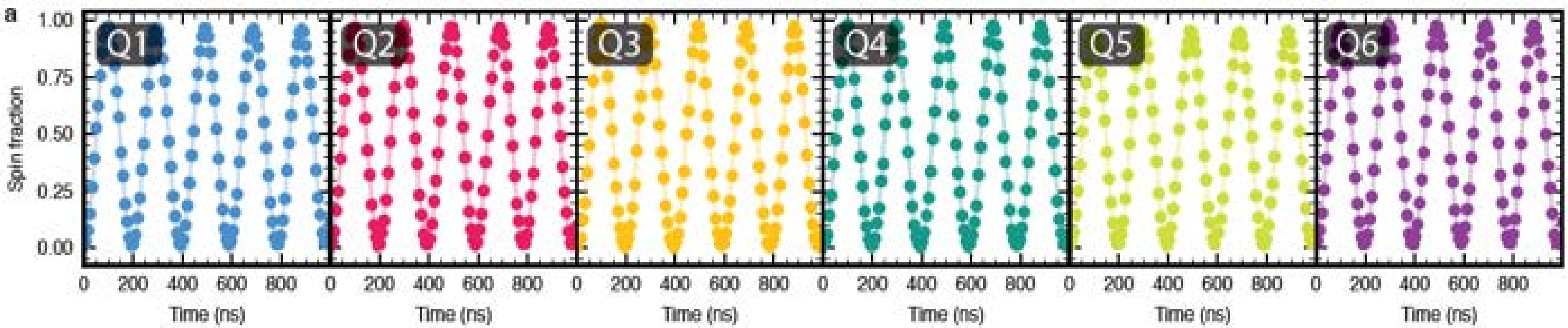

Fidelity = 99.77 to 99.96 %

Spin Qubits using a μ-magnet Method

28Si/SiGe   Rabi oscillaition

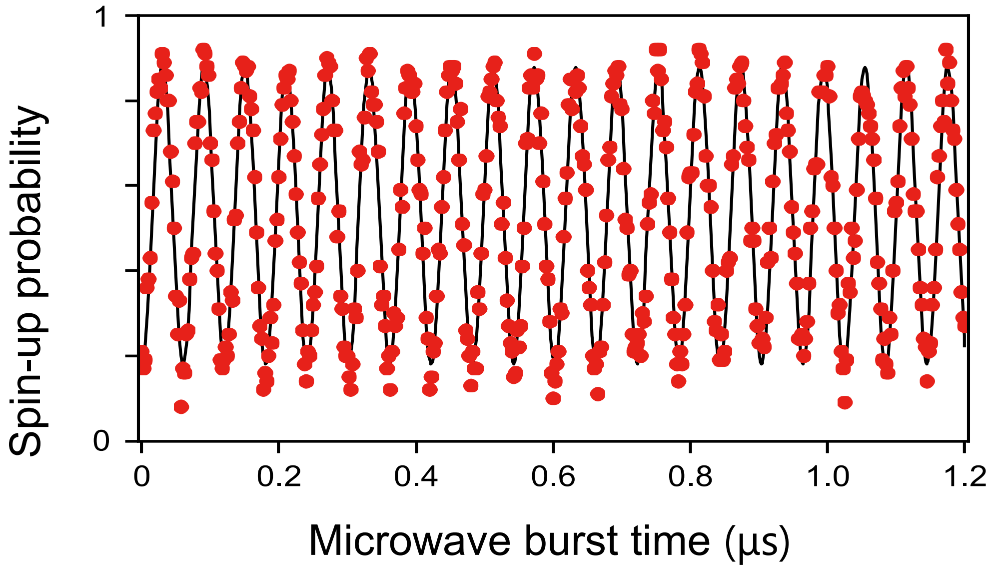

T2*=20 μsec   F= 99.93%

J. Yoneda et al., Nat. Nanotechnol. 2018

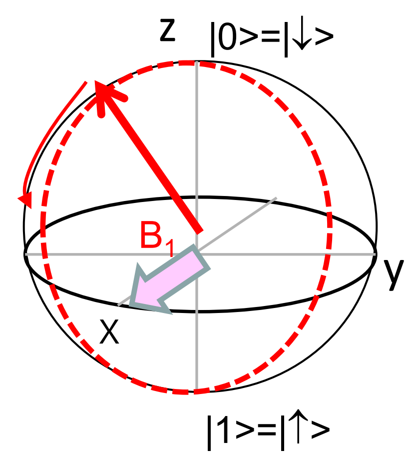

Environment Noise Limited Fidelity in $^{28}Si/SiGe$

Random Bench Marking Qubit
Fidelity > 99.9 %

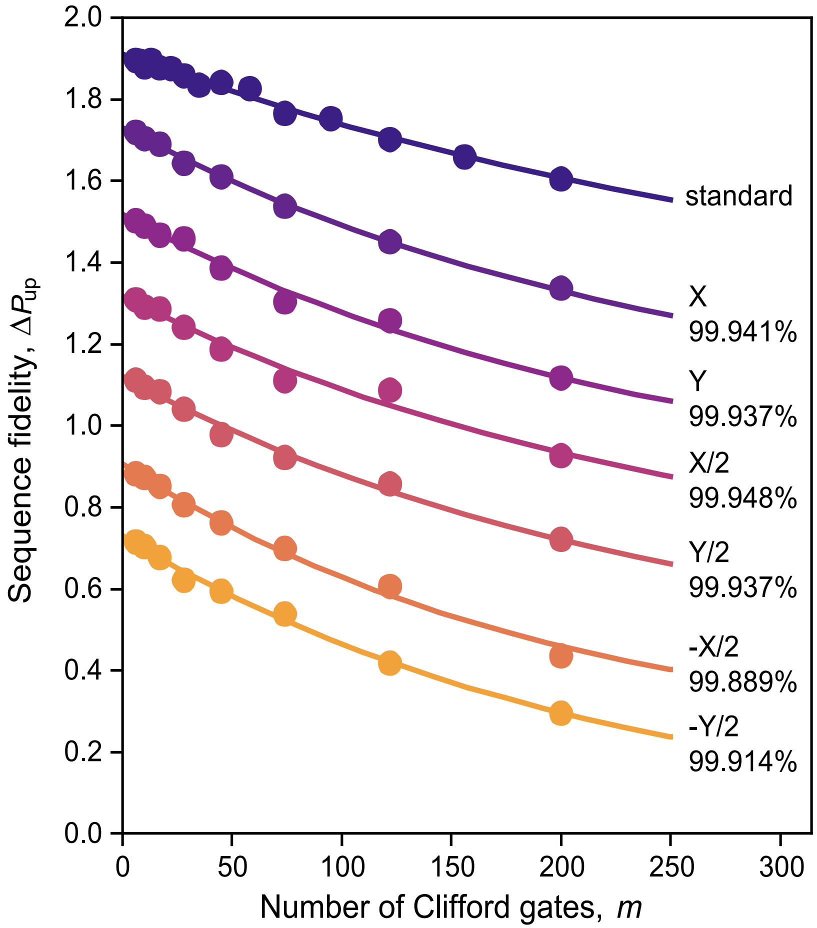

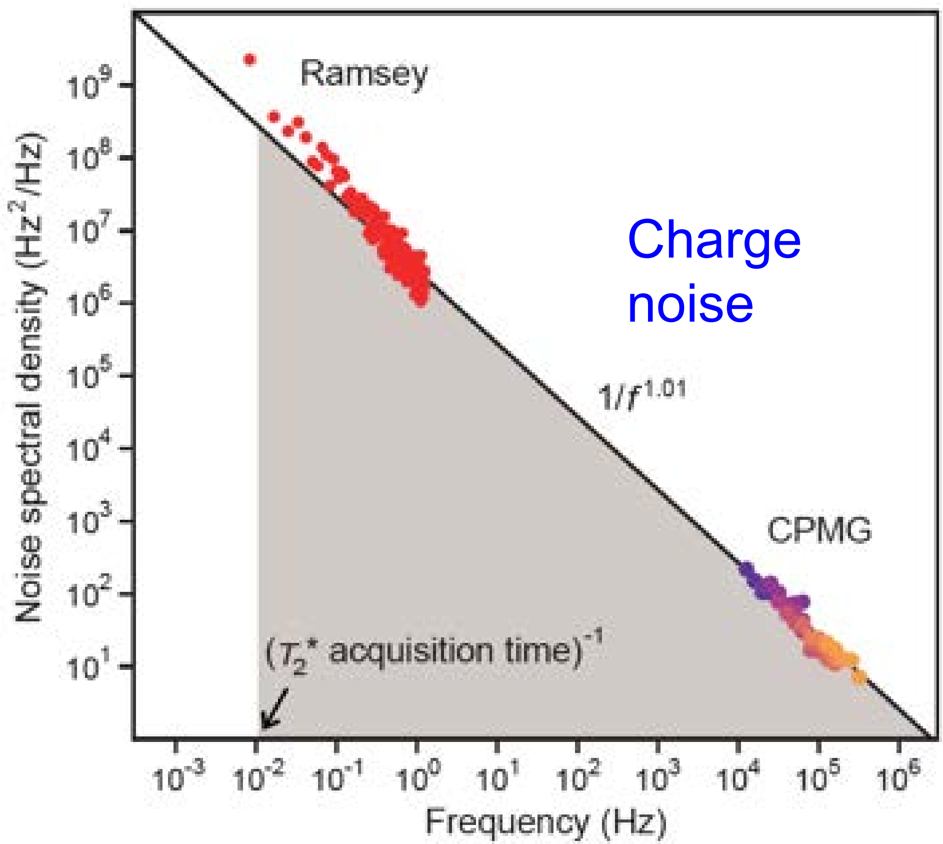

Charge noise

J. Yoneda et al. Nat. Nanotechnol. 2018

High-fidelity Two-qubit Gates

Two-qubit gate using spin-exchange interaction and Zeeman energy difference

Exchange coupling controlled by tunnel coupling (up to 10MHz)

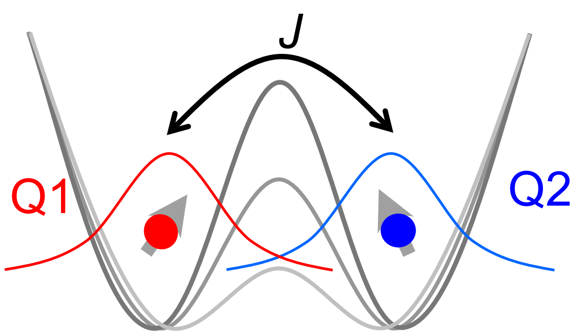

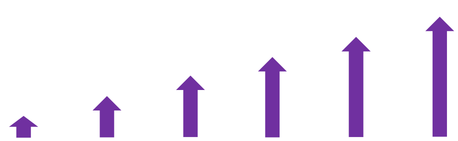

Zeeman energy gradient (ΔE_Z) induced by MM

ΔE_Z ~ a few 100 MHz

$\Delta E_Z \gg J$

"Heisenberg" *"Ising"*

$$H_{\text{int}} = \frac{J}{4}\boldsymbol{\sigma}_1 \cdot \boldsymbol{\sigma}_2 \approx \frac{J_{12}}{4}\sigma_{z1}\sigma_{z2}$$

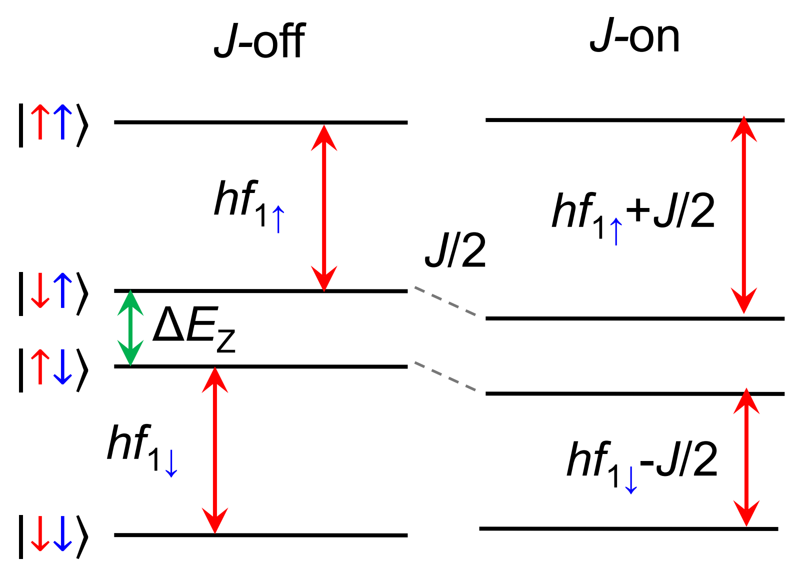

Single-step Two Qubit Gate

Basis states

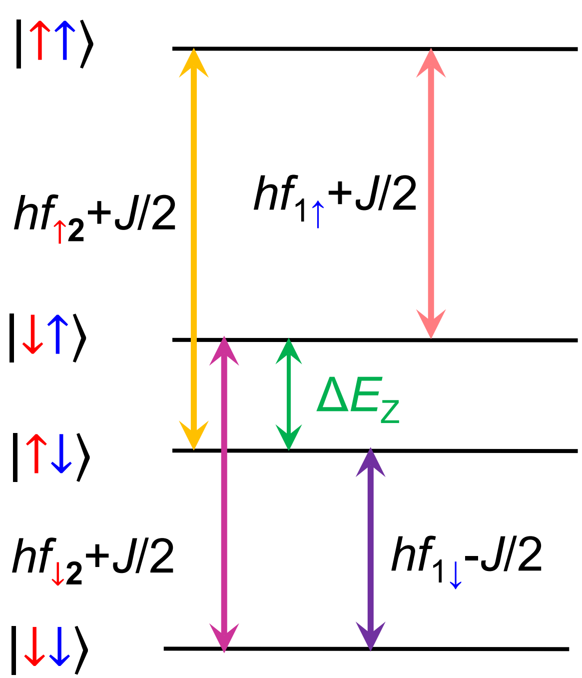

Each transition induced by
μ-wave excitation

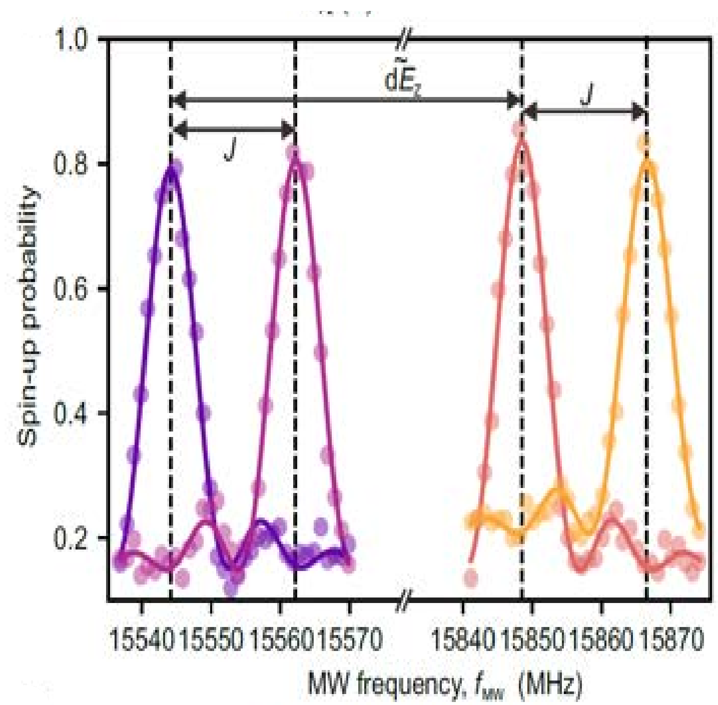

Conditional transitions to rotate one of the two spins depending on the other spin's orientation, up or down

Single-step Two Qubit Gate

Basis states

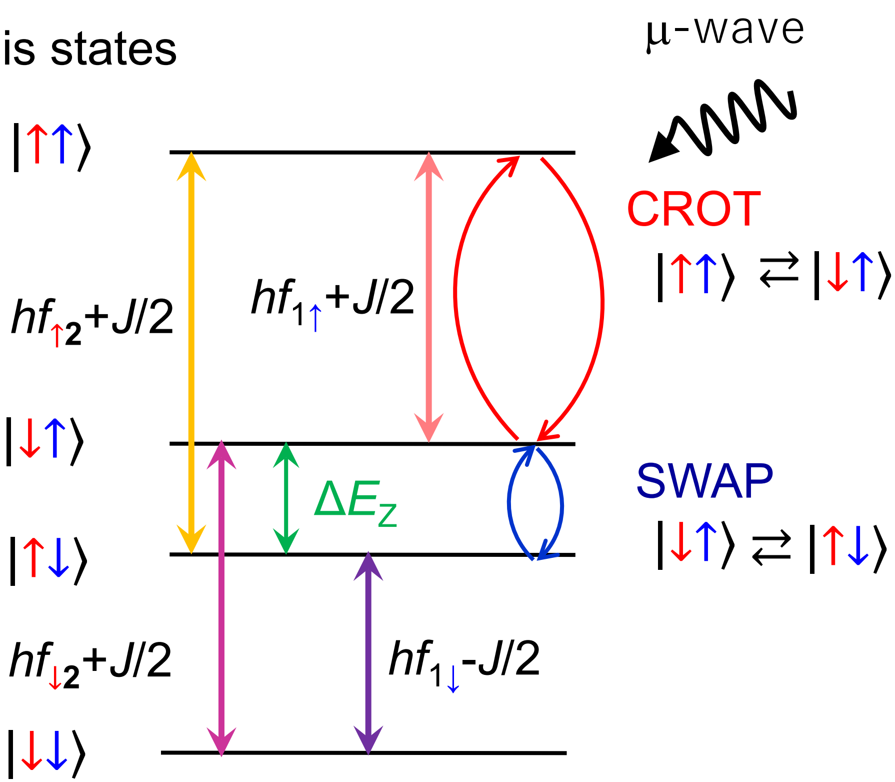

target control

$CNOT|\downarrow\downarrow\rangle = |\downarrow\downarrow\rangle$

$CNOT|\uparrow\downarrow\rangle = |\uparrow\downarrow\rangle$

$CNOT|\downarrow\uparrow\rangle = |\uparrow\uparrow\rangle$

$CNOT|\uparrow\uparrow\rangle = |\downarrow\uparrow\rangle$

With resonant μ-wave excitation, left spin flips when right spin up

SWAP and CNOT

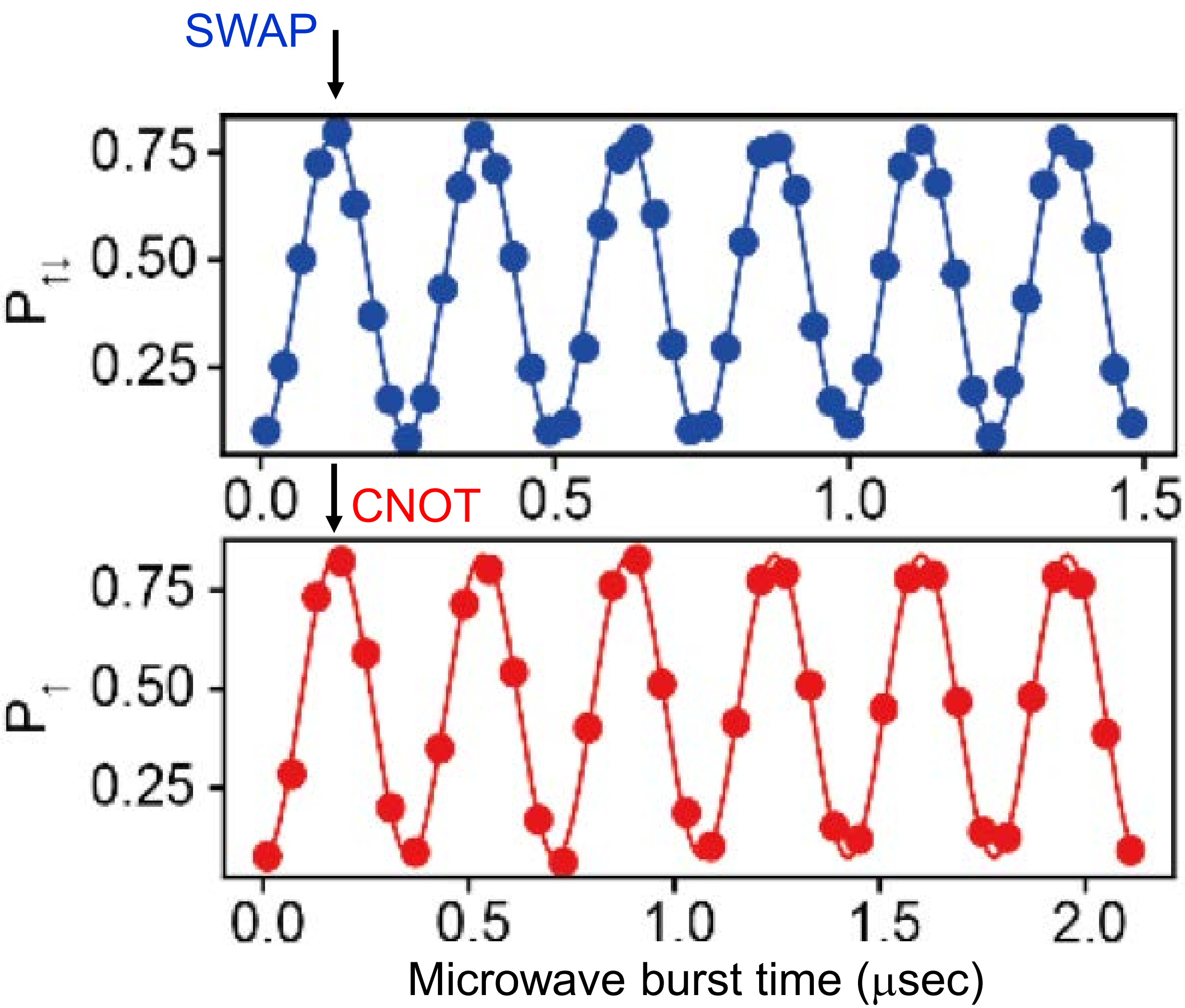

F=99.5%

T_{CPHASE} = 5.5.nsec to 1 msec

A. Noiri et al. Nat. Commun. 2018

Fidelities of Two Qubit Gates

A. Noiri et al. Nature 2022

Clifford gate random benchmark

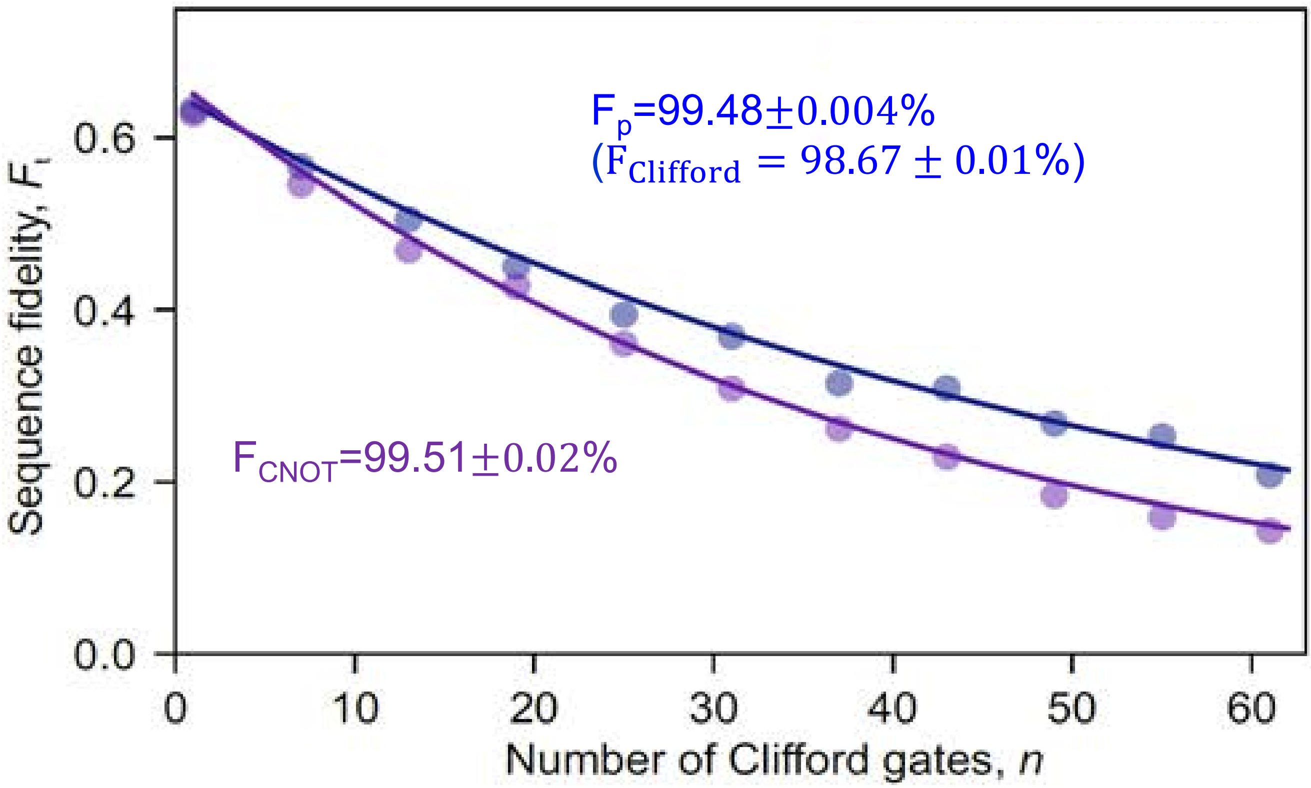

- The Rabi freq. range of 3 to 5 MHz is an order of magnitude higher than in previous work.

Two-spin qubit gate fidelity

> 99.5 % for 28Si/SiGe from TuDelft, Nature 2022; > 99% for 28Si/SiGe from Princeton Adv. Sci. 2022

99.4 % for two 31P nuclear qubits with a shared electron from UNSW, Nature 2022

Single and Two-qubit Gate Fidelities

A. Noiri et al. Nature 2022

28Si/SiGe (G. Scappuci)

Max. fidelity 99.8 %

Single qubit

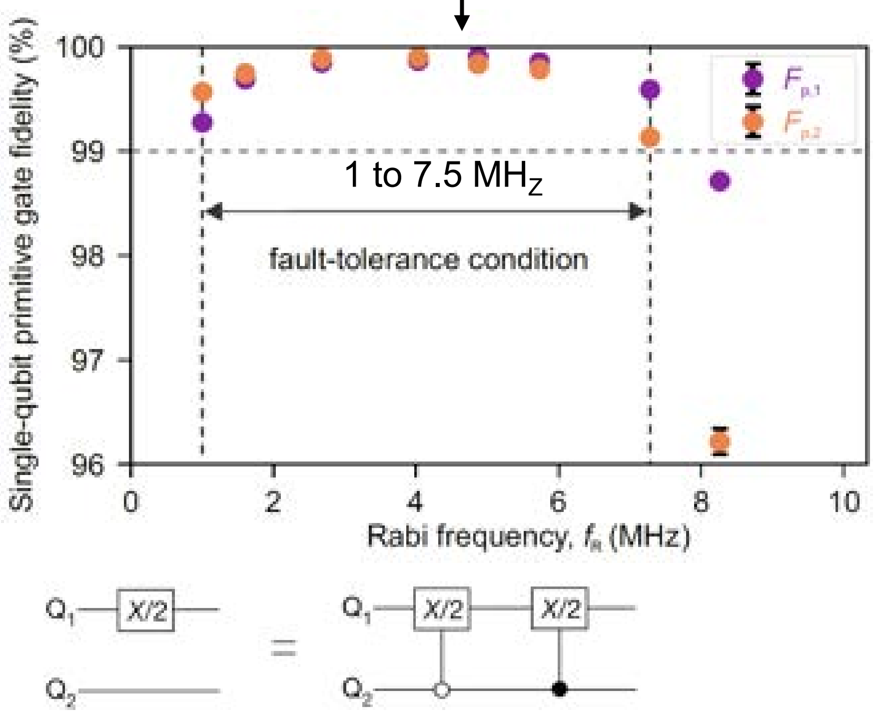

Max. fidelity 99.5 %

Two qubits

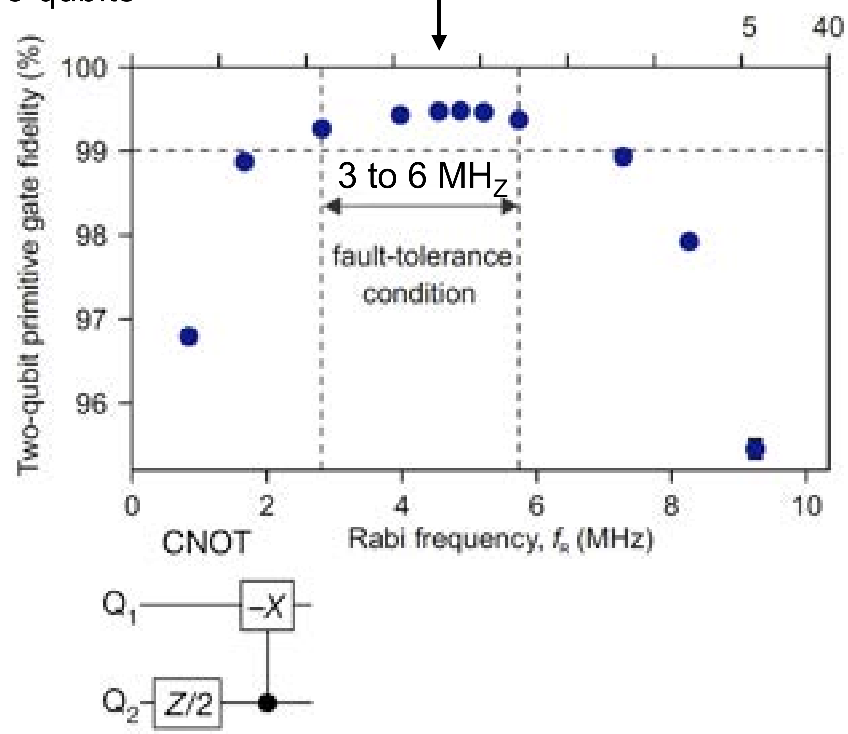

- The freq. range of 3 to 5 MHz is an order of magnitude higher than in previous work.

Part I Basics of semiconductor QC

- Concepts of quantum bits and computation
- Implementation of single and two qubit gates
- Readout and initialization
- Quantum coherence and phase noise

Part II Advances in semiconductor QC

- Features of quantum computing in silicon
- High-fidelity quantum gates and readout
- Quantum error correction
- Multi-qubit devices for scale-up

Errors in Quantum Bits

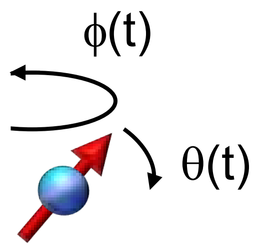

$$|\varphi\rangle = \cos\frac{\theta}{2}\,|0\rangle + e^{i\phi}\sin\frac{\theta}{2}\,|1\rangle$$

Fluctuation of ϕ : phase error
Fluctuation of θ : bit error

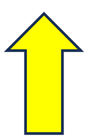

Detect and correction of phase error

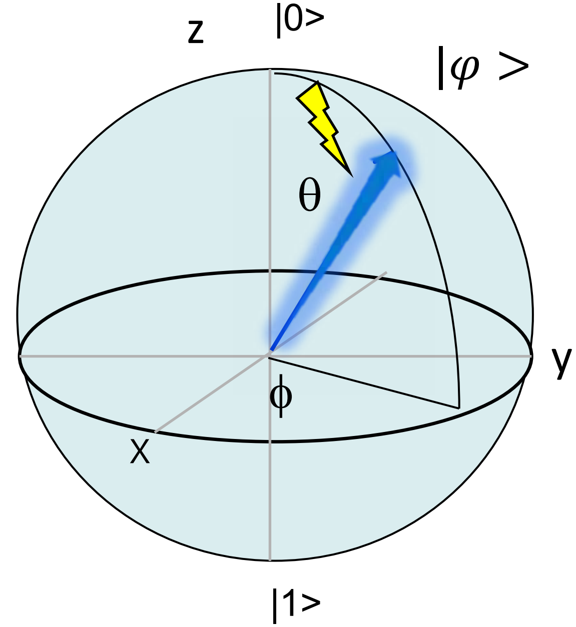

Phase error >> Bit error in semiconductors

Circuit of 3Q Quantum Error Correction (QEC)

QEC for phase error (Phase error rate >> Bit error rate)

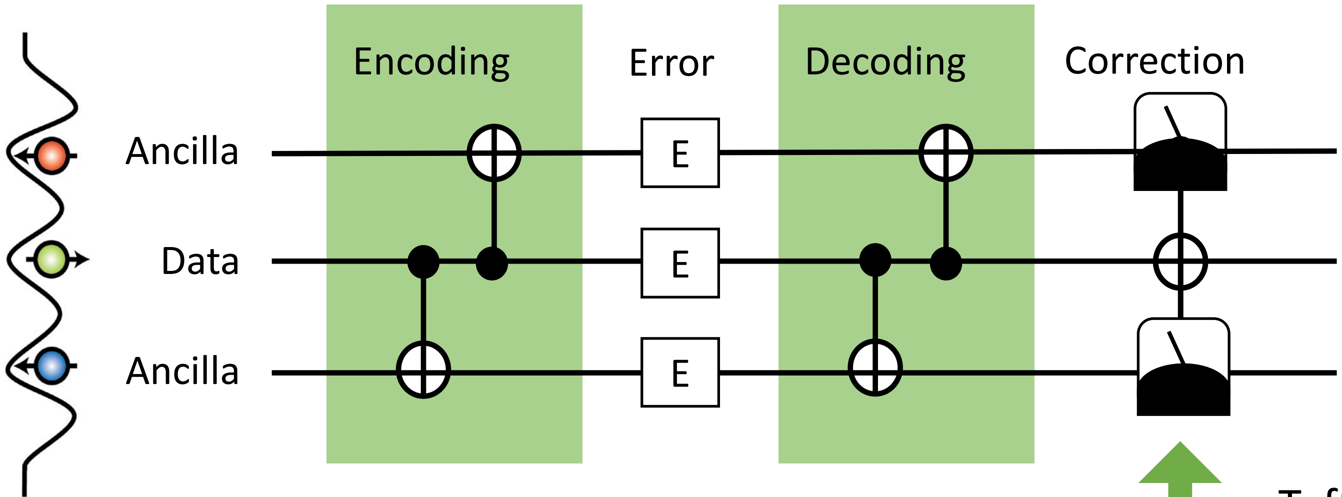

QEC time < T2*

$\alpha|\downarrow\rangle + \beta|\uparrow\rangle$ Phase error

$\boldsymbol{\alpha}|\downarrow\downarrow\downarrow\rangle + \boldsymbol{\beta}|\uparrow\uparrow\uparrow\rangle$ $\hat{Z}_1\hat{Z}_3$

Toffoli gate:

Rotates data qubit only when $Z_1 = Z_3 = 1$

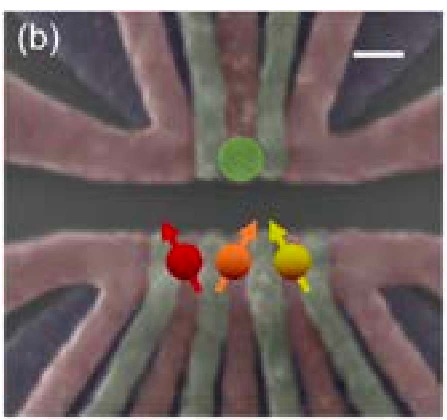

Generation of GHZ State

Input:
Product state

Output:
GHZ-state with various phase conditions

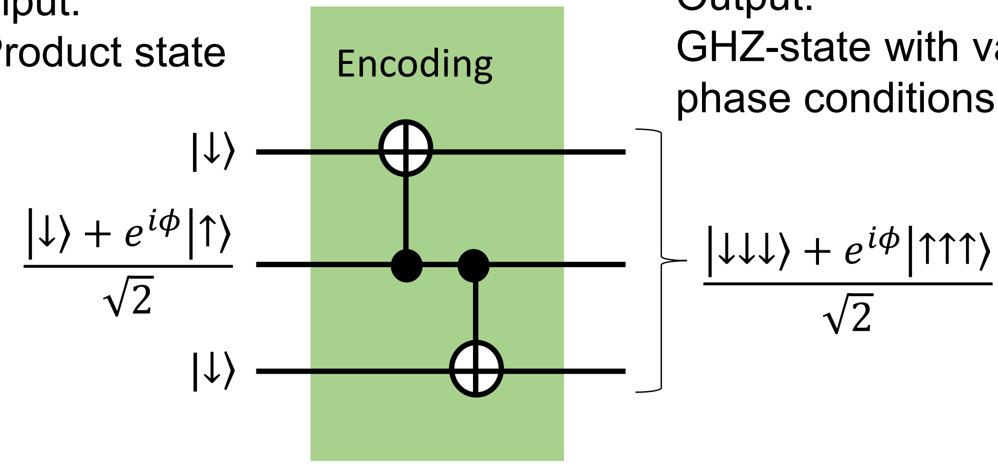

$\phi = 0$

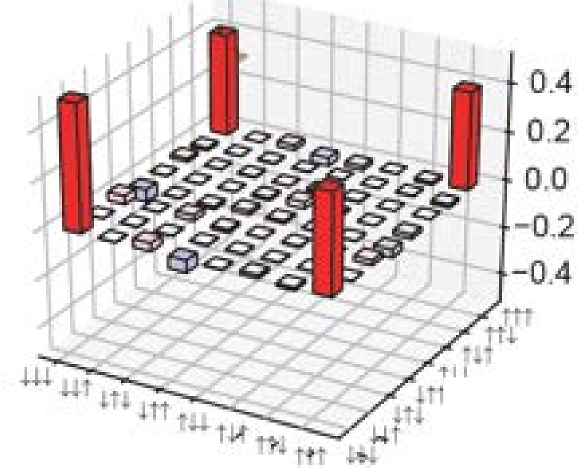

Fidelity 88%

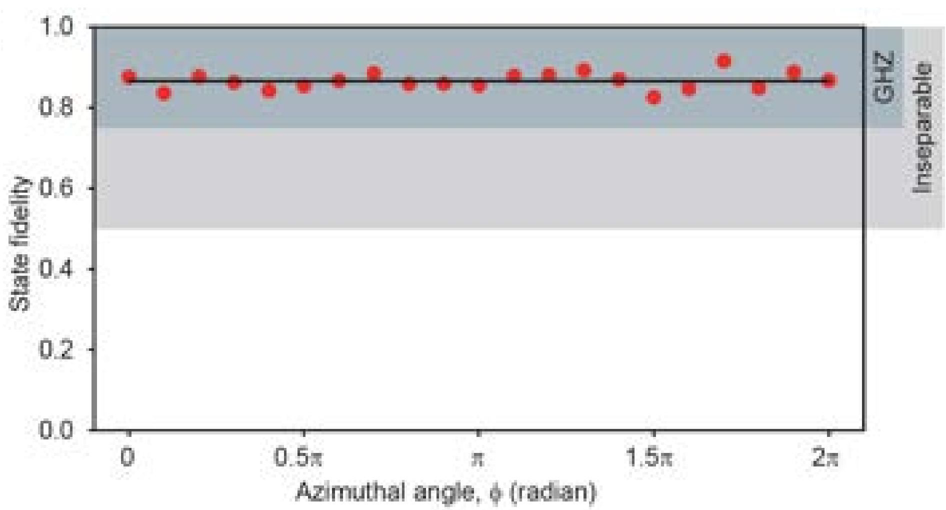

$\phi = \pi$

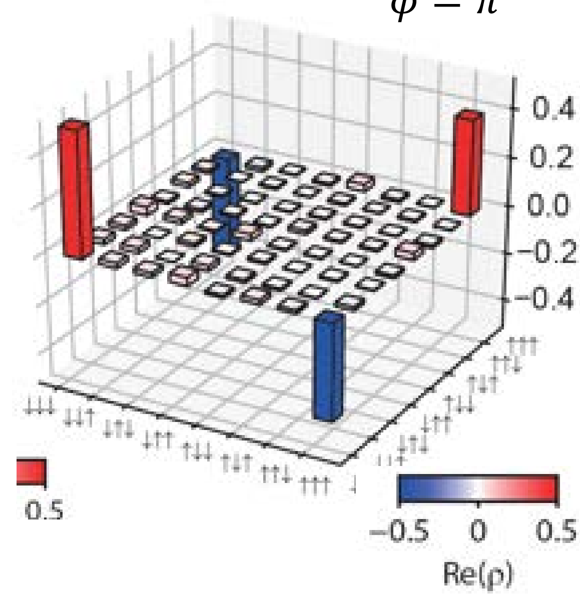

Error Correction by Single Step Toffoli Gate

K. Takeda et al. Nature 2022

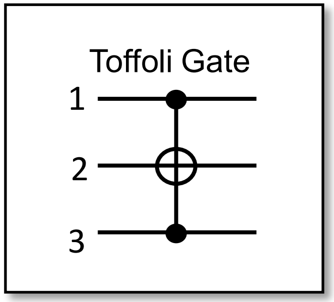

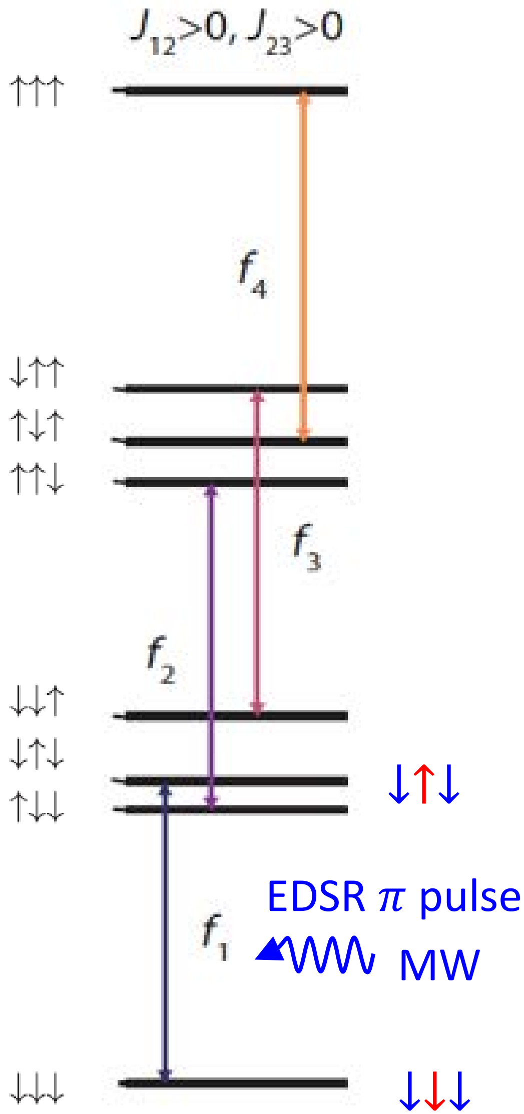

Flipping the center spin with the other two spins fixed

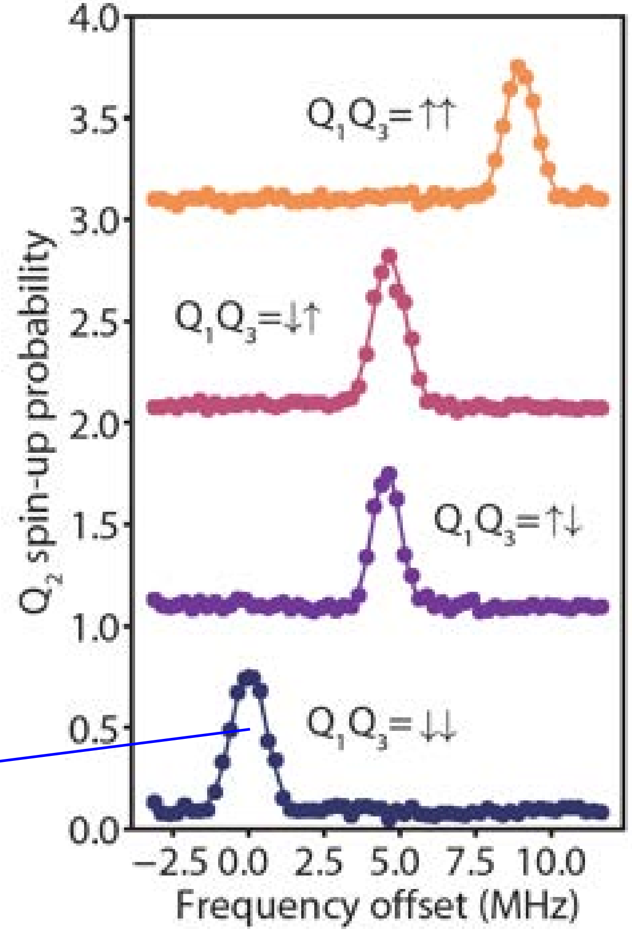

MJ Gullans and JP Petta, PRB 2019

1 Qubit Phase Error Correction Experiment

K. Takeda et al. Nature 2022

Nat.Si/SiGe

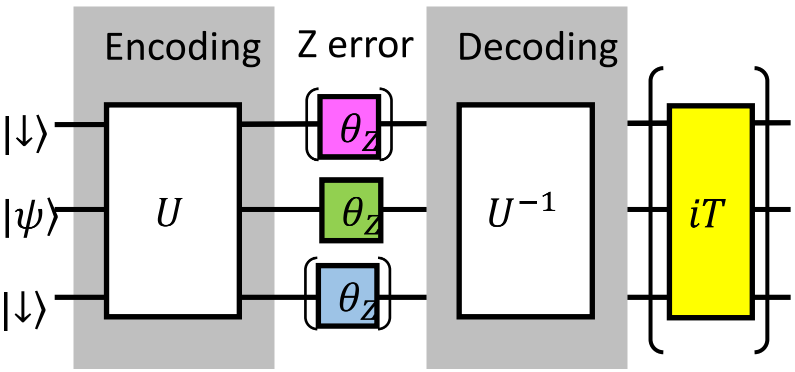

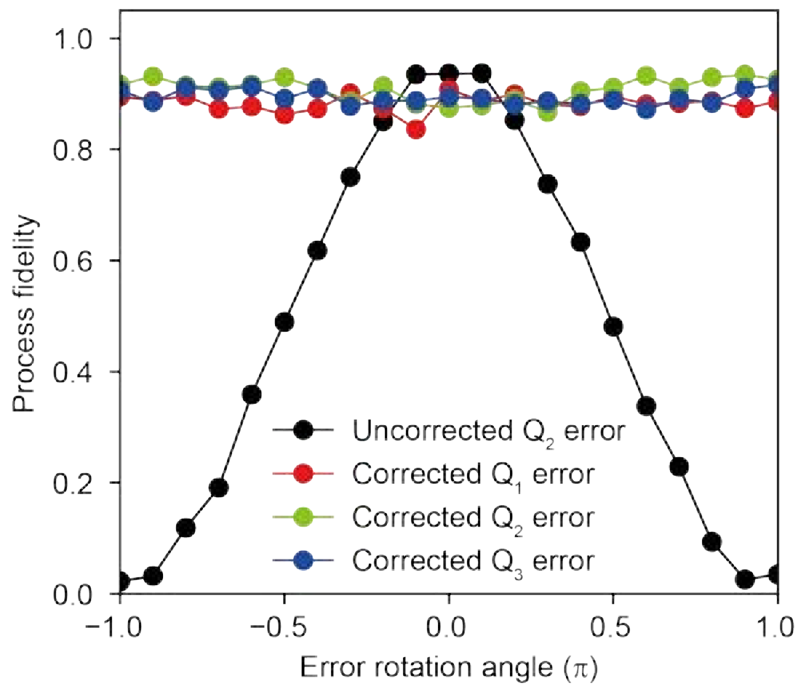

Phase error with angle θ

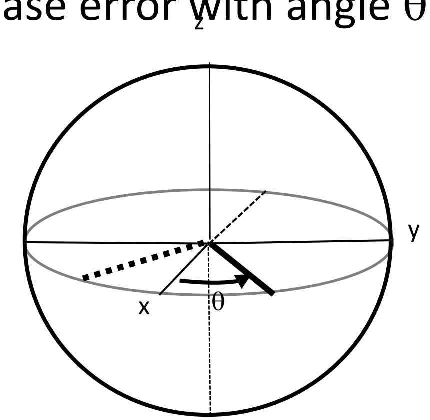

Outline of 3Q Quantum Error Correction

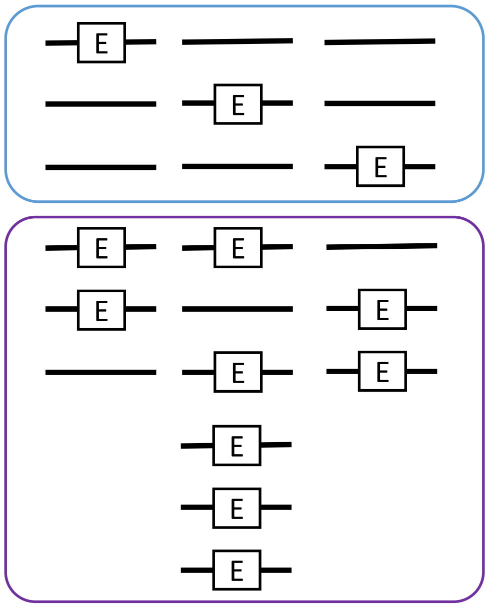

1Q error: corrected

2Q & 3Q error: uncorrected

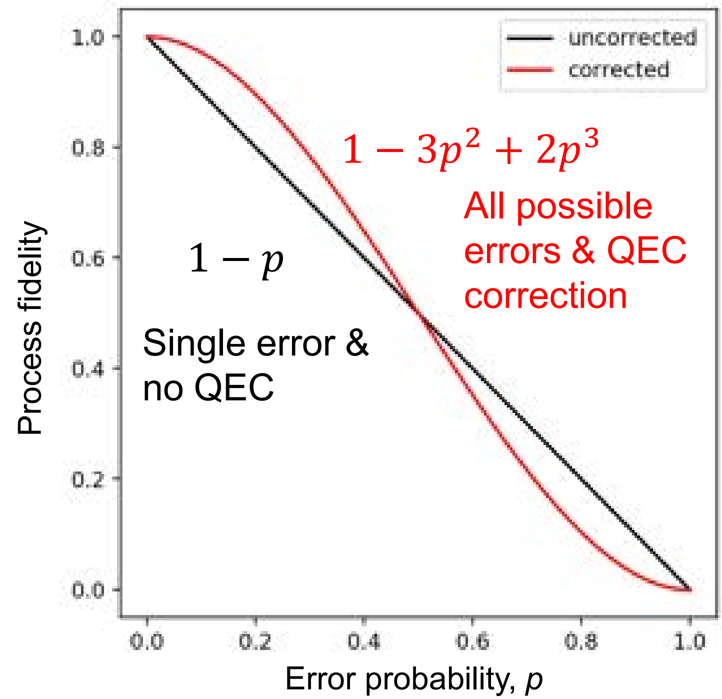

p=sin²θ/2

- Corrected infidelity $1 - F(p) = O(p^2)$
- Improvement for $p < 0.5$ if all qubits have the same error rate

QEC for Three-qubit Phase Error

K. Takeda et al. Nature 2022

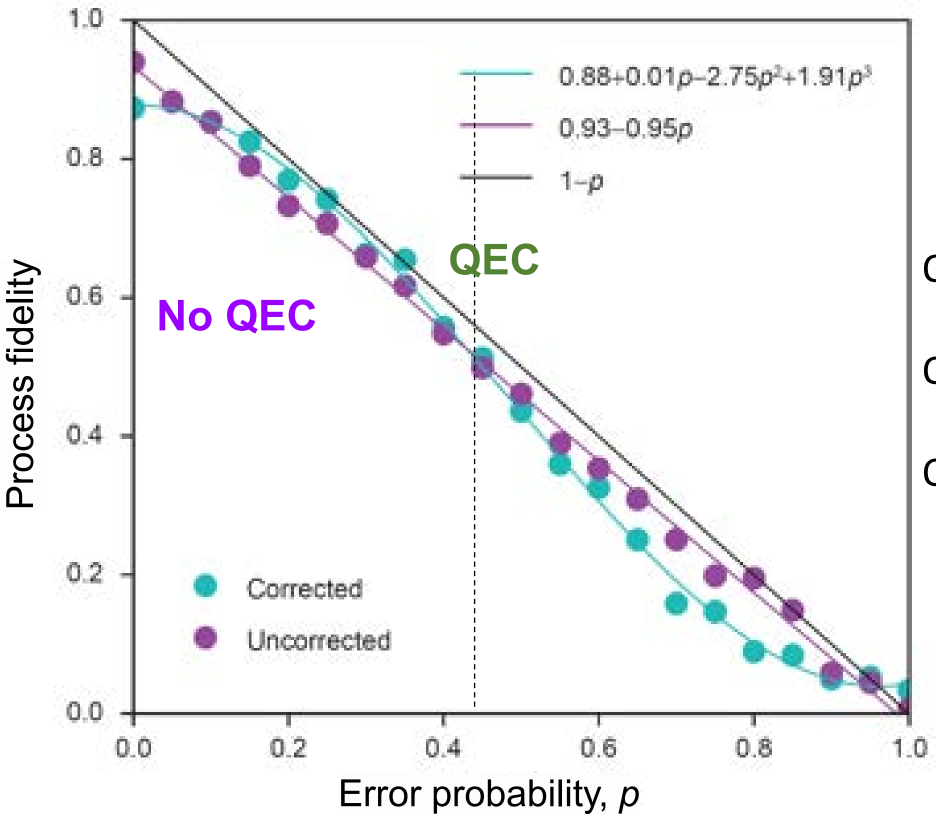

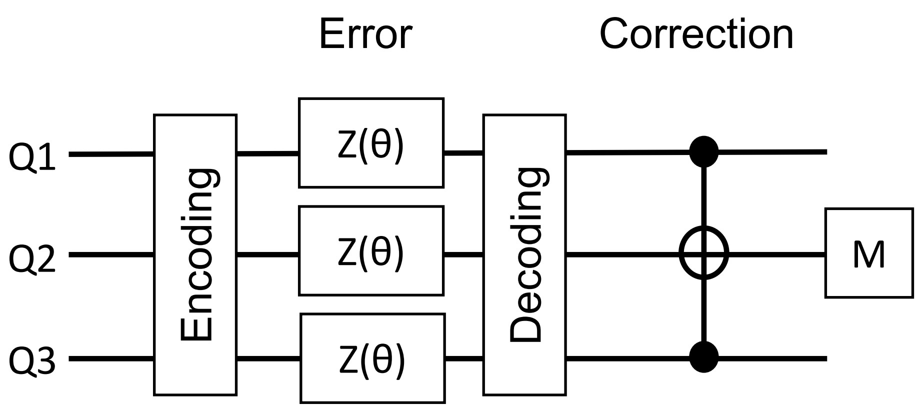

- Fidelity almost first-order insensitive to p
- Improvement for $p < 0.45$

➡ Indication of presence of correlated phase error between qubits

Error Detection and Correction

Toffoli

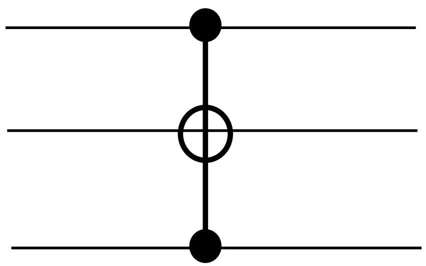

Measurement & correction

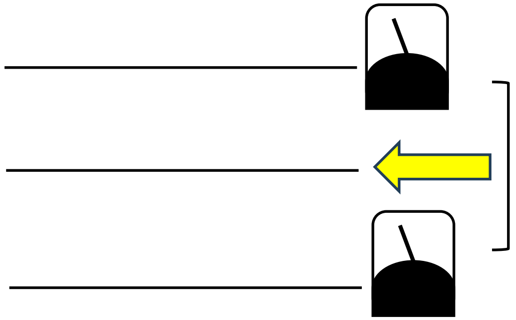

Fast

Relatively slow to retain high F> 99%

$T_{Tofolli}$ < T2* (~10 μsec)

T^{Meas} > T2*

Small code

Large code

Fast (< 1 μsec) and High-fidelity (> 99%) measurement

Realizing Repeated Quantum Error Correction in a Distance-Three Surface Code

Krinner et al. Nature 2022

17 physical qubits

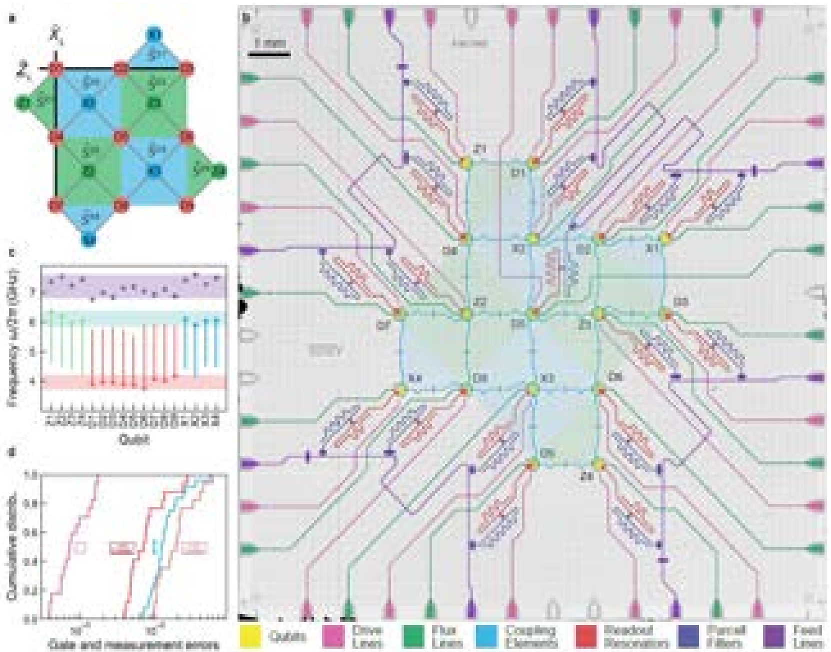

3x3 data qubits
4 & 4 auxiliary qubits
2 or 4 data qubit measurements

Suppressing quantum errors by scaling a surface code logical qubit

-Exceeding the QEC break-even point-

Google Quantum AI, Nature 2023

Superconducting 49 qubits

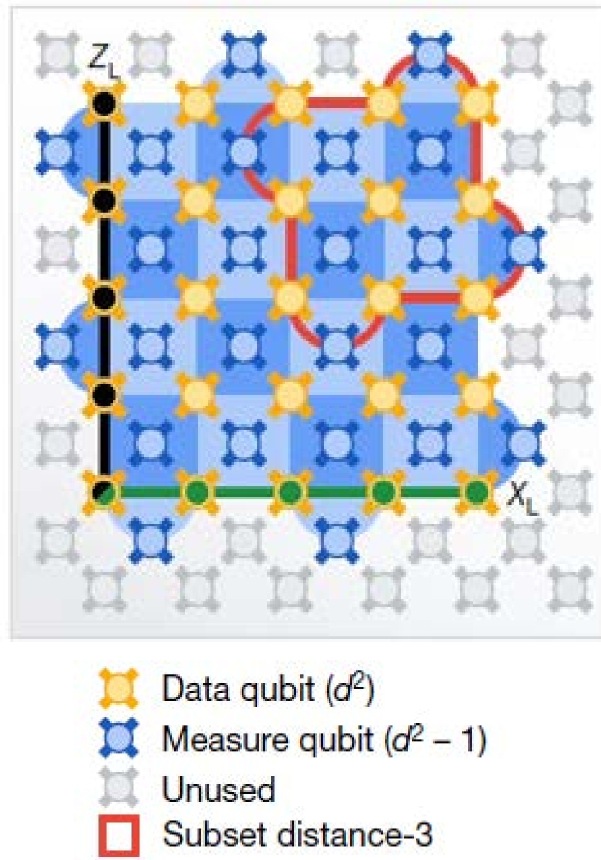

Distance 5
5x5 data qubits
24 measurement qubits

Fast, High-fidelity Spin Readout for QEC

K. Takeda et al. npj QI (2024)

Singlet-triplet probability using Pauli Spin Blockade

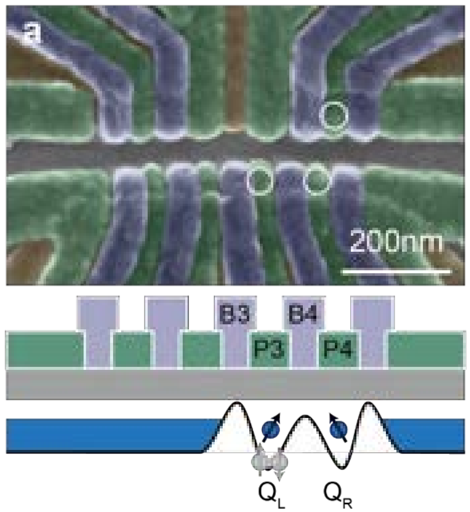

t_{int}=3 μs

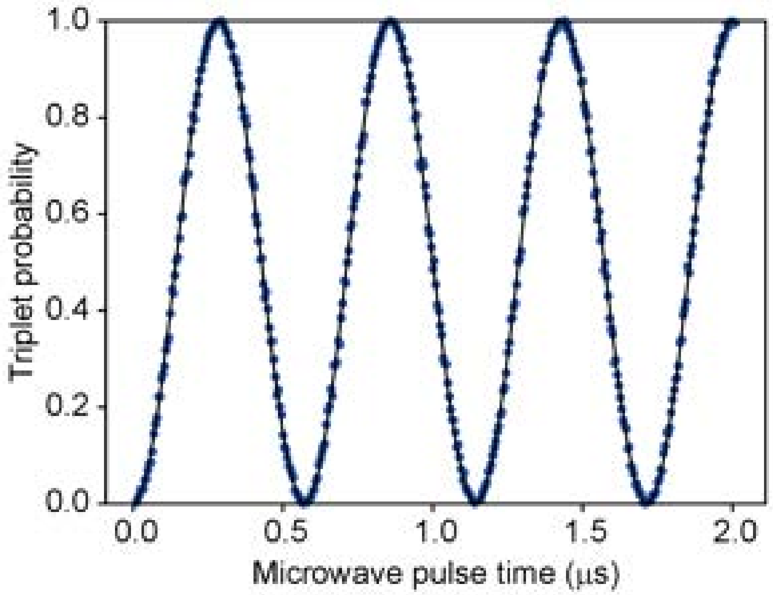

Rabi visibility
= 99.6%

RF refletometry signal from charge sensor

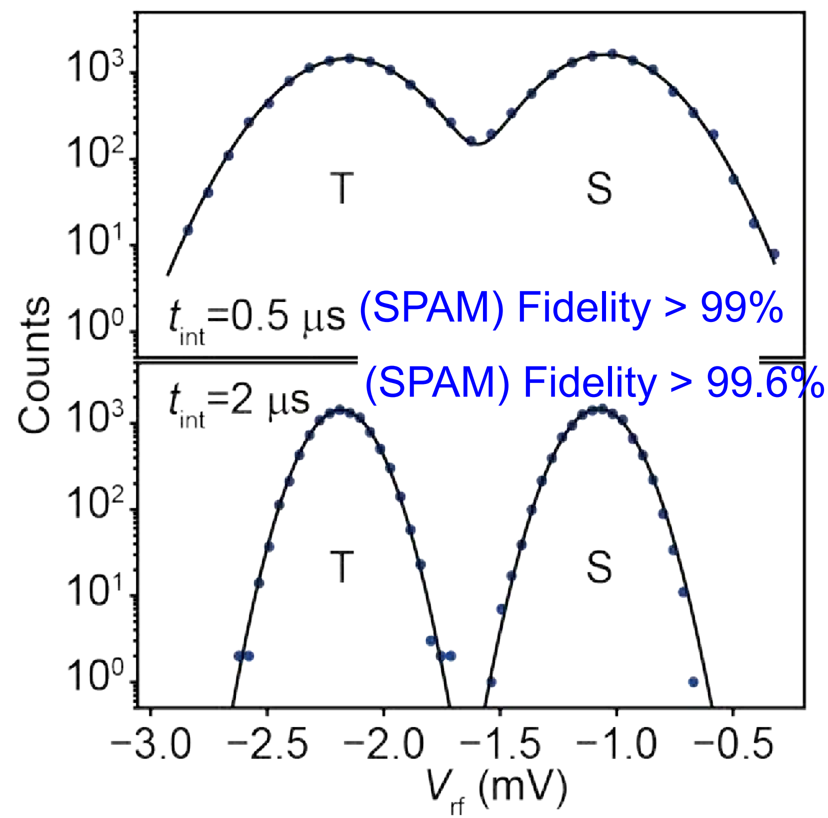

Initial. error : 0.2%

Part I Basics of semiconductor QC

- Concepts of quantum bits and computation
- Implementation of single and two qubit gates
- Readout and initialization
- Quantum coherence and phase noise

Part II Advances in semiconductor QC

- Features of quantum computing in silicon
- High-fidelity quantum gates and readout
- Quantum error correction
- Multi-qubit devices for scale-up

Probing single electrons across 300 mm spin qubit wafers

Intel

Neyens et al., arXiv: 2307.04812v1

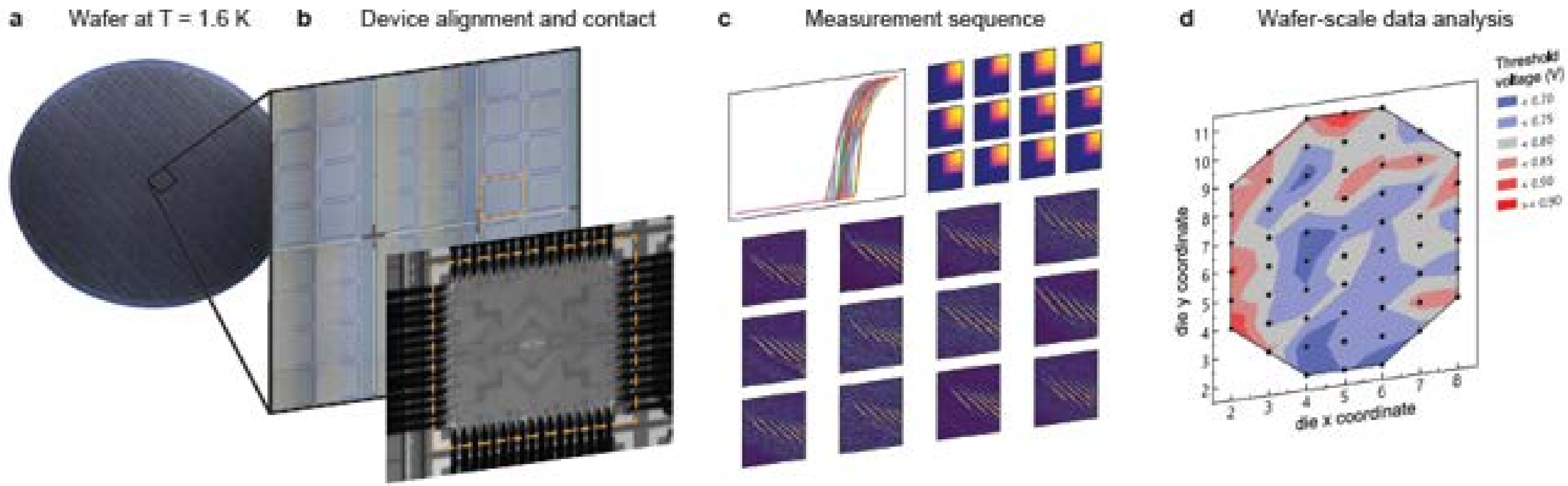

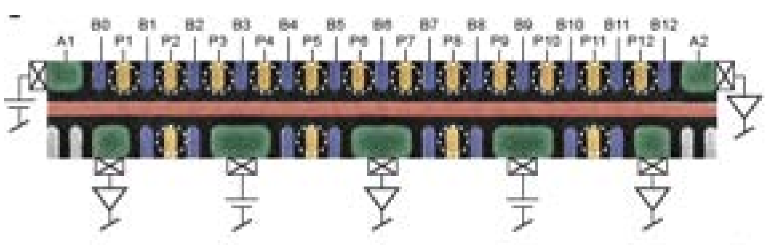

Component	Yield	Good count	Total count
Ohmics	100%	1624	1624
Gates	100%	10208	10208
Quantum dots	99.8%	3703	3712
12QD arrays	96%	223	232

Development of Multi-qubit Devices

2D array

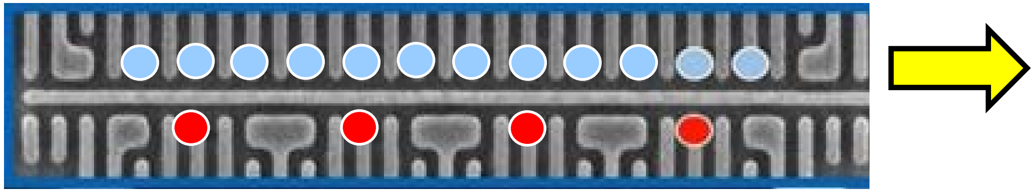

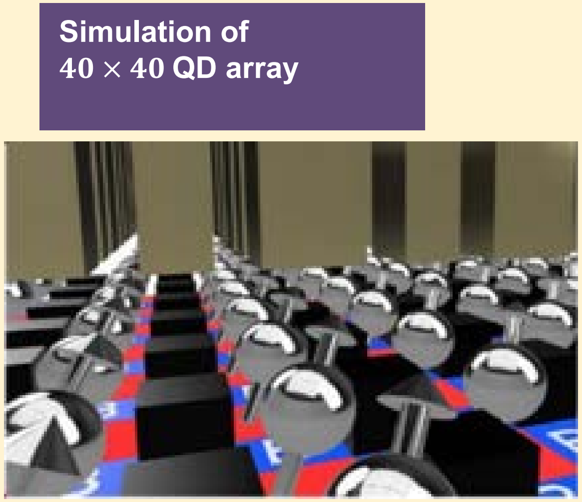

Tadokoro et al. Sci. Rep. 2021

Industrial tech. for Si/SiGe and
MOS 1D qubit array

12 qubit chips in Conf. talks
by J. Clark, Intel

Jun 15 2023
https://www.intc.com/news-events/press-releases/detail/1626/intels-new-chip-to-advance-silicon-spin-qubit-research

Quantum
link

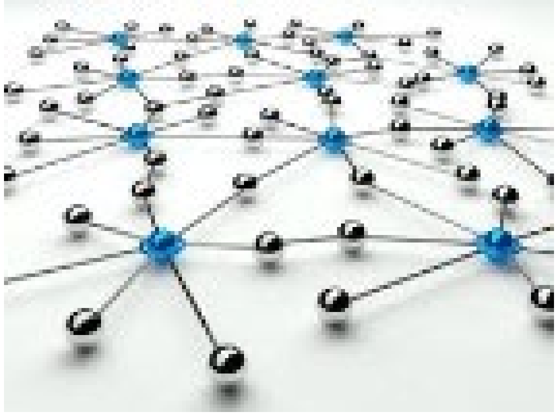

Shuttling-based two-qubit gate
Noiri et al., Nat. Commun. 2022

Toward Multiple Qubits

2x2 qubits in Si/SiGe

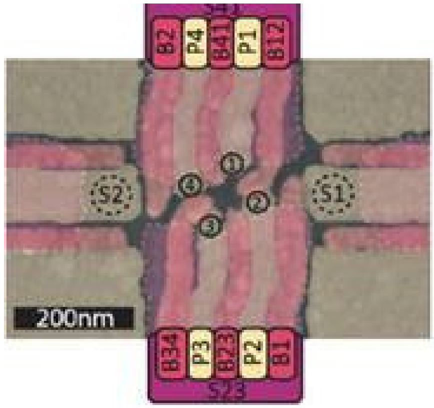

FK. Unseld et al. APL 2023
(APS March 2024)

2x2 qubits in Ge/SiGe QDs

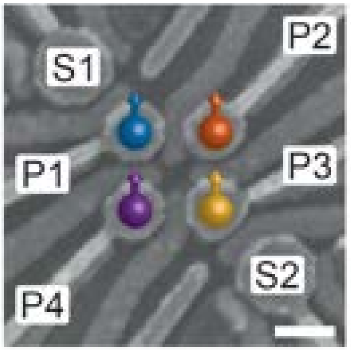

N.W. Hendrickx et al. Nature 2020

3x3 GaAs QDs

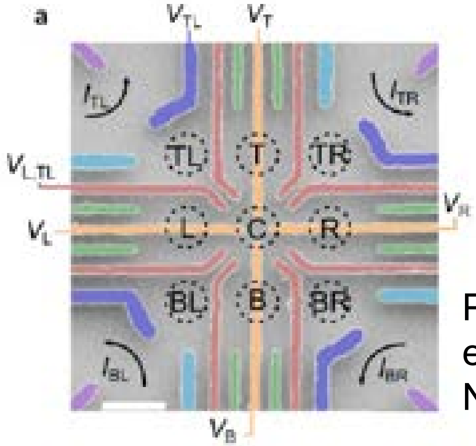

P-A. Mortemousque et al. Nat. Nanotechnol. 2020

4x4 Ge QDs with shared control

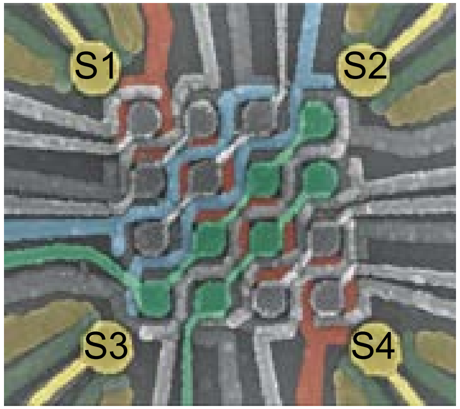

F. Borsoi et al. Nat. Nanotechnol 2023

Quantum Links between Qubits

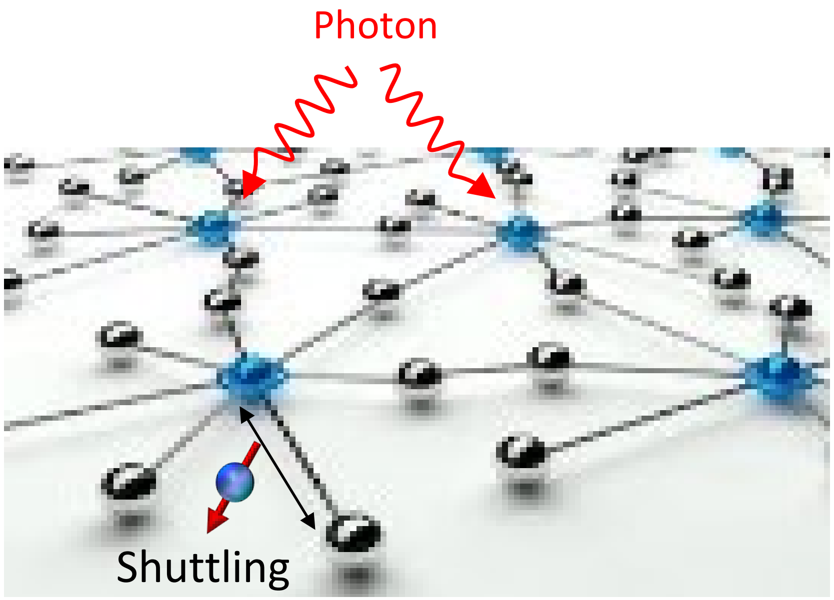

Quantum Link with Spin-photon Coupling

Spin-photon coupling

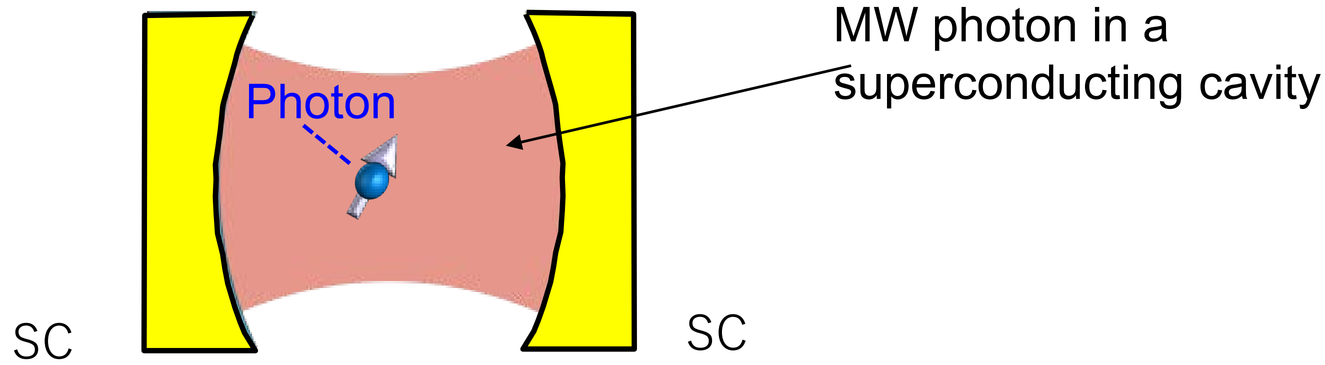

Photon-mediated spin-spin coupling

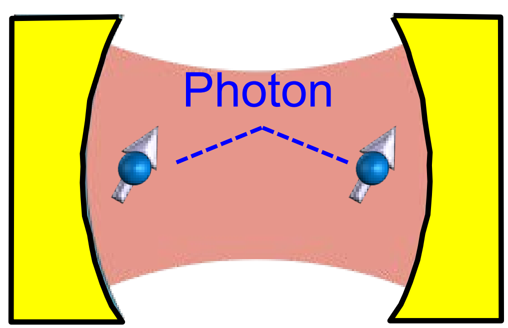

Spin-photon Coupling in a Superconducting Cavity

Spin-photon coupling in a super-
conducting resonator (~6 GHz) ^{28}Si/SiGe

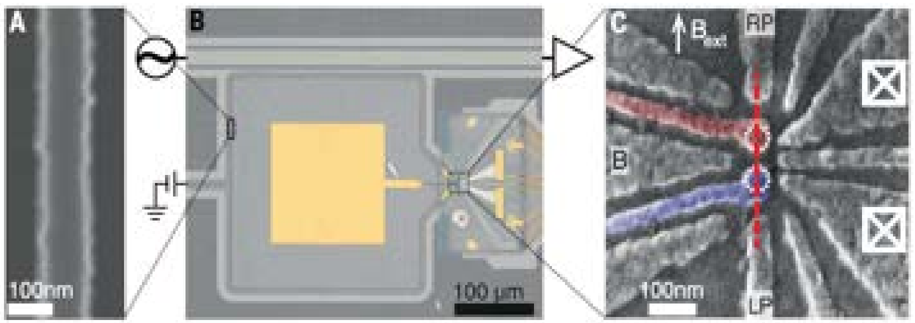

N. Samkharadze et al., Science 2018

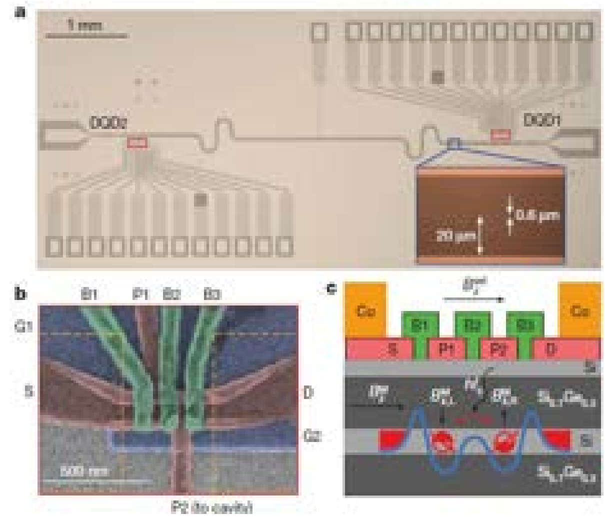

^{nat}Si/SiGe

X. Mi et al., Nature 2018

Note: GaAs QD, A.J. Landig et al., Nature 2018;
Carbon nanotube. T. Cubaynes et al., npj QuInfo 2019

Photon-mediated coupling of
two spins over 250 μm apart

P. Harvey-Collard et al., PRX
12, 021026 (2022); J. Dijikema
et al., arXiv:2310.16805v1

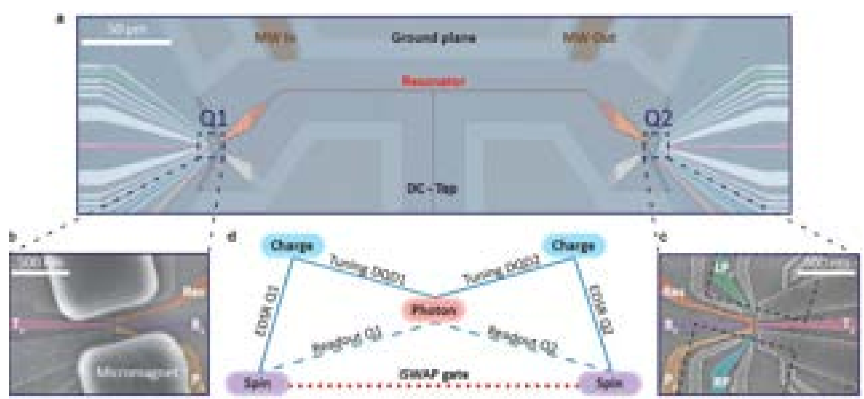

^{28}Si/SiGe

Quantum Link with Spin Shuttling

Gating using two distant spins

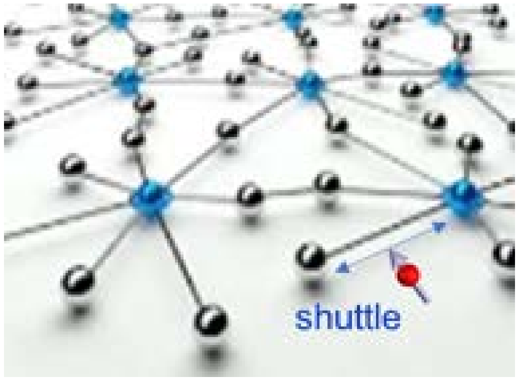

Spin Shuttling

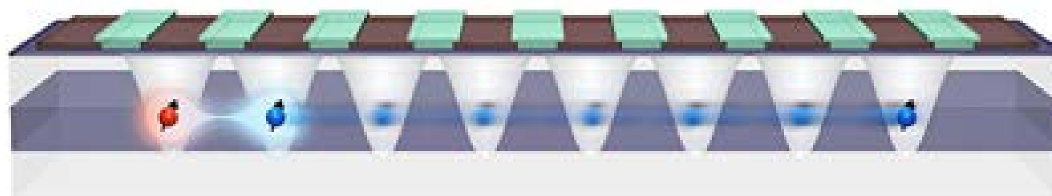

Electron shuttling

Bucket-brigade mode

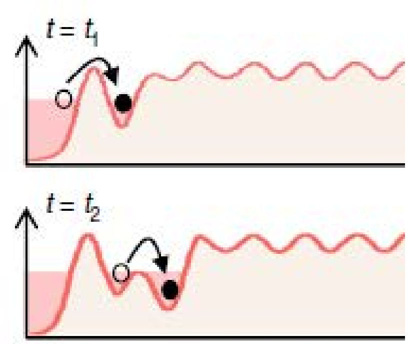

A.R. Mills et al., Nat. Commun. 2019

Belt-conveyor mode

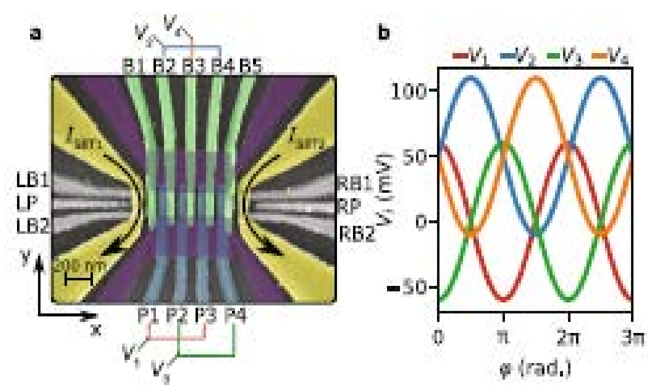

I. Seidler et al., npj QuInfo. 2022

Spin Shuttling through QD Channels

Bucket brigate mode

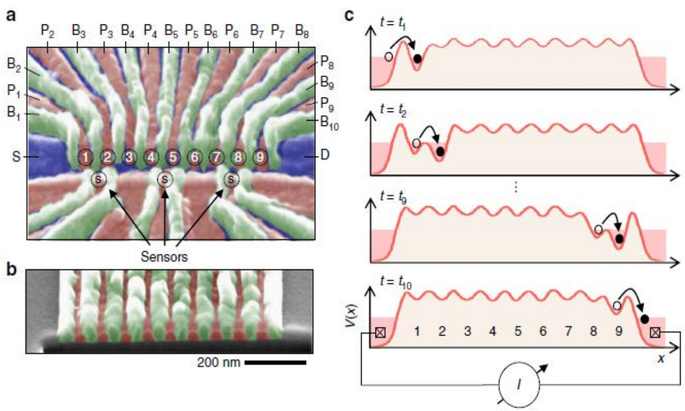

Charge move across 9 QDs in ^{28}Si/SiGe

A.R. Mills et al., Nat. Commun. 2019

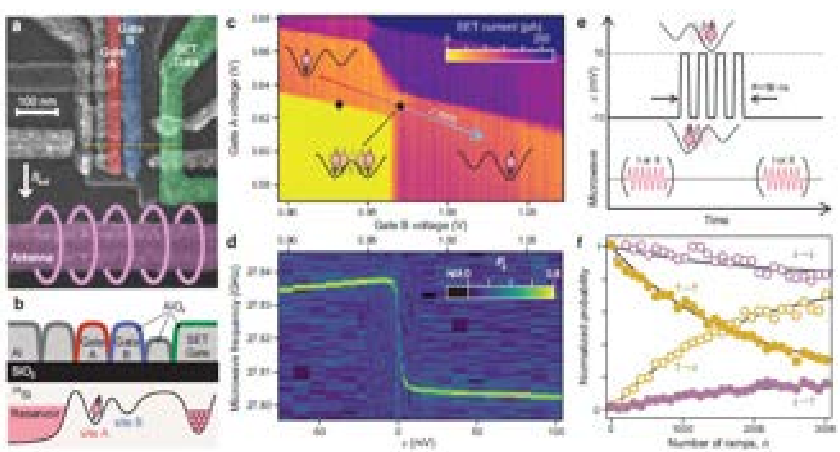

Spin move in DQD in ^{28}Si-MOS

Polarization F=99.97%; Coherence F=99.4%

J. Yoneda et al., Nat. Commun. 2021

Conveyor-belt mode

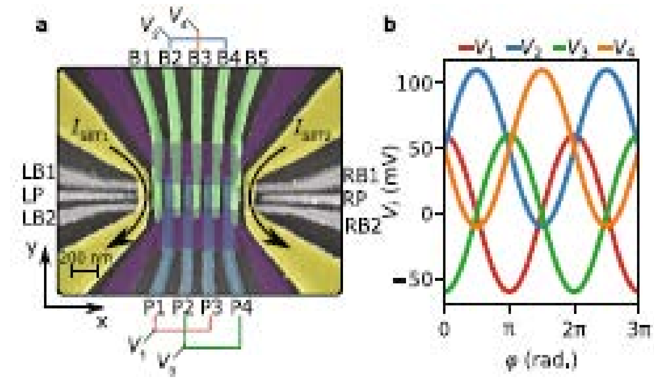

4 sinusoidal voltages for driving a spin across 4 QDs (420 nm) in Si/SiGe

Single electron shuttling with F=99.4%

I. Seidler et al., npj QuInfo. 2022

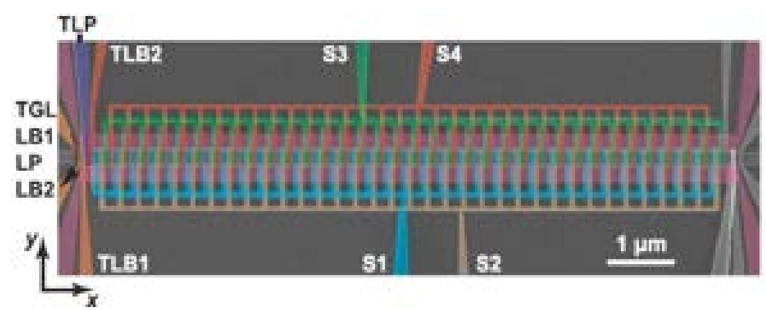

Spin shuttling across a 10 μm long channel of 34 QDs (19 μm) in Si/SiGe

Single electron shuttling with F=99.7%

R. Xue et al., Nat. Commun. 2023

Quantum Link between Distant Qubits

Exchange coupling on
between neighboring spins

Exchange coupling off
between distant spins

Q1 Q2

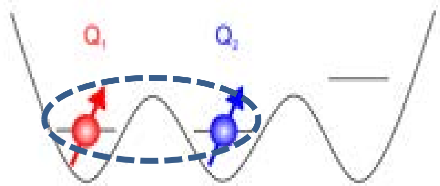

Shuttling

Q1 Q2

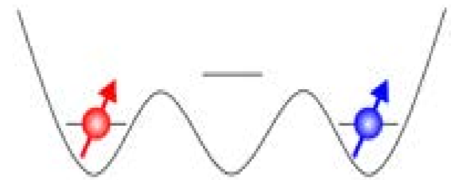

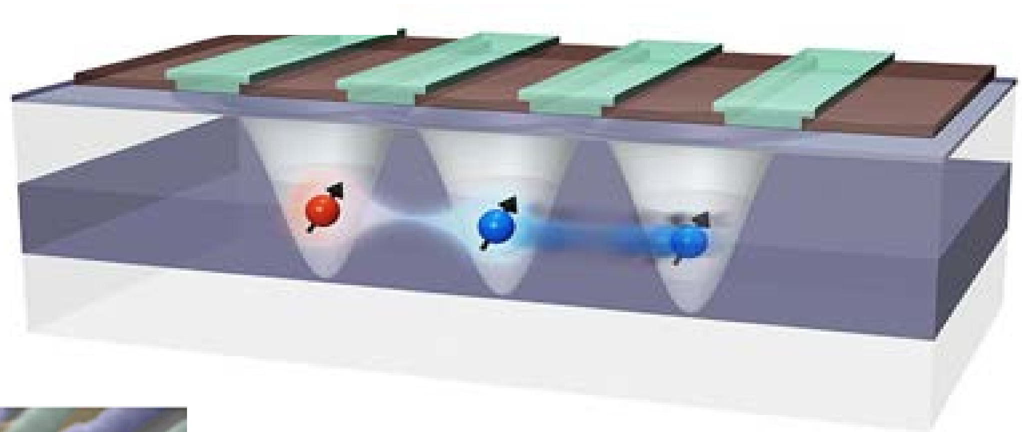

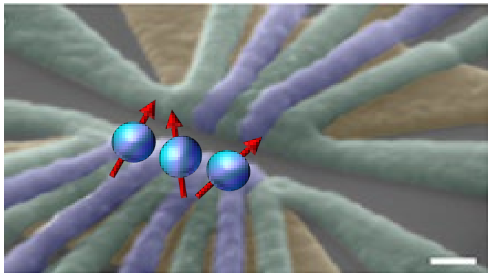

A. Noiri et al. Nat. Commun. 2022

Shuttling Based CPHASE Gate in a Triple QD

A. Noiri et al. Nat. Commun. 2022

Exchange off before electron-move

Exchange on after electron-move

T2* = 3 to 4 us

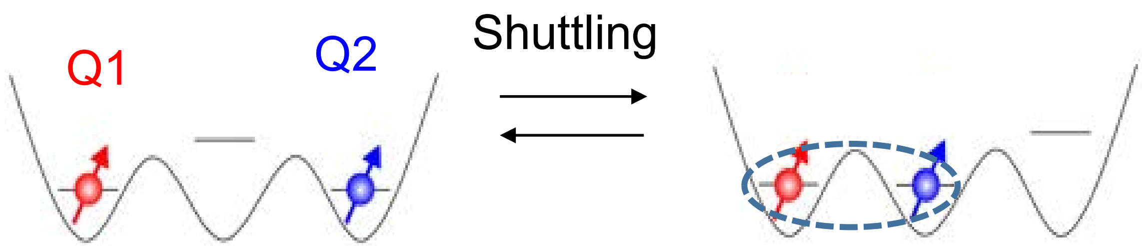

Transfer time
= 3 ns

CPHASE time
= 0.4 us

Shuttling

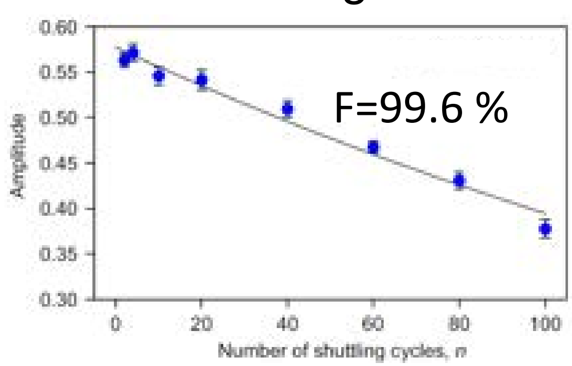

Two-qubit CHPASE gate

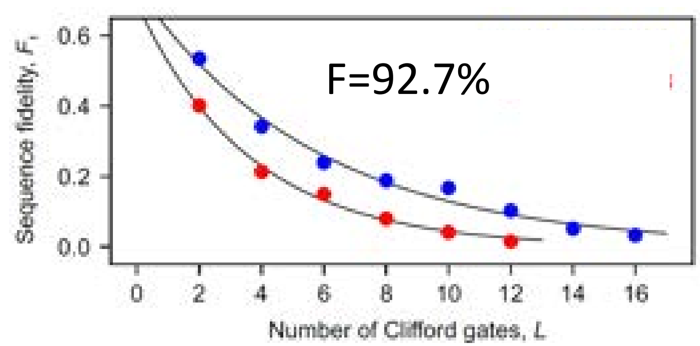

Limited by slow CPHASE

Summary

Basics of QC
: Superposition, entanglement and computation

Implementation of semiconductor qubits
: Spin qubits using concept of spin resonance
Two-qubit operation using spin exchange coupling
Readout and initialization
Spin dynamics

Operation of spin qubits
: High-fidelity quantum gates
Error correction

Challenges for semiconductor QC
: Multi-qubit devices
2D qubit arrays and quantum links for scale-up